EUROPEAN COMMISSION
5th EURATOM FRAMEWORK PROGRAMME 1998-2002
KEY ACTION : NUCLEAR FISSION

LONG-TERM PERFORMANCE OF CANDIDATE MATERIALS FOR HLW/SPENT FUEL DISPOSAL CONTAINERS

CONTRACT N°:
FIKW-CT-2000-00004

FINAL REPORT

E. Smailos[1)], M.Á. Cuñado[2)], B. Kursten[3)], I. Azkarate[4)], G. Marx[5)]

1) FZK.INE, Germany (Co-ordinator); 2) ENRESA, Spain; 3) SCK.CEN, Belgium; 4) INASMET, Spain; 5) GNF.IUT, Germany

Reporting Period:
November 2000 – January 2004

Dissemination level :
Confidential, only for partners of the [acronym] project

ACKNOWLEDGEMENT

The authors gratefully acknowledge the persons listed below for their contributions to the preparation of this report:

B. Fiehn, R. Weiler, FZK.INE, Forschungszentrum Karlsruhe (DE).

F. Druyts, S. Lunardi and K. Penasse, SCK.CEN, Belgian Nuclear Research Centre (B).

Prof. Klaus Richter, Dr. H. Günther, Dr. Henning, GNF.IUT, Gesellschaft zur Förderung der Naturwissenschaftlich-technischen Forschung in Berlin-Adlershof (DE).

V. Madina, INASMET, Asociación de Investigatión Metalúrgica del País Vasco (ES).

The European Commission, and the national authorities and institutions of the authors are also gratefully acknowledged for the funding of this project.

ABSTRACT

In-depth corrosion studies were performed on preselected container materials such as steels, nickel-base alloys (Hastelloy C-4 and C-22), Ti99.8-Pd and Cu-base materials in rock salt, granite and clay environments. The objectives of the studies were: to determine the influence of essential parameters on corrosion, to gain a better understanding of corrosion mechanisms, and to provide more accurate data for modeling the corrosion of the containers over hundred of years. To achieve these objectives, a combination of long-term immersion experiments, electrochemical studies, and stress corrosion cracking studies were performed.

The results in salt brines (T=150°C) confirm previous findings that the passively corroded alloy Ti99.8-Pd has an excellent resistance to general and localized corrosion, and, therefore, it is the strongest candidate for the realization of the **corrosion-resistant container concept.** The TStE355 carbon steel is subject to general corrosion and its corrosion rate implies corrosion allowances acceptable for thick-walled containers (**corrosion-allowance container concept**). EB and TIG welding decrease the corrosion resistance of the carbon steel in $MgCl_2$-rich brine, but this problem can be solved by a thermal stress relief treatment of the welds. However, by use of carbon steel containers it must be taken into account that the corrosion of carbon steel in brines, especially in $MgCl_2$-rich brine, results in high amounts of H_2 in the repository. If it cannot be tolerated, the steel containers can be corrosion protected by Ti99.8-Pd (best material) or Cu-base materials (resistant to pitting corrosion, reasonable corrosion rates). However, the investigation of material pairs indicates that by failure of the corrosion protection materials and presence of $MgCl_2$-rich brine and gamma radiation (10 Gy/h) galvanic corrosion occurs which results in a significant increase in the corrosion rate of the less noble carbon steel and in a decrease in the corrosion rate of the more noble Cu-base materials. The corrosion rate of Ti99.8-Pd remains unchanged.

In granitic environments (Cl^- up to 50,000 mg/L, temperature up to 90°C), Hastelloy C-22 exhibits the highest corrosion resistance. It is resistant to pitting corrosion, crevice corrosion, stress corrosion cracking (SCC) and microbiologically induced corrosion (MIC). Cu shows a slight susceptibility to MIC, and Cu-Ni 70-30 to MIC and SCC at very low strain rates (10^{-6} and $2x10^{-7}$ s^{-1}). The corrosion rates of Cu, Cu-Ni 90-10 and Cu-Ni 70-30 determined in long-term immersion experiments at 90°C in granitic water (initial oxidizing conditions, 98 mg/l Cl^-, pH=9.1) are small (1-7 µm/a), but for Cu pitting and intergranular corrosion were observed. In granitic water (initial oxidizing conditions, T=90°C)) having a low Cl^- concentration (98 mg/L) and a pH=9.1, the carbon steel is sufficient resistant to pitting corrosion. However, in granitic-bentonite environment having a high Cl^- concentration (6,280 mg/L) and a pH=7.3, pitting corrosion occurs.

In clay water (100-50,000 mg/L Cl^-, 16-140°C), the actively corroded TStE355 carbon steel is subject to general corrosion. Among the passively corroded materials only Ti99.8-Pd is resistant to pitting and crevice corrosion under all test conditions. Hastelloy C-4 and Hastelloy C-22 show under severe test conditions (oxidizing conditions, 140°C, Cl^- higher than 20,000 mg/L) a slight crevice corrosion. The stainless steels investigated show a lower resistance to pitting corrosion than the Hastelloy, but pitting corrosion occurs at Cl^- concentrations which are significantly higher than those expected in the near field environment of the Belgian disposal concept. Therefore, stainless steels are the first candidate container material for clay.

TABLE OF CONTENTS

EXECUTIVE SUMMARY

I. Background and Objectives

The waste container as a part of the multibarrier system contributes to the safety disposal of HLW/Spent Fuel in geological formations by protecting the waste forms against radionuclide mobilization by attack of salt brines or groundwater. The main requirement on the container materials is long-term corrosion resistance under normal operating and accident conditions in the repository.

In the present project in-depth corrosion studies have been performed on preselected container materials in simulated rock salt, granite and clay environments at FZK.INE, GNF.IUT, ENRESA/INASMET and SCK.CEN in the frame of a joint programme.The objectives of these studies are: to determine the influence of essential parameters (e.g., composition of the medium, temperature etc.) on corrosion, to gain a better understanding of corrosion mechanisms, and to provide more accurate data for modeling the corrosion of the containers over hundred of years. The materials investigated were:

- In salt environments: the passively corroding alloy Ti99.8-Pd, the actively corroding TStE355 carbon steel, Cu, and Cu-Ni alloys.

- In granitic environments: Ni-base materials, the TStE355 carbon steel, Cu, and Cu-Ni alloys.

- In clay environments: Ti99.8-Pd, Ni-base alloys, stainless steels, and the TStE355 carbon steel.

To achieve the objectives of the project, a combination of chemical experiments (long-term immersion tests), electrochemical studies and stress corrosion cracking studies were performed in the EU-partners´ laboratories. FZK.INE considered both disposal in rock salt and in granite. Work of GNF.IUT has concentrated on disposal in rock salt, ENRESA/INASMET considered disposal in granite, and SCK.CEN covered disposal in clay. The whole programme was coordinated by FZK.INE.

The corrosion results obtained from these studies can be used to develop materials degradation models in order to predict the lifetime of the containers over very many years. A container corrosion model can be combined with other models (e.g. spent fuel and HLW glass models) to describe the source term in the near field in the framework of safety analyses for a repository.

II. Investigations and Results

II.1 Salt environment

II.1.1 Long-term immersion studies on candidate container materials (FZK.INE)

Long-term immersion studies were performed on the candidate container materials Ti99.8-Pd, Cu-base materials and carbon steel in disposal-relevant salt brines at 150°C. In these studies was investigated:

- The effect of welding and thermal stress relief treatment of welds on corrosion of the preselected TStE355 carbon steel.
- The galvanic corrosion between the TStE355 carbon steel and Ti99.8-Pd. Such investigations are relevant by using material pairs for double-walled containers.
- The long-term corrosion behaviour of Cu-base materials such as Cu, Cu-Ni 90-10 and Cu-Ni 70-30.
- The galvanic corrosion between Cu-Ni alloys and TStE355 carbon steel.

All materials were evaluated for general corrosion and local corrosion by using gravimetry, measurements of pit depths, surface profilometry and metallography.

II. 1.1.1 Influence of welding and thermal stress relief treatment of welds on corrosion of TStE355 steel in brines

To examine the effect of electron beam (EB) and tungsten-inert-gas (TIG) welding (potential container closure techniques), and thermal treatment of welds on corrosion of the preselected TStE355 steel, the steel was investigated in three material conditions: unwelded (parent material), only-welded, and welded plus stress-relief thermal treated. The steel was examined at 150°C in NaCl-rich brine (25.9 wt% NaCl) without gamma radiation, and in $MgCl_2$-rich brine (Q-brine, 26 wt% $MgCl_2$) in the presence of a gamma radiation field of 10 Gy/h. The results indicate that the unwelded steel is resistant to pitting corrosion in the sense of an active-passive corrosion element and its general corrosion rates (15.3 µm/a in NaCl-brine and 72.6 µm/a in $MgCl_2$-brine) imply corrosion allowances acceptable for thick-walled containers. The EB- and TIG-welding decrease significantly the corrosion resistance of the steel to localized corrosion, but only in the $MgCl_2$-rich brine. The only-welded specimens suffer in this brine from severe local corrosion attacks in the welds and in the heat-affected zone (HAZ). However, the stress relief thermal treatment of the welds improves the corrosion resistance of the welded material in the $MgCl_2$-rich brine, so that the thermal treated welded steel is resistant to pitting corrosion, as does also the unwelded material.

In view of these results, the TStE355 carbon steel continues to be considered promising for long-lived containers. To avoid local corrosion problems in the region of the welded container cover, a stress-relief thermal treatment of the welds is recommended.

II. 1.1.2 Galvanic corrosion between TStE355 carbon steel and Ti99.8-Pd in brines

In NaCl-rich-brine both with and without gamma radiation and in $MgCl_2$-rich brine in the absence of gamma radiation no galvanic corrosion occurs on the coupled material pair Ti99.8-Pd/TStE355 carbon steel because both materials form protecting corrosion layers. However, in $MgCl_2$-rich brine and in the presence of gamma radiation field of 10 Gy/h a significant galvanic corrosion occurs which leads in the case of the coupled steel in strong local corrosion attacks and in a high increase in the corrosion rate (370 µm/a) compared to the value of the uncoupled steel specimens (72 µm/a). This is attributed to the fact that the oxidants (mainly O_2) formed by the radiolysis of water are reduced at the Ti99.8-Pd alloy which results in an increase of the oxidation rate of Fe analog to a local element.

II. 1.1.3 Long-term corrosion behaviour of Cu-base materials and galvanic corrosion between Cu base meterials and TStE355 carbon steel

Cu and the alloys Cu-Ni 90-10 and Cu-Ni 70-30 are potential materials for long-lived HLW/Spent Fuel disposal containers. They are resistant to pitting corrosion in salt brines and their corrosion rates (in NaCl-brine: 3-12 µm/a, in $MgCl_2$-brine: 24-46 µm/a) determined imply corrosion allowances reasonable for long-lived containers.

In the NaCl-rich brine with and without gamma radiation (10 Gy/h) the coupled material pairs Cu-Ni 90-10/TStE355 carbon steel and Cu-Ni 70-30/TStE355 carbon steel form stable corrosion protective surface layers, and, therefore, no galvanic corrosion occurs. In $MgCl_2$-rich brine, however, both in irradiated and unirradited brine environment, galvanic corrosion occurs due to local break down of the corrosion surface layer of the steel. This results in localized corrosion on the less noble coupled carbon steel and significant increase in its general corrosion rate (123-564 µm/a) compared to the value of the uncoupled steel specimens (47-72 µm/a). For the more noble coupled Cu-Ni alloys a clear decrease in corrosion rate (6-6.2 µm/a) is observed in the unirradiated $MgCl_2$-rich brine compared to the values of the uncoupled specimens (37-46 µm/a). This means that in this brine the Cu-Ni alloys are cathodically protected by the carbon steel.

II.1.2 <u>Electrochemical corrosion studies and surface analytical investigations on</u> candidate container materials in salt brines (GNF.IUT)

Electrochemical investigations into the corrosion behaviour of TStE355 carbon steel, Ni, Cu and Cu-Ni-alloys in the $MgCl_2$-rich Q-brine and in NaCl-rich brine were performed by applying potentiostatic and potentiodynamic measurements, measurements at rest potentials (free corrosion potentials) and at galvanic potentials at 25°C and at 80°C. The electrochemical procedures were combined with analytical methods, mostly with gravimetric ones, but in some cases also with ICP-MS and TXRF.

The results obtained demonstrate that among the materials investigated theTStE355 carbon steel is the less resistant material in Q-brine and in NaCl-rich brine, due to its negative potential with respect to its oxidant H_3O^+, which is reduced to H_2.The corrosion rates of carbon steel are higher in Q-brine than in NaCl-rich brine. The higher corrosivity of the Q-brine is attributed to its higher Cl^- concentration and lower pH (pH=4.5 at 25°C) compared to the NaCl-rich brine (pH=6.5 at 25°C), and to the Mg^{2+} containing in the Q-brine, which influence the formation of the corrosion surface layer.

In general higher temperatures enhance the corrosion rates of all the materials under investigation. At 25°C the corrosion rate of Ni is only R_{Ni} = 8 µm/a in Q-brine due to its being passivated by a NiO surface layer. At this temperature the corrosion rate of Cu is significant higher, R_{Cu} = 24 µm/a in this medium, because its potential is shifted more to the negative range due to the $[CuCl_2]^-$-complex formation.

On the other hand, at 80°C in NaCl-rich brine it is R_{Ni} = 215 µm/a and R_{Cu} = 105 µm/a. This behaviour is caused by the passive range of Ni being shortened at higher temperature due to the disruption of the passivating NiO surface layer. At 80°C the oxidant of Ni and Cu in brines is O_2 to be reduced to H_2O or OH^- , respectively. At 80°C the O_2 concentration of the brines is smaller than at 25°C, which causes the

shift of the relevant rest potentials of Ni and Cu to more negative values, because the cathodic potential current density is decreased.

In case of galvanic coupling of carbon steel with Cu, Ni and Cu-Ni alloys, respectively, carbon steel is the anode in the two brines at both temperatures. The galvanic potentials are near to the relevant rest potentials of carbon steel which acts as a cathode protector. In accordance with the theory, the corrosion rates of the cathodic materials are decreased. From the contact pair Cu/Ni, which is of importance from the theoretical point of view, it was demonstrated that Cu is the anode and Ni the cathode in brine due to the existence of the $[CuCl_2]^-$-complex and the NiO layer.

The relevant thermodynamic data (Reaction Free Enthalpy $\Delta_R G$; Reaction Enthalpy $\Delta_R H$ and Reaction Entropy $\Delta_R S$) were calculated from Gibbs-Helmholtz and the dependence of the EMF on temperature, assuming $\Delta_R H$ to be independent from T. The reasonable data obtained confirm the assumptions made. They represent the few data which have been calculated for brines uptil now.

Referring to all the corrosion data obtained by applying electrochemical methods it always must be kept in mind that only the starting period of the relevant corrosion processes and, therefore, the initial corrosion rate of the materials could be determined. The long-term corrosion behaviour and the final corrosion rate of the materials, which are needed for the evaluation of the suitability of the materials as container materials, were determined from the long-term immersion experiments. The most important benefit of the electrochemical studies compared to the chemical immersion experiments, however, is the possibility to study in detail the corrosion mechanisms, which allows a better interpretation of the corrosion results obtained from the long-term immersion experiments. Both the electrochemical and the long-term corrosion studies, and the investigation of the surface of corroded specimens by means of EPMA/SEM allow a reasonable description of the long-term corrosion behaviour of the investigated materials.

The surface analytical investigations of corroded material specimens have shown that in the case of the electrode couples Cu/steel and Ni/steel in Q-brine, the steel electrode corrodes very strongly. A thick layer (μm-range) arises on the surface, which consists of crystallites of (Fe,Mg)-oxides, -hydroxides and -chlorides. The corrosion of the Cu and the Ni partner, respectively, is comparatively small. In the case of the electrode couple Cu/Ni in Q-brine at 26 °C, the corrosion of copper is very high, whereas the corrosion of Ni is small due to its strong passivation by an oxide/hydroxide layer. At 80°C Ni is deposited on the Cu electrode. In some experiments carried out at 80°C Ag is deposited on the more negative metal, especially on Cu; this is due to the complex formation of $[AgCl_2]^-$, which happens to AgCl of the reference electrode in Q-brine.

Besides the element composition and morphology being already analyzed, first investigations were undertaken and further investigations are urgently needed to determine also the phase composition and the structure of the surface layers by means of diffraction methods. The results from the investigation into the element composition and the morphology of the corroded surfaces of the Cu, Ni and steel electrodes by means of EPMA/EDX and SEM prove to be a valuable addition as well as a confirmation of those obtained electrochemically.

II.2 Granitic environment

II.2.1 Long-term immersion studies on candidate container materials (FZK.INE)

The long-term corrosion behaviour of the preselected TStE355 carbon steel and three Cu-base materials (Cu, Cu-Ni 90-10 and Cu-Ni 70-30) was investigated in disposal relevant granitic environments by using immersion experiments.

All materials were examined under initial oxidizing conditions in a granitic water having a moderate Cl^- content of 98 mg/L and a pH value of 9.1 at 22°C (granitic water 1). In order to examine the influence of the Cl^- content of granitic water on the steel corrosion, the steel was additionally investigated in a granitic water which was in contact with bentonite and had a very high Cl^- content of 6260 mg/L and a pH value of 7.3 at 22°C (granitic water 2).

The corrosion results obtained from the long-term immersion experiments in the synthetic granitic waters at 90°C can be summarized as follows:

- In the granitic water having the low Cl^- content (98 mg/L Cl^-) and a pH=9.1, the TStE355 carbon steel performs well as HLW/Spent Fuel container material. Under the test conditions applied it is resistant to pitting corrosion and its general corrosion rate (21 µm/a) is acceptable for thick-walled containers.

- In the granitic water having the high Cl^- content (6280 mg/L Cl^-) and a pH=7.3, the steel suffers from severe pitting corrosion.

- The general corrosion rates of Cu, Cu-Ni 90-10 and Cu-Ni 70-30 in the test granitic water (oxidizing conditions, pH=9.1, 98 mg/L Cl^-) are small (1-7 µm/a). Furthermore, the alloys Cu-Ni 90-10 and Cu-Ni 70-30 resist localized corrosion. However, Cu is susceptible to pitting and intergranular corrosion.

II.2.2 Stress corrosion cracking, electrochemical and crevice corrosion studies on candidate container materials in salt brines (ENRESA/INASMET)

The corrosion behaviour of three preselected container materials has been investigated in simulated saturated granitic-bentonite water with chloride contents between 6,500 and 50,000 mg/L. Localized corrosion phenomena such as stress corrosion cracking (SCC), pitting, crevice, and microbiologically influenced corrosion (MIC) have been studied. The container materials examined were the nickel base alloy Hastelloy C22 (HC22), the oxygen free high purity copper CuOF and the cupronickel alloy Cu30Ni (Cu-Ni 70-30). Besides the parent metal, welded specimens provided with different welding procedures simulating possible container closure techniques were investigated. The resistance to SCC has been evaluated at 90°C by means of the Slow Strain Rate Technique (SSRT). Pitting, general corrosion, and MIC have been evaluated by electrochemical methods at 25°C. Finally the crevice corrosion behaviour has been studied at 90°C creating artificial assemblies on test specimens.

The results obtained have shown that the HC22 alloy is resistant to SCC, pitting, and crevice corrosion at temperatures up to 90ºC and chloride contents up to 50,000 mg/L. No MIC due to Suphate Reducing Bacteria (SRB) is detected on HC22 specimens. CuOF and Cu30Ni alloys are resistant to crevice and pitting corrosion. The Cu30Ni alloy exhibits shallow secondary cracking when tested at 90ºC in the granitic-bentonitic water with chloride contents up to 6,500 mg/L, thus revealing a certain sensitivity to SCC. No susceptibility to SCC, at any of the testing conditions is observed for CuOF specimens. CuOF and Cu30Ni alloys show a certain sensitivity to MIC phenomenon due to the action of SRB.

II.3 Clay Environment (SCK.CEN)

The resistance of eight preselected container materials to pitting corrosion was investigated under conditions representative for underground disposal in clay. These materials are: carbon steel (TStE 355), stainless steels (AISI 316L, AISI 316L hMo, AISI 316Ti, UHB 904L), nickel-base alloys (Hastelloy C-4, Hastelloy C-22), and the titanium alloy Ti/0.2Pd (Ti99.8-Pd). The influence of four environmental parameters on the pitting corrosion of the materials was investigated, namely the oxygen level, the temperature, the chemical composition of the underground disposal environment (chloride, sulphate, and thiosulphate), and the presence of the most important radiolytic product hydrogen peroxide (H_2O_2). The oxygen content reflects the aerobic and anaerobic phases of the disposal. The tests were conducted at three temperatures, namely 16°C, 90°C, and 140°C. The chloride concentration was varied up to 50,000 mg/L. The influence of thiosulphate was investigated in the range 20-200 mg/L. Experiments were performed in solutions containing 0.2, 216, 1700, and 5400 mg/L sulphate. The influence of hydrogen peroxide, which occurs as a radiolytic product from the interaction of gamma radiation with the aqueous surroundings, was studied in the range 8.10^{-3}-8.10^{-1} mol/L. Experiments were performed in solutions which are representative for either Boom Clay backfill (SICW and SOCW under anaerobic and aerobic conditions, respectively) or a bentonitic backfill material (SBW).

The long-term susceptibility to pitting corrosion was evaluated by comparing the critical potential for pitting (E_{NP}) and the protection potential (E_{PP}), which were determined from CPP-measurements, to the actual corrosion potential, which was determined by monitoring the free corrosion potential as a function of time.

The results indicate that among the materials investigated only the alloy Ti/0.2Pd was completely resistant to pitting corrosion under all experimental conditions applied. The results obtained for the other materials under the various experimental conditions can be summarized as follows:

II.3.1 Anaerobic experiments at 16°C

The carbon steel TStE 355 remains unaffected in SBW-solutions without thiosulphate at 16°C. Under all other conditions, TStE 355 is subject to general corrosion. Hastelloy C-4, Hastelloy C-22, and UHB 904L are resistant to pitting corrosion. The stainless steels AISI 316L, AISI 316L hMo, and AISI 316Ti are resistant to piting in all SBW-solutions (up to 50,000 mg/L Cl^-) and in SICW up to 1,000 mg/L Cl^-. Although at

$[Cl^-] \geq 1{,}000$ mg/L slight signs of pitting were observed, the E_{NP}-values remained much more positive than the actual E_{CORR} (-10 mV_{SHE}).

II.3.2 Anaerobic experiments at 90°C

The carbon steel TStE 355 exhibits uniform attack in all SICW- and SBW-solutions. Hastelloy C-4 and Hastelloy C-22 are resistant to pitting. Although under some conditions the CPP-curves revealed a hysteresis, it was found that this was probably the result of an alteration of the passive layer.

UHB 904L has a slightly higher pitting resistance than the three 316 grade stainless steels. The E_{NP}-values for AISI 316L, AISI 316L hMo, and AISI 316Ti are situated well above the actual E_{CORR} in all SICW- and SBW-solutions. The E_{PP}-values drop below the actual E_{CORR} for $[Cl^-] > 10{,}000$ mg/L.

II.3.3 Aerobic experiments at 90°C (Influence of the radiolytic product H_2O_2)

The addition of hydrogen peroxide (H_2O_2) to the solutions does not affect the corrosion behaviour of Hastelloy C-4, Hastelloy C-22 and carbon steel TStE 355. In the case of the stainless steels AISI 316L, AISI 316L hMo, AISI 316Ti, and UHB 904L the addition of H_2O_2 to the solutions exerts a dual effect on the susceptibility to pitting corrosion: a beneficial effect by promoting passivation and inhibiting pitting, and a detrimental effect by increasing the OCP significantly and eliminating repassivation completely.

II.3.4 Aerobic experiments, 140°C

The carbon steel TStE 355 exhibits uniform corrosion in all SOCW- and SBW-solutions. Hastelloy C-4 and Hastelloy C-22 are resistant to pitting. However, in SOCW-solutions containing high $[Cl^-]$ (> 20,000 mg/L), the Hastelloy samples show signs of pitting at the interface between the sample and the mounting resin. This indicates that under these severe test conditions, Hastelloy C-4 and Hastelloy C-22 could be susceptible to crevice corrosion.

UHB 904L has a slightly higher resistance to pitting than the other stainless steels. The three grades of AISI 316 type stainless steels have comparable pitting characteristics. The pitting resistance decreases with increasing chloride concentration. In SOCW, E_{NP} drops below the actual E_{CORR} when the chloride concentration is increased to 1,000 mg/L (except for UHB 904L). In SBW, E_{NP} remains well above the actual E_{CORR} for chloride concentrations up to 10,000 mg/L. E_{PP} is more negative than the actual E_{CORR} in all SOCW- and SBW-solutions. Sulphate has an inhibitive effect on pitting, i.e., the higher the sulphate concentration, the more chloride is required to initiate pitting. This inhibitive effect diminishes with increasing $[Cl^-]$. An increase in temperature causes a steep decrease of E_{NP}.

The oxygen level has a significant influence on the pitting resistance. As oxygen will be consumed in the underground repository, the tested stainless steels become much more resistant to pitting.

The 'critical chloride content' approach is a useful tool to determine the suitability of stainless steels in other argillaceous disposal environments containing Cl^- by estimating the maximum chloride level below which pitting is not expected to occur.

III. Conclusions and Recommendations for Future Work

- The results of this study confirm previous findings that the passively corroded alloy Ti99.8-Pd is the strongest candidate for the realization of the **corrosion-resistant container concept** in rock salt. Such a **corrosion-resistant container concept** could consist of a carbon steel container as mechanical support provided with a corrosion protection (layer or surrounding thin-walled container) made of Ti99.8-Pd. It must be mentioned that due to the high rock pressure in a rock salt repository thick-walled containers are needed in any case for mechanical reasons.

- The TStE355 carbon steel, Cu and the alloys Cu-Ni 90-10 and Cu-Ni 70-30 are promising materials for the realization of the **corrosion-allowance container concept** in rock salt. A benefit of the use of carbon steel containers is the establishment of reducing conditions in the near field of the repository by corroded iron and, therefore, the expected high retardation of radionuclides by iron corrosion products (e.g. Fe_3O_4, Fe_2O_3, $Fe(OH)_2$).

The problem of the susceptibility of welded steel (welded container lid) to pitting corrosion in $MgCl_2$-rich brine can be avoided by thermal stress relief treatment of the welds. An important question which still needs to be clarified with a view to the use of the corrosion-allowance carbon steels is namely, whether the large amount of hydrogen generated by the corrosion of iron or by the radiolysis of brines (especially $MgCl_2$-rich brines) can be tolerated in the repository. If not, the carbon steel containers can be corrosion protected by Ti99-Pd (best choice) or Cu-base materials.

- The most promising materials for containers to be disposed of in granitic formations are Hastelloy C-22, Cu and Cu-Ni-alloys. Very probably the alloy Ti99.8-Pd is also a strong candidate for containers, but this material was not examined in the present study. Carbon steel is also a option for the thick-walled **corrosion-allowance container concept.**

- Stainless steels, Ni-base alloys (Hastelloy C-4 and C-22), and the Ti-Pd alloy Ti99.8-Pd are the most important candidate materials for thin-walled containers in clay formations, while carbon steels are considered as the prime choice for the thick-walled **corrosion-allowance container concept.** Considering material costs and fabrication aspects for containers, stainless steels are the first candidate container material in the Belgian disposal concept in clay.

Various areas for which more in-depth investigations are required were identified and the most important of them are summarised below. The level of scientific knowledge already available and priority differ according to the type of candidate rock formation.

- microbiologically induced corrosion (MIC).
- atmospheric corrosion (corrosion during interim storage).
- effect of fabrication aspects and container design on corrosion.

- long-term metallurgical modifications.
- influence of radiation effects.
- production of nitric acid (and its influence on the integrity of the container).
- information from archeological analogues .
- studies of the sorption of radionuclides on iron corrosion products.
- corrosion models in order to predict the lifetime of waste containers under disposal conditions.

1. INTRODUCTION AND OBJECTIVES

In present concepts for the disposal of vitrified high-level waste (HLW) and spent fuel in geological formations such as rock salt, granite and clay, the disposal container (overpack) is an important component of the multibarrier system against the mobilization of radionuclides from the waste forms. Its function is to isolate the waste from the disposal environment for as long as practicable. Depending on the disposal medium and concept container lifetimes between some hundreds and thousands of years are required. The main threat to container integrity is corrosion induced by contact with salt brines or groundwater which may be present in the disposal area under certain conditions. Accordingly, extended studies have been undertaken in various EU-laboratories aimed at identifying corrosion resistant materials for long-lived containers. In previous EU-programmes extended corrosion studies were performed on a large number of metallic materials [1,2,3,4,5] in rock salt, granite and clay environments. In these studies some materials were identified as promising for the manufacture of long-lived containers. These are:

- The passively corroded titanium-palladium alloy Ti99.8-Pd as the strongest candidate for **the corrosion-resistant** container concept in rock salt, granite and clay. This consists of a carbon steel container as mechanical support against the rock pressure provided with a corrosion protection made of Ti99.8-Pd.

- The actively corroded carbon steel as the most promising material for the **corrosion-allowance** container concept in the above-mentioned three geological media. This concept consists of a thick-walled carbon steel container without a corrosion protection. However, the general corrosion rate of carbon steels at high temperature (150°C) in salt brines, especially in $MgCl_2$-rich brines, is very high which leads to very thick-walled containers as corrosion allowance and to undesirable high amounts of H_2 in the repository. Therefore, copper (Cu) and copper-nickel alloys (Cu-Ni alloys) were investigated in the present study as alternative materials for the corrosion-allowance concept or as corrosion protection material for carbon steel containers.

- The nickel-base alloy Hastelloy and high alloyed stainless steels seem to be potential container materials for disposal in clay at realistic Cl^- concentrations.

In the present project in-depth corrosion studies have been performed on the above-mentioned candidate materials (steels, Hastelloy, Ti99.8-Pd, Cu, and Cu-Ni alloys) in simulated rock salt, granite and clay environments at FZK.INE, GNF.IUT, ENRESA/INASMET, and SCK.CEN in the frame of a joint programme.The objectives of these studies are: to determine the influence of essential parameters (e.g., composition of the medium, temperature etc.) on corrosion, to gain a better understanding of corrosion mechanisms, and to provide more accurate data for modeling the corrosion of the containers over hundred of years.

To achieve the objectives of the project, a combination of chemical experiments (long-term immersion tests), electrochemical studies and stress corrosion cracking studies were performed in the EU-partners´ laboratories. FZK.INE considered both disposal in rock salt and in granite. Work of GNF.IUT has concentrated on disposal in

rock salt, ENRESA/INASMET considered disposal in granite, and SCK.CEN covered disposal in clay. The whole programme was coordinated by FZK.INE.
The corrosion results obtained from these studies can be used to develop materials degradation models in order to predict the lifetime of the containers over very many years. A container corrosion model can be combined with other models (e.g. spent fuel and HLW glass models) to describe the source term in the near field in the framework of safety analyses for a repository.

The results will be disseminated to organizations responsible for implementing the programmes for disposal of radioactive waste and will be published in accordance with the rules set up by the European Commission. Since all partners are involved in research into repository safety, the participating organizations will be also end-users of the results. The results of the project could be used in all European Union countries as the project is independent of the type of fuel cycle of HLW waste (spent fuel or glass) and the characteristics of the host rock environment.

In the present final project report, the progress achieved in the research programme from November 2000 to January 2004 is described.

2. WORK PROGRAMME

The work programme consists of three work packages (WP):

WP 1: Corrosion studies in salt environments (FZK.INE, GNF.IUT)

Both long-term immersion studies (FZK.INE) and electrochemical studies (GNF.IUT) were performed on presected materials in disposal-relevant salt brines. In these studies was investigated:

- The effect of welding and thermal stress relief treatment of the welds on the corrosion of carbon steel.
- The galvanic corrosion between carbon steel and Ti99.8-Pd. Such investigations are relevant by using a double-walled container.
- The long-term corrosion behaviour of Cu-base materials such as Cu, Cu-Ni 90-10 and Cu-Ni 70-30.
- The galvanic corrosion between Cu-base materials and carbon steel.
- The electrochemical corrosion behaviour of Cu, Ni and Cu-Ni alloys.

WP 2: Corrosion studies in granitic environments (ENRESA/INASMET, FZK.INE)

ENRESA/INASMET investigated the corrosion resistance of Cu- and Ni-base materials to pitting corrosion, crevice corrosion, stress corrosion cracking, and microbiologically induced corrosion. FZK.INE studied the general and localized corrosion behaviour of carbon steel and Cu-base materials by using long-term immersion experiments.

WP 3: Corrosion studies in clay environments (SCK.CEN)

SCK.CEN investigated the influence of various parameters such as oxygen content, elevated temperature, and radiolytic products of clay water on the localized corrosion behaviour of a large number of preselected container materials (carbon steel, stainless steels Ni-base alloys, alloy Ti99.8-Pd) in clay environments.

3. LONG-TERM CORROSION STUDIES IN SALT ENVIRONMENTS (WP1) (FZK.INE,GNF.IUT)

3.1 Influence of welding and heat treatment of welds on corrosion of TStE355 carbon steel in salt brines (WP1.1) (FZK.INE)

Welding techniques such as Electron Beam welding (EB-welding) and Tungsten Inert Gas welding (TIG-welding) are considered as potential closure techniques for carbon steel containers.

To ensure the desired lifetime of the containers, the welded container cover should have a corrosion resistance similar to that of the parent material. Under this aspect, comparative corrosion investigations on unwelded (parent material) and TIG- and EB-welded steel specimens with and without heat treatment of the welds were performed in this study. The investigation of welds is important because welding causes changes in the material structure and generates tensile stresses in the weld region and in the Heat Affected Zone (HAZ), which in turn can cause an unfavourable corrosion behaviour of the welded material.

3.1.1 Steel investigated and experimental

The preselected carbon steel TStE355 was investigated in the hot-rolled and annealed condition and had the following composition in wt.%: 0.17% C; 0.44% Si; 1.49% Mn; bal. Fe.

For the investigations, flat specimens having the dimensions 40mmx20mmx4mm were used. The steel was examined in three material conditions:

- Unwelded (parent material).
- Only-welded (EB- and TIG-welded).
- Welded and thermal treated. These specimens were welded by EB and TIG, and subsequently stress-relief thermal treated for 2 hours at 600°C.

In the case of the welded specimens, the weld was located in the center of the specimens in the transverse direction.

The steel specimens were examined up to 16 months in two disposal-relevant brines at a temperature of 150°C, which roughly corresponds to the maximum surface temperature of the disposal containers (≤200°C) according to the disposal concept discussed in Germany. The brines had at 55°C the following compositions in wt.%:

- $MgCl_2$-rich “Q-brine” (brine 1): 26.8 $MgCl_2$; 4.7 KCl; 1.4 NaCl; 1.4 $MgSO_4$; 65.7 H_2O (pH = 4.6).
- NaCl-rich brine (brine 3): 25.9 NaCl; 0.23 K_2SO_4; 0.21 $CaSO_4$; 0.16 $MgSO_4$; 73.5 H_2O (pH = 6.5).

The experiments in Q-brine were performed in the presence of a gamma radiation field of 10 Gy/h. This dose rate corresponds to the value on the surface of the containers having mechanical and corrosion allowances of about 90 mm for a lifetime of 500 years. The experiments in NaCl-rich brine were conducted without gamma radiation because previous investigations [6] have shown that in this brine the gamma radiation of 10 Gy/h does not affect the corrosion behaviour of the steel.

The experimental setups used for the experiments are described in previous work [5]. Briefly, for the experiments without irradiation, stainless steel pressure vessels provided with corrosion resistant insert vessels made of PTFE were used to avoid evaporation of the brines (boiling point: about 115°C). The experiments under gamma irradiation were performed in the spent fuel storage pool of KFA Jülich. For these experiments, autoclaves made of Ti99.8-Pd were used. With these experimental equipments, the initial test conditions were oxidizing. The total amount of oxygen available in the systems was about 15 mg, corresponding to 0.19 mg O_2/cm^2 specimen. This oxygen amount was consumed very fast by reactions with Fe so that after a few days reducing conditions were established. Evaluation of the specimens regarding general and local corrosion was carried out by gravimetry, measurements of pit depth, surface profilometry and metallography. The integral corrosion rate of the specimens was calculated from the experimental determined weight losses and the material density.

3.1.2 Results in the $MgCl_2$-rich “Q-brine”

Figure 3.1 shows the time-dependence of the general corrosion, expressed as the integral thickness reduction, of the unwelded and only-welded steel specimens in the Q-brine at 150°C and 10 Gy/h. The data indicate that the thickness reduction of the specimens increases linearly with the exposure time in the brine over the test duration of the study. The integral thickness reduction of the welded specimens is lower than that of the unwelded specimens. This is attributed to the formation of a dense layer on the specimens surface after welding which was observed in the metallographic examinations. However, the slope of the curves indicates that the linear thickness reduction of the only-welded specimens, which is the basis for the determination of the long-term corrosion rate, is very close to that of the unwelded specimens.

The linear corrosion rates of the unwelded and only-welded specimens, calculated from the slope of the curves, are compiled in Table 3.1. In this Table the results of the localized corrosion of the specimens are also summarized, which were obtained from the surface profilometry and the metallographic examinations. The Table 3.1 shows that the linear corrosion rates of the only-welded specimens (66-68 µm/a) are very close to the value of the unwelded specimens (73 µm/a). For the unwelded specimens, a non-uniform general corrosion with a maximum depth of only 60 µm after 550 days was observed. In the case of the EB- and TIG- welded specimens,

however, severe local corrosion attacks occurred in the weld region and in the HAZ with maximum pit depths of about 1350-1500 µm after 300 days test time.

Generally, it can be stated that the EB- and TIG-welded specimens have a very similar corrosion behaviour in the brine, and that they exhibit a significantly lower corrosion resistance than the base material

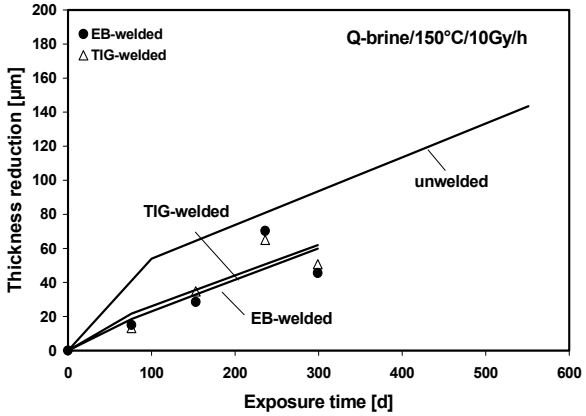

Figure 3.1: Time-dependence of the general corrosion of welded and unwelded TStE355 steel in $MgCl_2$-rich Q-brine at 150°C and 10 Gy/h

Table 3.1: Comparison of the corrosion results obtained for welded and unwelded TStE355 steel in Q-brine at 150°C and a gamma-dose rate of 10 Gy/h

Material condition	Max. test duration (d)	Linear corrosion rate (µm/a)	Max. localized corrosion (µm)		
			Base mat.	HAZ	Weld
unwelded	550	72.6 ± 11	60	—	—
EB-welded	300	67.7 ± 41	90	1500	1200
TIG-welded	300	65.8 ± 40	180	1250	1350

HAZ= Heat Affected Zone

The results on general and localized corrosion obtained for the thermal treated welded steel specimens in Q-brine at 150°C and 10 Gy/h are given in Figure 3.2 and Table 3.2. For comparison, the results obtained on unwelded and only-welded specimens are also given. The thickness reduction of the thermal treated welded specimens increases linearly with the exposure time in the brine (Figure 3.2), as do so also unwelded and only-welded specimens.

The linear corrosion rates (Table 3.2) of the thermal treated EB- and TIG-welded specimens (95 µm/a – 112 µm/a) are higher than the values of the unwelded (73 µm/a) and only welded specimens (66-68 µm/a). However, a such increase is not significant for the thick-walled containers discussed. Very important is the fact that corrosion of the thermal treated welded specimens is only slightly non-uniform (maximum corrosion depth 90-120 µm after 480 days) as in the case of the unwelded

specimens. Severe localized corrosion in the welds or in the HAZ, as was determined on the only-welded specimens, was not observed on the thermal treated welded specimens. In general it can be stated that, in contrast to the only-welded specimens, the thermal treated welded specimens show a sufficient resistance to localized corrosion in the brine, and that their corrosion behaviour is similar to that of the parent material. As in the case of the only-welded specimens, there are not noticeable differences in the corrosion behaviour of the thermal treated EB- and TIG-welded specimens.

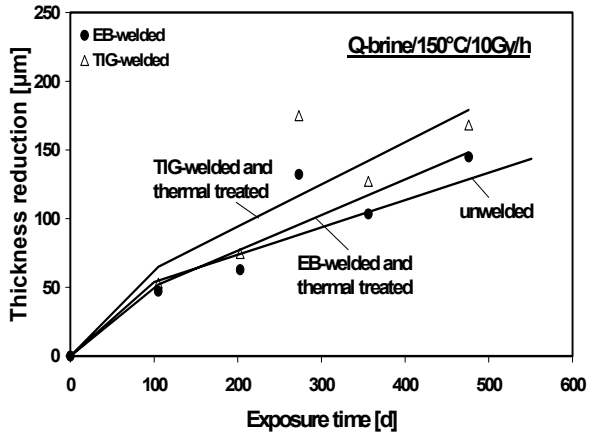

Figure 3.2: Time-dependence of the general corrosion of unwelded and thermal treated welded TStE355 steel in MgCl-rich Q-brine at 150°C and 10 Gy/h

Table 3.2: Comparison of the corrosion results obtained for unwelded, welded, and heat treated welded TStE355 steel in $MgCl_2$-rich brine (Q-brine) at 150°C and a gamma-dose rate of 10 Gy/h

Material condition	Max. test duration (d)	Linear corrosion rate (µm/a)	Max. localized corrosion (µm)		
			Base mat.	HAZ	Weld
unwelded	550	72.6 ± 11	60	—	—
EB-welded	300	67.7 ± 41	90	1500	1200
TIG-welded	300	65.8 ± 40	180	1250	1350
EB-welded and heat treated *	480	94.7 ± 31	80	90	100
TIG-welded and heat treated *	480	112 ± 49	100	120	100

*2h,600°C

3.1.3 Results in NaCl-rich brine

Figure 3.3 shows the time-dependence of the general corrosion of the unwelded and only-welded steel specimens in the NaCl-rich brine at 150°C. As in the $MgCl_2$-rich "Q-brine", the thickness reduction of the specimens increases linearly with the exposure time in the brine. The linear corrosion rates of the unwelded and only-welded spacimens, calculated from the slope of the curves are compiled in Table 3.3. As in the $MgCl_2$-rich Q-brine, the corrosion rates of the welded specimens (18.6 µm/a – 19.1 µm/a) are very close to the value of the unwelded specimens (15.3 µm/a). The metallographic examinations of corroded specimens show that corrosion of the welded specimens is uniform, as in the case of the unwelded specimens. In general it can be stated that the corrosion behaviour of the EB- and TIG-welded steel specimens is very similar to that of the unwelded specimens.

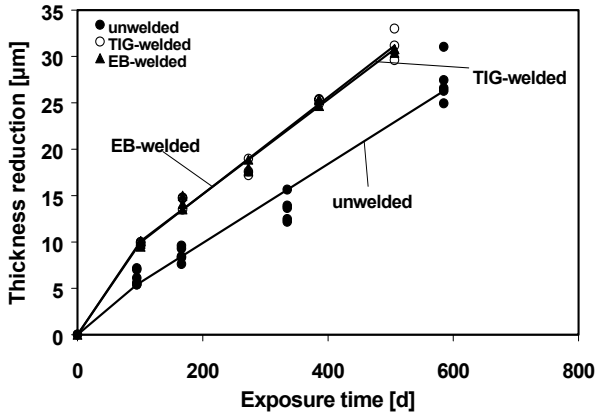

Figure 3.3: Time-dependence of the general corrosion of welded and unwelded TStE355 steel in NaCl-rich brine at 150°C

Table 3.3: Comparison of the corrosion rates of welded and unwelded TStE355 steel in NaCl-rich brine at 150°C

Material condition	Max. test duration (d)	Linear corrosion rate (µm/a)
unwelded	585	15.3 ± 1.0
EB-welded	506	18.6 ± 0.7
TIG-welded	506	19.1 ± 1.0

The corrosion results obtained for the thermal treated welded steel specimens in NaCl-rich brine at 150°C are given in Figure 3.4 and Table 3.4. For comparison, the results obtained on unwelded and only-welded specimens are also given. The general corrosion of all specimens increases linearly with the exposure time during the whole test duration (Figure 3.4). The linear corrosion rates of the heat treated welded steel specimens of 22.6 µm/a – 25.9 µm/a (Table 3.4) are somewhat higher than the values of the unwelded and only-welded specimens (15.1 µm/a – 19.1 µm/a) as in the Q-brine. However, this increase in the values is not significant. The surface profiles and the

metallographic examinations of the heat treated welded specimens do not show any signs of pitting corrosion. In general it can be stated that considering an NaCl-rich brine as corrosion medium in a rock salt-repository, a heat treatment of the welds of steel containers is not necessary because it does not improve its corrosion behaviour.

The comparison of the corrosion rates of the steel in Q-brine and NaCl-rich brine (Tables 3.2 and 3.4) shows that the values in the $MgCl_2$-rich "Q-brine" are significatly higher than in the NaCl-rich brine. The higher corrosivity of the $MgCl_2$-rich brine compared to the NaCl-rich brine is attributed to its higher Cl^- concentration and to the presence of Mg^{2+}. It appears that the Mg^{2+} intrude into the ferrous hydroxide layer for $Fe2^+$ interfere with the normally expected conversion of $Fe(OH)_2$ to Fe_3O_4. The (Fe, Mg) $(OH)_2$ appears to have little or no ability to protect the carbon steel from corrosion. The acceleration of the steel corrosion in brines containing high amounts of $MgCl_2$ is in line with the results reported by Westerman et al.[7].

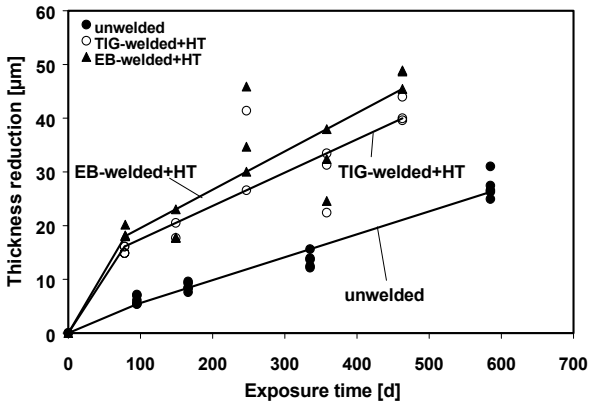

Figure 3.4: Time-dependence of the general corrosion of unwelded and thermal treated (HT) welded TStE355 steel in NaCl-rich brine at 150°C

Table 3.4: Comparison of the corrosion results obtained for unwelded, welded, and heat treated welded TStE355 steel in NaCl-rich brine at 150°C

Material condition	Max. test duration (d)	Linear corrosion rate (µm/a)
unwelded	585	15.3 ± 1.0
EB-welded	506	18.6 ± 0.7
TIG-welded	506	19.1 ± 1.1
EB-welded and heat treated *	463	25.9 ± 7.0
TIG-welded and heat treated *	463	22.6 ± 6.8

* 2h,600°C

3.2 Galvanic corrosion between Ti99.8-Pd and TStE355 carbon steel in brines (WP1.2) (FZK.INE)

On the base of our previous results [4,5,8,9], two container concepts based on carbon steel were developed in Germany for the direct disposal of spent fuel elements in a rock salt repository. These are: Self shielding casks for disposal in drifts (reference concept), and canisters for disposal in boreholes (backup concept). Both concepts are described in detail in [10,11]. Shortly, the cask consists of the disposal container made of carbon steel which is surrounded by a shielding container made of nodular cast iron. The thickness of the disposal container of 160 mm is designed according to the mechanical and shielding requirements. In the alternative concept (non-shielding concept), the canisters consist of carbon steel with a 50 mm wall thickness for mechanical support against the rock pressure. To this thickness a suitable corrosion allowance must be added.

In June 2001, the German government expressed “doubts” about the suitability of the Gorleben site as repository for high-level radioactive wastes [12]. These doubts covered different aspects. One of these is the formation of high gas pressures in the disposal area resulting from the hydrogen formation by the corrosion of the carbon steel containers by attack of brines. Therefore, in order to avoid the formation of large amounts of hydrogen in the disposal area, an improved container concept is discussed, in which the carbon steel containers will be corrosion protected by a thin-walled container made of the alloy Ti99.8-Pd of copper-base materials. Both materials were identified in our previous studies as promising for corrosion-resistant containers [4,13,14]. However, by use of material pairs a galvanic corrosion can occur. In this study has been examined if by pitting corrosion of the outer container material made of Ti99.8-Pd and resulting contact of salt brine with both container materials, a galvanic corrosion occurs between the steel and the Ti-Pd alloy that results in a strong change of the corrosion behaviour of the individual materials. For this, long-term corrosion experiments have been performed on galvanic coupled Ti99.8-Pd/TStE355 carbon steel specimens (contact specimens) in two disposal-relevant salt brines. Experimental results of corresponding galvanic corrosion studies on the material pairs Cu-Ni alloys//TStE355 carbon steel in salt brines are reported in session 3.4.

3.2.1 Experimental

The materials TStE355 carbon steel and Ti99.8-Pd were investigated in the hot-rolled and annealed condition and had the following composition in wt.%:

- TStE355 steel: 0.17 % C; 0.44 % Si; 1.49 % Mn; bal. Fe.
- Ti99.8: 0.18 % Pd; 0.05 % Fe; 0.01 % C; 0.04 % O_2; bal. Ti.

Galvanic coupled specimens were formed by bolting one flat coupon of Ti99.8-Pd (40 mm x 20 mm x 4 mm) with one flat coupon of carbon steel (40mm x 20mm x 4mm). The two coupons were provided with bores in both ends and were fastened with titanium screws. The bores were isolated by PTFE. With this specimens type, the metals were joined very tight. The long-term corrosion of the galvanic coupled materials was investigated in two disposal relevant brines. One of them is NaCl-rich, the other one $MgCl_2$-rich (Q-brine). The composition and the pH values of the brines are given in

session 3.1.1. The experiments lasted up to about 18 months and were performed at a temperature of 150°C. Experiments were performed both with and without gamma radiation of 10 Gy/h. Experiments under gamma radiation are important because the interaction of gamma radiation exerted by the waste with brines produces reducing/oxidizing reactive particles and stable products (e.g., H_2, O_2, ClO_3^-) which may change the rate and mechanism of corrosion. Furthermore, the absorption of gamma radiation in passive oxide layers of metals (e.g. Ti) will induce photoradiation effects, which may change the corrosion rate.

The experimental setups used for the experiments are described in previous work [5]. The experimental conditions are described in session 3.1.1. Shortly, for the experiments, autoclaves made of Ti99.8-Pd were used. Every autoclave contained 160 ml brine and two coupled specimens of 80 cm^2 total surface. This gave a brine volume-to-specimen surface ratio of 2 ml/cm^2. With these experimental equipments, the initial test conditions were oxidizing. The initial total amount of the oxygen available in the systems was about 15 mg, corresponding to 0.19 mg O_2/cm^2 specimen. This oxygen amount was consumed very fast by reactions with Fe so that after a few days reducing conditions were established.

Evaluation of the galvanic coupled specimens regarding general and local corrosion was carried out by gravimetry, measurements of pit depth, surface profilometry and metallography. Both the contact area and the free specimen area were investigated for local corrosion attacks. The integral corrosion rate of the specimens was calculated from the experimental determined weight losses and the material density.

3.2.2 Results in the $MgCl_2$-rich Q-brine

The time-dependence of the integral thickness reduction (general corrosion) of the coupled specimens of Ti99.8-Pd and TStE355 carbon steel at 150°C in Q-brine with and without a gamma radiation field is plotted in Figures 3.5 and 3.6. The data indicate that the thickness reduction of Ti99.8-Pd in the brine both with and without radiation (0.2 µm at the maximum) is only a little higher than the detection limit (0.01 µm). This is attributed to the formation of a very stable passive oxide surface film consisting of TiO_2.

The thickness reduction of the steel in the brine without irradiation (Figure 3.5) remains during the test time between 147 days and 340 days fairly constant, which means that the corrosion rate decreases with time. This is due to the formation of a protective corrosion layer on the specimens surface consisting of (Fe, Mg)$(OH)_2$. However, after longer test duration than 340 days, the corrosion layer was locally penetrated which resulted to an increase of the corrosion rate. In Q-brine and in the presence of gamma radiation (Figure 3.6), the thickness reduction of the specimens increases linearly over the whole test duration and is significantly higher (about 320 µm after 310 days) than the value without irradiation. In addition, very deep local corrosion was observed on the steel specimens exposed to irradiated brine.

The calculated integral corrosion rates of the coupled specimens of Ti99.8-Pd and carbon steel in Q-brine at 150°C with and without gamma radiation are compiled in Table 3.5. For comparison, the values of uncoupled (single) specimens of these materials determined in previous investigations [3,5] are also given in the Table. For

Ti99.8-Pd, the corrosion rates of the coupled specimens both with and without gamma radiation are negligible low (0.08 µm/a – 0.25 µm/a) and very close to the values of the uncoupled specimens (0.02 µm/a – 0.2 µm/a). Also for the carbon steel, the corrosion rate of the coupled specimens in the absence of radiation (36.6 µm/a ± 14.5 µm/a) corresponds well to the value of the unirradiated uncoupled specimens (47.1 µm/a ± 2.5 µm/a). This indicates that the solid corrosion product (Fe, Mg)$(OH)_2$ can sufficiently protect the actively corroded steel against galvanic corrosion, and that the galvanic corrosion potential lies apparently near to the rest corrosion potential of the steel. The small differences between the corrosion rates found for Ti99.8-Pd and carbon steel in the brine are in the range of the standard deviation of the values. In the Q-brine and in the presence of gamma radiation , however, the corrosion rate of the coupled steel specimens (369 µm/a) increases significantly, compared to that without radiation (36.6 µm/a ± 14.5 µm/a) and is by a factor of about 5 higher than the value of the irradiated uncoupled specimens (72.6 µm/a ± 11 µm/a). A possible explanation for the strong increase of the corrosion rate of the coupled steel specimens in irradiated Q-brine is that the oxidants, mainly O_2, formed by the radiolysis of water are reduced at the Ti99.8-Pd cathode, which results to an increase of the oxidation rate of Fe analog to a local element.

The metallographic examinations of coupled Ti99.8-Pd specimens exposed to irradiated and unirradiated Q-brine do not show any signs of localized corrosion neither in the contact area to the steel nor in the free specimen area. For all Ti99.8-Pd specimens a completely uniform corrosion was observed. The coupled steel specimens corroded in the Q-brine without irradiation non-uniformly, but the maximum depth of this uneven general corrosion was only about 70 µm after 538 days. In the presence of gamma radiation, however, the coupled steel specimens suffered from very strong localized corrosion in the brine. The maximum localized corrosion depth after 538 days exposure to the irradiated Q-brine was about 500 µm. This explains the high average general corrosion rate of the steel in the irradiated Q-brine environment.

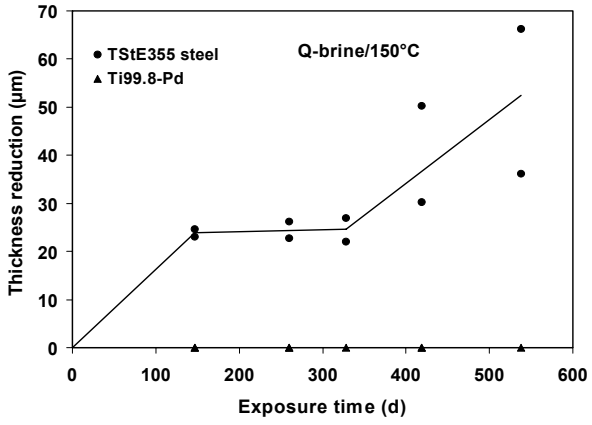

Figure 3.5:Time-dependence of the general corrosion of galvanic coupled Ti99.8-Pd and TStE355 stee in Q- brine at 150°C

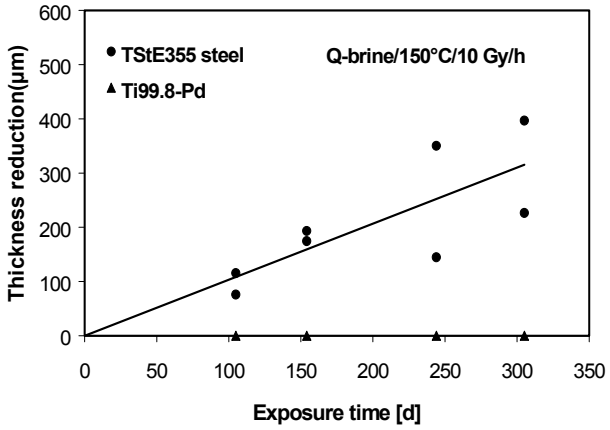

Figure 3.6: Time-dependence of the general corrosion of galvanic coupled Ti99.8-Pd and TStE355 steel in Q-brine at 150°C and 10 Gy/h

Table 3.5: Corrosion rates of coupled and uncoupled Ti99.8-Pd and TStE355 steel in $MgCl_2$-rich brine (Q-brine) at 150°C

Material	Corrosion conditions	Corrosion rate (µm/a)	
		coupled specimens	uncoupled specimens
Ti99.8-Pd	Q-brine	0.08 ± 0.02	0.02 ± 0.01
TStE355 steel		36.6 ± 14.5	47.1 ± 2.5
Ti99.8-Pd	Q-brine/10 Gy/h	0.25 ± 0.02	0.20 ± 0.02
TStE355 steel		369.5 ± 46.7	72.6 ± 11.0

3.2.3 Results in NaCl-rich brine

The thickness reduction (general corrosion) of the coupled specimens of Ti99.8-Pd and TStE355 carbon steel in irradiated and unirradiated NaCl-rich brine at 150°C is plotted in Figures 3.7 and 3.8. In both cases with and without gamma radiation the thickness reduction of the alloy Ti99.8-Pd (0.1 µm at the maximum) is only a little higher than the detection limit (0.01 µm), as is the case also in the $MgCl_2$-rich Q-brine. This is attributed, as already discussed, to the fact that this alloy corrodes in the brine by forming a very stable passive oxide surface film consisting of TiO_2. The thickness reduction of the carbon steel in the brine with and without gamma radiation increases linearly with the exposure time over the test duration of this study between 3 and 18 months, and is, as expected, significantly higher than that of Ti99.8-Pd. For the time less than 3 months (initial corrosion phase), the corrosion could be influenced by the oxygen available in the experimental equipment (15 mg O_2). After corrosion in the irradiated and unirradiated brine, the surface of the steel specimens was covered with a black corrosion film. The X-ray diffraction analysis has shown that this film consists of magnetite (Fe_3O_4).

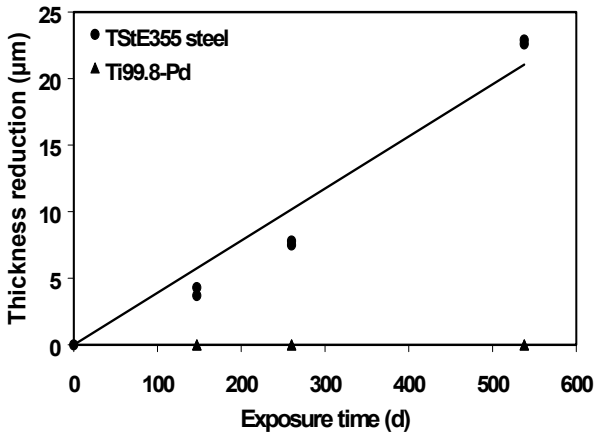

Figure 3.7: General corrosion of coupled specimens of Ti99.8-Pd and TStE355 carbon steel in NaCl-rich brine at 150°C

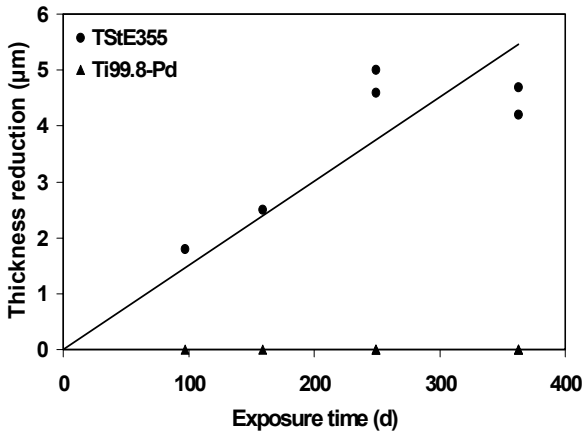

Figure 3.8: General corrosion of coupled specimens of Ti99.8-Pd and TStE355 carbon steel in NaCl-rich brine at 150°C and Gy/h

The calculated integral corrosion rates of the coupled specimens of Ti99.8-Pd and carbon steel in the irradiated and unirradiated NaCl-rich brine (T = 150°C) are given in Table 3.6. For comparison, the values of uncoupled (single) specimens of these materials determined in previous investigations [2,3] are also given. For Ti99.8-Pd, the corrosion rates of the coupled specimens both with and without radiation are negligible low (0.07 µm/a - 0.1 µm/a) and very close to the values of the uncoupled specimens (0.02 µm/a - 0.05 µm/a), as do also in the Q-brine. Also in the case of the carbon steel the corrosion rates of the coupled specimens in NaCl-rich brine of 14.2 without radiation and 10.8 µm/a with radiation, respectively, correspond very well to the values of the uncoupled specimens (13.5 -15.3 µm/a). This indicates that the galvanic corrosion potential is very near to the rest corrosion potential of the steel. The small differences between the corrosion rates found for Ti99.8-Pd and carbon steel in the irradiated and unirradiated brine are in the range of the standard deviation of the values. This means

that a gamma radiation field of 10 Gy/h does not increase noticeably the corrosion rate of both materials.

Table 3.6: Corrosion rates of coupled and uncoupled Ti99.8-Pd and TStE355 steel in NaCl-rich brine at 150°C

Material	Corrosion conditions	Corrosion rate (µm/a)	
		coupled specimens	uncoupled specimens
Ti99.8-Pd	NaCl-brine	0.07 ± 0.01	0.02 ± 0.01
TStE355 steel		14.2 ± 1.6	15.3 ± 1.0
Ti99.8-Pd	NaCl-brine/10 Gy/h	0.10 ± 0.05	0.05 ± 0.02
TStE355 steel		10.8 ± 3.5	13.5 ± 1.8

The metallographic examinations of coupled Ti99.8-Pd specimens exposed to irradiated and unirradiated brine do not show any signs of localized corrosion neither in the contact area to steel nor in the free specimen area. The corrosion of the Ti99.8-Pd specimens was completely uniform. For the steel specimens, a slight non-uniform corrosion (10 - 15 µm after one year immersion) was observed in the contact area to Ti99.8-Pd and in the free area of the specimens after exposure to irradiated and unirradiated brine. The non-uniform corrosion of the steel specimens is due to minor local defects of the Fe_3O_4 corrosion film. In the contact area to Ti99.8-Pd no preferencial corrosion attack was observed, compared to the free specimen area.

In general, it can be stated that by coupling of Ti99.8-Pd and TStE355 carbon steel no galvanic corrosion occurs in the NaCl-rich brine both with and without gamma radiation of 10 Gy/h. This is attributed to the fact that both materials form in this brine passive oxide surface layers such as TiO_2 and Fe_3O_4, respectively.

3.3 Corrosion behaviour of copper-base materials in salt brines (WP1.3) (FZK.INE)

In the present work, the suitability of three Cu-base materials (Cu, Cu-Ni 90-10 and Cu-Ni 70-30) as corrosion barrier materials was examined. For this, the long-term corrosion behaviour of the materials was investigated in two disposal relevant brines by using immersion tests.

3.3.1 Materials and experimental

The Cu-base materials were investigated in the brines in the hot-rolled and annealed condition and had the following composition in wt.%:

Cu: 99.9995 Cu; O: 0.0005
Cu-Ni 90-10: 88.5 Cu; 9.9 Ni; 1.3 Fe; Rest: C, Mn, P, S
Cu-Ni 70-30: 69.3 Cu; 29.3 Ni; 0.6 Fe; Rest: C, Mn, P, S

For the experiments plane specimens having the dimensions 40mmx20mmx4mm were used.

The corrosion media were two disposal relevant brines. One of them is NaCl-rich, the other one $MgCl_2$-rich (Q-brine). The composition and pH values of the brines are given in session 3.1.1.

The materials were investigated in the brines for up to 15 month at the temperature of 150°C. In order to get information on the influence of gamma radiation on the corrosion behaviour of the materials, additionally experiments were performed in the NaCl-rich brine in the presence of a gamma radiation field of 10 Gy/h. The experimental setups and the methods used for the corrosion evaluation of the materials are described in section 3.1.1.

3.3.2 Results

Figures 3.9-3.11 show the time-dependence of the general corrosion, expressed as the integral thickness reduction of the three Cu-base materials in the brines at 150°C. The data indicate that the general corrosion of the specimens both with and without gamma radiation increases linearly with the exposure time in the brines over the test duration of this study. The linear corrosion rates of the materials in the brines were calculated from the slope of the curves and are compiled in Tables 3.7 and 3.8.

In the NaCl-rich brine (Table 3.7) the corrosion rates of the materials are very low (3-12 µm/a), and the imposition of a 10 Gy/h gamma radiation field does not increase the corrosion rate of the materials in this brine. In fact, the corrosion rates under gamma radiation (0.4-1.3 µm/a) are lower than those without irradiation. This is attributed to the formation of more dense Fe_3O_4-corrosion protective surface layers than in the unirradiated brine, as was observed in the metallographic examinations. In the $MgCl_2$-rich Q-brine (Table 3.8) the corrosion rates of the Cu-base materials amount 24-46 µm/a and are clearly higher than in the NaCl-rich brine. The higher corrosivity of the $MgCl_2$-rich brine compared to the NaCl-rich brine is attributed to its higher Cl^- concentration and to the presence of Mg^{2+}, as discussed in session 3.1.3.

It is evident from the surface profiles and the metallographic examinations of corroded specimens that all three Cu-base materials investigated are resistant to pitting corrosion in the brines in the sense of an active-passive corrosion element. In NaCl-rich brine, the materials corrode uniformly. In the $MgCl_2$-rich Q-brine, the materials were subject to non-uniform general corrosion. In addition, in this brine intergranular corrosion was observed on Cu and the alloy Cu-Ni 90-10. However, the maximum penetration depth of the non-uniform corrosion corresponds to the values of the average thickness reduction of the specimens, and the intergranular corrosion after 15 months is only about 100 µm at the maximum.

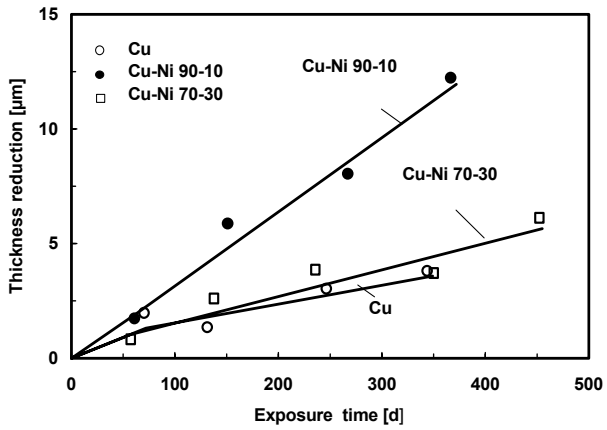

Figure 3.9: Time-dependence of the thickness reduction of the Cu- base materials in NaCl-rich brine at 150°C

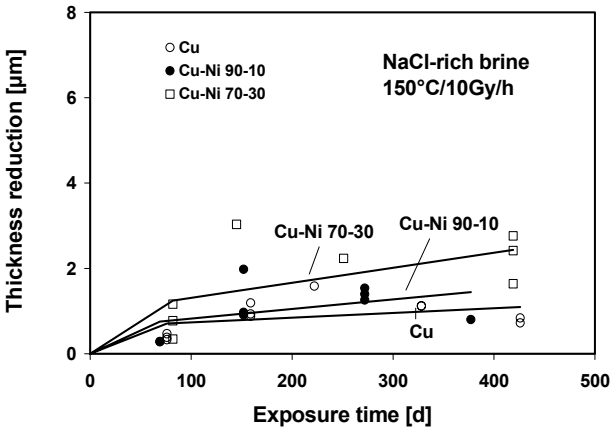

Figure 3.10: Time-dependence of the thickness reduction of the Cu-base materials in NaCl-rich brine at150°C and 10 Gy/h

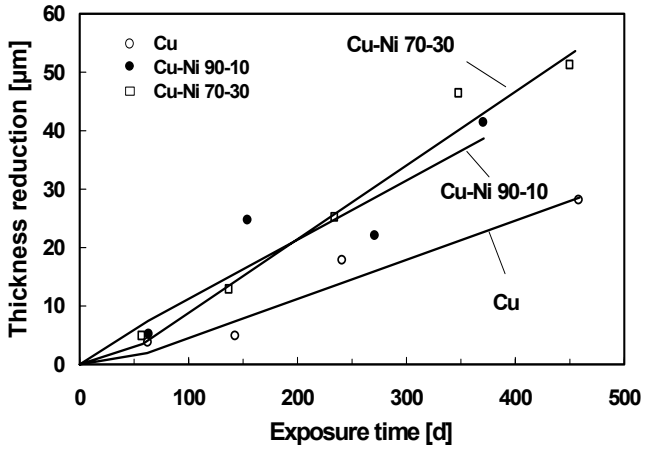

Figure 3.11: Time-dependence of the thickness reduction of the Cu-base materials at 150°C in the $MgCl_2$-rich Q-brine

Table 3.7: Linear corrosion rates of Cu-base materials in NaCl-rich brine at 150°C

Material	Linear corrosion rate (µm/a)	
	without γ-radiation	with γ (10 Gy/h)
Cu	3.0 ± 0.5	0.4 ± 0.3
Cu-Ni 90-10	11.8 ± 0.6	0.8 ± 0.6
Cu-Ni 70-30	4.2 ± 0.4	1.3 ± 0.7

Table 3.8: Linear corrosion rates of Cu-base materials in the $MgCl_2$-rich Q-brine at 150°C

Material	Corrosion rate (µm/a)
Cu	24.4 ± 2.6
Cu-Ni 90-10	37.0 ± 4.7
Cu-Ni 70-30	46.0 ± 2.0

3.4 Galvanic corrosion between Cu-Ni alloys and TStE355 steel in salt brines

Analog to the galvanic corrosion experiments on the material pair Ti99.8-Pd/ TStE355 carbon steel (session 3.2), the galvanic corrosion between Cu-Ni alloys and TStE355 carbon steel was investigated by long-term corrosion experiments on galvanic coupled specimens (contact specimens) of the material pairs Cu-Ni 90-10/carbon steel and Cu-Ni 70-30/carbon steel, respectively, in two disposal-relevant salt brines. In addition, the influence of gamma radiation (10 Gy/h) on the corrosion behaviour of galvanic coupled specimens of Cu-Ni 70-30 and carbon steel in the brines was examined.

3.4.1 Materials investigated and experimental

The galvanic corrosion of the material pairs Cu-Ni 90-10/TStE355 and Cu-Ni 70-30/TStE355, respectively, was investigated in two salt brines. One of them is rich in NaCl, the other one is rich in $MgCl_2$. The composition of the brines are given in session 3.1.1. All materials were investigated in the hot-rolled and annealed condition and had the following composition in wt.%:

Cu-Ni 90-10: 88.5 Cu; 9.9 Ni; 1.3 Fe; Rest: C, Mn, P, S
Cu-Ni 70-30: 69.3 Cu; 29.3 Ni; 0.6 Fe; Rest: C, Mn, P, S
TStE355 steel: 0.17 % C; 0.44 % Si; 1.49 % Mn; bal. Fe.

The pH values of the brines at 25°C measured with a glass electrode are for the NaCl-rich brine 5.7 and for the $MgCl_2$-rich brine 4.0. In order to compare the influence of the pH on the corrosion processes in the two different brines, one has to care about the liquid junction potentials (diffusion potentials) and the pH splitting convention which differ in the brines of different ionic strength. By calibrating the pH electrode with a Cl^- sensitive electrode in more or less concentrated NaCl and $MgCl_2$ solutions, correction terms could be obtained [15,16]. In the Pitzer convention, the corrected pH is obtained by $pH_{corr} = pH_{meas} + \Delta pH$. The correction term ΔpH is 0.41 for saturated NaCl brine and 1.53 for the $MgCl_2$-rich Q-brine. These pH values do not represent H^+ activity at the experimental temperature conditions. The pH effect of quenching (cooling) solutions from higher temperatures is discussed in reference [17].

For the galvanic corrosion tests, specimens were prepared by bolting one flat coupon of Cu-Ni alloy with one flat coupon of carbon steel. The specimens were polished with 1200-grit SiC paper up to a final surface roughness of 4 µm and ultrasonically cleaned in alcohol. The specimens of all materials had the dimensions 40 mm x 20 mm x 4 mm. This gave a surface area ratio of the two coupled specimens of 1:1. The two coupons were provided with bores in both ends and were fastened with titanium screws.

The experiments lasted up to about 18 months and were performed at a temperature of 150°C, which roughly corresponds to the maximum surface temperature of the disposal containers for spent fuel elements (≤200°C) according to the disposal concept in Germany [11]. In addition, in order to examine the influence of gamma radiation on the galvanic corrosion, experiments were performed on the material pair Cu-Ni 70-30/TStE355 steel in the two brines at a gamma dose rate of 10 Gy/h. This dose rate corresponds to the value on the surface of the canisters for the disposal of spent fuel

elements in boreholes having mechanical and corrosion allowances of about 90 mm for a lifetime of 500 years. Experiments under gamma radiation are important because the interaction of gamma radiation exerted by the waste with brines produces reducing/oxidizing reactive particles and stable products such as H_2, O_2 and ClO_3^- [18] which may change the rate and mechanism of corrosion.

The experimental setups used are described in previous work [5]. With the experimental equipments used, the initial test conditions were oxidizing. The initial total amount of the oxygen available in the systems was about 15 mg (0.19 mg O_2/cm² specimen). It consisted of the oxygen content in the 50 ml of air space (15 mgO_2) above the brine and the dissolved oxygen (0.2 mg) in the 160 ml of brine. This oxygen amount was consumed very fast for reactions with Fe, so that after a few days reducing conditions were established. After 20 days corrosion of the Cu-Ni/steel coupled specimens, the redox potential (Eh) of the NaCl-rich brine measured with a platin electrode at 25°C was -180 to -190 mV vs. SHE. The corresponding Eh-values in the $MgCl_2$-rich Q-brine were -170 to -180 mV vs. SHE, and, therefore, very closed to the values in the NaCl-rich brine.

When the specified test duration has been achieved, the specimens were removed from the brines and cleaned. The specimens were freed from the adhering salts and corrosion products by cleaning in distilled H_2O and pickling in diluted HCl (Cu-materials) or in the Clark solution (carbon steel) (37% HCl+Sb_2O_3+$SnCl_2$). Subsequently, the specimens were cleaned in distilled H_2O and alcohol. After drying in hot air, the specimens were weighed and the weight losses determined were used to calculate the integral corrosion rate. The examination to localized corrosion was made by measurements of pit depth, surface profilometry and metallography. Both the contact area and the free specimen area were investigated for localized corrosion attacks.

3.4.2 Results

3.4.2.1 Galvanic corrosion of the material pairs Cu-Ni 90-10/TStE355 Steel and Cu-Ni 70-30/TStE355 steel in NaCl-rich brine

After completion of the experiments, the Eh value (T=25°C) was measured to be -240 to -270 mV vs. SHE. This value as well as the value measured after 20 days corrosion time(-180 to -190 mV vs. SHE) indicate that, except few days, during the whole long test duration reducing conditions were available in the experimental system. After the end of the corrosion experiments, the pH values of the brine measured at 25°C were 5.8-6.3 (pH_{corr}=6.2-6.7) and, therefore, they correspond very well to the initial pH value of 5.7 (pH_{corr}=6.1).

The thickness reduction (general corrosion) of the galvanically coupled material pairs Cu-Ni 90-10/TStE355 steel and Cu-Ni 70-30/TStE355 steel in irradiated and unirradiated NaCl-rich brine at 150°C is plotted in Figures 3.12-3.14. In both cases with and without gamma radiation the thickness reduction of the coupled Cu-Ni alloys is very small (1.7-2.3 µm after 520 days test duration). This is attributed to the fact that the Cu-Ni alloys corrode in the NaCl-rich brine by forming a stable corrosion protective surface layer. This layer was identified by X-rays diffraction as $Cu_2(OH)_3Cl$ which is a good agreement with literature [19]. The thickness reduction of carbon steel in the brine with

and without gamma radiation increases linearly with the exposure time over the whole test duration of this study and is clearly higher than that of the Cu-Ni alloys. After corrosion in the irradiated and unirradiated NaCl-rich brine, the surface of the steel specimens was covered with a black corrosion film. The X-ray diffraction analysis has shown that this film consists of magnetite (Fe_3O_4).

The calculated integral corrosion rates of the galvanically coupled material pairs Cu-Ni 90-10/TStE355 steel and Cu-Ni 70-30/TStE355 steel in the irradiated and unirradiated NaCl-rich brine (T=150°C) are given in Table 3.9. For comparison, the values of uncoupled (single) specimens of these materials determined in this study and in our previous investigations [6] are also given. For the Cu-Ni alloys, the corrosion rates of the coupled specimens both with and without radiation are very small (1.2 µm/y - 1.6 µm/y) and very close to the values of the uncoupled specimens (1.3 µm/y – 1.6 µm/y). Also in the case of carbon steel the corrosion rates of the coupled specimens in NaCl-rich brine of 15 µm/y - 16.4 µm/y without radiation and 16.2 µm/y with radiation, respectively, correspond very well to the values of the uncoupled specimens (13.5 -15.3 µm/y). This indicates that the solid corrosion product Fe_3O_4 can sufficiently protect the less noble carbon steel against galvanic corrosion, and that the galvanic corrosion potential lies apparently near to the rest corrosion potential of the steel. The small differences in corrosion rates of the Cu-Ni alloys and carbon steel in the irradiated and unirradiated NaCl-rich brine are in the range of the standard deviation of the values. A gamma radiation field of 10 Gy/h does not increase noticeably the corrosion rate neither of the Cu-Ni alloys nor of the TStE355 carbon steel.

The metallographic examination of the galvanically coupled Cu-Ni and carbon steel specimens after exposure to irradiated or unirradiated NaCl-rich brine shows a slight non-uniform corrosion both in the contact specimen area and in the free specimen area. The maximum depth of this uneven corrosion was about 20-30 µm after one year immersion into the brine. In the contact specimen area no preferencial corrosion attack was observed, compared to the free specimen area. Furthermore, the titanium screws (specimen fastener) do not show any signs of pitting or crevice corrosion.

In general, it can be stated that by coupling of Cu-Ni alloys (90-10 and 70-30) with TStE355 carbon steel no galvanic corrosion occurs in the NaCl-rich brine both with and without gamma radiation of 10 Gy/h. This is attributed to the fact that in this brine both materials form stable corrosion protective surface layers of $Cu_2(OH)_3Cl$ and Fe_3O_4, respectively.

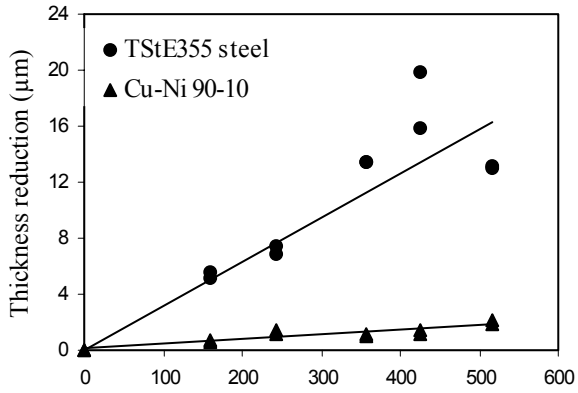

Figure 3.12: General corrosion of coupled Cu-Ni 90-10 and TStE355 steel in NaCl-rich brine at 150°C

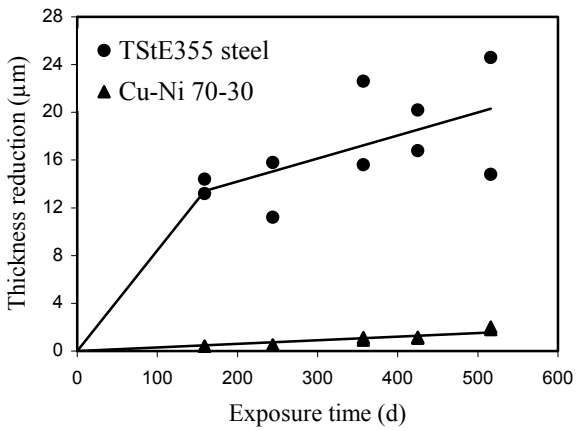

Figure 3.13: General corrosion of coupled Cu-Ni 70-30 and TStE35 steel in NaCl-rich brine at 150°C

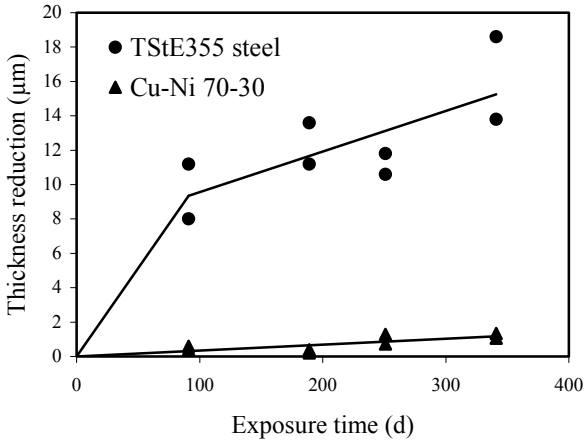

Figure 3.14: General corrosion of Cu-Ni 70-30 and TStE355 steel in NaCl-rich brine at 150°C and 10 Gy/h

Table 3.9: Integral corrosion rates of galvanic coupled and uncoupled Cu-Ni alloys and TStE355 steel in NaCl-rich brine at 150°C

Material	Corrosion conditions	Integral corrosion rate (µm/a)	
		Coupled specimens	Uncoupled specimens
Cu-Ni 90-10 Stahl	NaCl-brine	1.6 ± 0.2 15.0 ± 3.6	1.5 ± 0.3 15.3 ± 1.0
Cu-Ni 70-30 Stahl	NaCl-brine	1.2 ± 0.1 16.4 ± 1.4	1.6 ± 0.3 15.3 ± 1.0
Cu-Ni 70-30 Stahl	NaCl-brine and 10 Gy/h	1.4 ± 0.1 16.2 ± 1.8	1.3 ± 0.7 13.5 ± 1.8

3.4.2.2 Galvanic corrosion of the material pairs Cu-Ni 90-10/TStE355 steel and Cu-Ni 70-30/TStE355 steel in the $MgCl_2$-rich Q-brine

After completion of the experiments, the Eh value (T=25°C) was measured to be -270 to -280 mV vs. SHE. This value as well as the value measured after 20 days (-170 to -180 mV vs. SHE) indicate , as in the case of the NaCl-rich brine, that, except few days, during the whole long test duration reducing conditions were available in the experimental system. After the finish of the corrosion experiments, the measured pH values of the brine at 25°C were 4.2-4.4 (pH_{corr}=5.7-5.9), and, therefore, a little higher than the initial pH value of 4.0 (pH_{corr}=5.5).

The time-dependence of the integral thickness reduction (general corrosion) of the galvaninically coupled material pairs Cu-Ni 90-10/TStE355 steel and Cu-Ni 70-30/TStE355 steel at 150°C in the $MgCl_2$-rich Q-brine with and without a gamma radiation field is plotted in Figures 3.15-3.17. The data indicate that the thickness reduction of the coupled Cu-Ni alloys both in the irradiated and in the unirradiated $MgCl_2$-rich brine are small (0.4 µm - 8 µm after 480 days immersion into the brine), as in the NaCl-rich brine. This is attributed to the formation of a stable corrosion protection layer on the specimen surface ($Cu_2(OH)_3Cl$), as already discussed above. The slope of the curves (Figures 3.15 and 3.16) indicates that up to 210 days exposure to the unirradiated Q-brine, the corrosion rate of the coupled steel is relatively low. This is due to the formation of a protective corrosion layer consisting of $(Fe, Mg)(OH)_2$. However, after longer test duration than 210 days, the corrosion layer is locally degradated which results in an increase in the corrosion rate of the steel. In addition, severe localized corrosion was observed on the steel specimens. In Q-brine under gamma radiation (Figure 3.17), the thickness reduction of the steel coupled to Cu-Ni 70-30 increases linearly over the whole test duration and is clearly higher (about 440 µm after 238 days) than the value without irradiation. This is attributed to the fact that the radiolytic oxidants formed, mainly O_2 [18], are reduced at the cathode Cu-Ni alloy which results in an increase of the Fe oxidation rate of the anode carbon steel.

The integral corrosion rates of the galvanically coupled material pairs Cu-Ni 90-10/TStE355 steel and Cu-Ni 70-30/TStE355 steel in irradiated and unirradiated Q-brine at 150°C are compiled in Table 3.10. For comparison, the values of uncoupled specimens of these materials determined in this study and in our previous investigations [20] are also given. In the unirradiated Q-brine the corrosion rates of the galvanically coupled Cu-Ni alloys are small (6 µm/y - 6.2 µm/y) and clearly lower than the values of the corresponding uncoupled materials (37 µm/y - 46 µm/y). On the other hand, the corrosion rates of the coupled steel increase significantly (123.2 µm/y - 157.4 µm/y) compared to the values of the uncoupled steel specimens. This means that the Cu-Ni alloys are cathodically protected by the carbon steel. In the irradiated Q-brine the corrosion rate of the coupled Cu-Ni 70-30 is extremely low (0.6 µm/y) which is similar to the value of the uncoupled Cu-Ni material (0.9 µm/y). In this irradiated Q-brine environment the corrosion rate of the coupled steel (563.9 µm/y) is significantly higher than the value of the uncoupled steel specimens (72.6 µm/y) and the values in the unirradiated brine environment (157.4 µm/y). The increase in the corrosion rate of the coupled steel in the irradiated Q-brine by a factor of about 4 compared to the value in the unirradiated brine environment is attributed, as already

discussed, to the reduction of the radiolytic formed oxidants at the cathode Cu-Ni 70-30.

The metallographic examination of galvanically coupled Cu-Ni specimens exposed to unirradiated Q-brine shows a non-uniform corrosion with a maximum depth of about 50 µm after exposure for 480 days to the brine. In the presence of gamma radiation the Cu-Ni specimens show in this brine a nearly uniform corrosion. In the case of the coupled TStE355 carbon steel severe localized corrosion (wide pits) was observed in the Q-brine both with and without gamma radiation. After exposure for 480 days to the brine maximum depths of about 100 µm in the unirradiated brine and 250 µm in the irradiated brine were measured. This explains the calculated high average general corrosion rate of the galvanically coupled steel in this $MgCl_2$-rich brine environment. As in the NaCl-rich brine, no localized corrosion was observed on the titanium screws in the Q-brine.

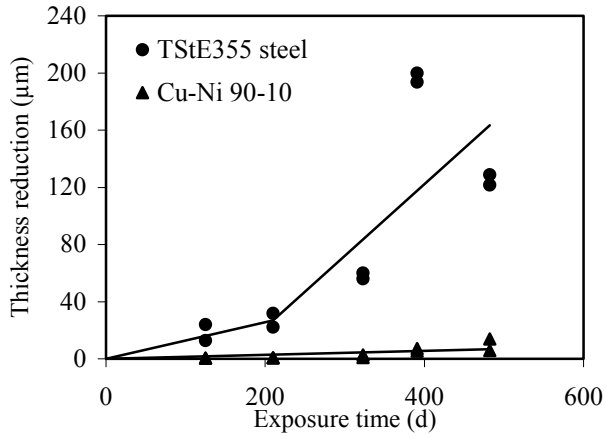

Figure 3.15: General corrosion of coupled Cu-Ni 90-10 and TStE355 steel in $MgCl_2$-rich brine at 150°C

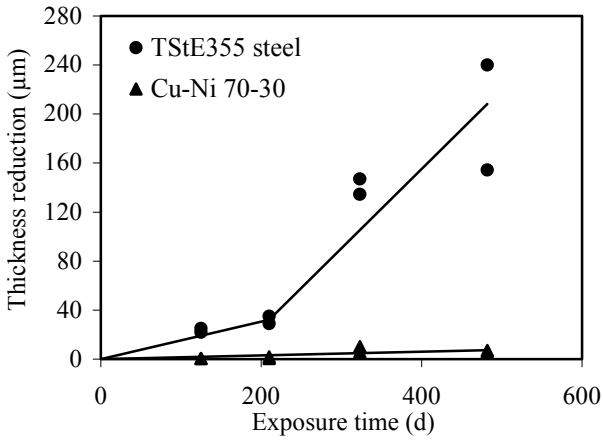

Figure 3.16: General corrosion of coupled Cu-Ni 70-30 and TStE355 steel in $MgCl_2$-rich brine at 150°C

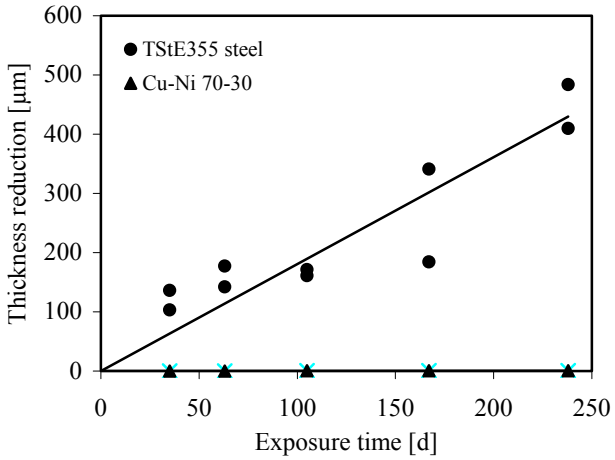

Figure 3.17: General corrosion of coupled Cu-Ni 70-30 and TStE355 steel in $MgCl_2$-rich brine at 150°C and 10 Gy/h

Table 3.10: Integral corrosion rates of galvanic coupled and uncoupled Cu-Ni alloys and TStE355 steel in $MgCl_2$-rich brine (Q-brine) at 150°C

Material	Corrosion conditions	Integral corrosion rate (µm/a)	
		Coupled specimens	Uncoupled specimens
Cu-Ni 90-10 Stahl	Q-brine	6.2 ± 0.6 123.2 ± 12.4	37.0 ± 4.7 47.1 ± 2.5
Cu-Ni 70-30 Stahl	Q-brine	6.0 ± 0.6 157.4 ± 15.8	46.0 ± 2.0 47.1 ± 2.5
Cu-Ni 70-30 Stahl	Q-brine and 10 Gy/h	0.6 ± 0.4 563.9. ± 90	0.9 ± 0.5 72.6 ± 11.0

3.5 Conclusions

The corrosion results obtained from the long-term immersion experiments in salt brines at 150°C allow the following conclusions:

- Under the test conditions applied, the TStE355 carbon steel is resistant to pitting corrosion both in NaCl-rich and in $MgCl_2$-rich brines, and the corrosion rates determined imply corrosion allowances acceptable for thick- walled containers. Electron Beam (EB) and Tungsten-Inert-Gas (TIG) welding decrease significantly the corrosion resistance of the steel to localized corrosion, but only in the $MgCl_2$-rich brine. The stress relief thermal treatment of the welds improves the corrosion resistance of the welded material in the $MgCl_2$-rich brine, so that the thermal treated welded steel is resistant to pitting corrosion, as does also the unwelded material.

- In NaCl-rich-brine both with and without gamma radiation and in $MgCl_2$-rich brine in the absence of gamma radiation no galvanic corrosion occurs on the coupled material pair Ti99.8-Pd/TStE355 carbon steel because both materials form protecting corrosion layers. However, in $MgCl_2$-rich brine and in the presence of a gamma radiation field of 10 Gy/h a significant galvanic corrosion occurs which leads in the case of the less noble coupled steel in strong localized corrosion and in a high increase in the corrosion rate compared to the value of the uncoupled steel specimens. This is attributed to the fact that the oxidants (mainly O_2) formed by the radiolysis of water are reduced at the Ti99.8-Pd alloy which results in an increase of the oxidation rate of Fe analog to a local element.

- Cu and the alloys Cu-Ni 90-10 and Cu-Ni 70-30 are potential materials for long-lived HLW/Spent Fuel disposal containers. They are resistant to pitting corrosion in salt brines and their corrosion rates determined imply corrosion allowances reasonable for long-lived containers.

- In the NaCl-rich brine with and without gamma radiation (10 Gy/h) the coupled material pairs Cu-Ni 90-10/TStE355 carbon steel and Cu-Ni 70-30/TStE355

carbon steel form stable corrosion protective surface layers, and, therefore, no galvanic corrosion occurs. In $MgCl_2$-rich brine, however, both in irradiated and unirradiated brine environment, galvanic corrosion occurs due to local break down of the corrosion surface layer of the steel. This results in localized corrosion on the less noble coupled carbon steel and significant increase its general corrosion rate compared to the value of the uncoupled steel specimens. For the more noble coupled Cu-Ni alloys a clear decrease in the corrosion rate is observed in the unirradiated $MgCl_2$-rich brine compared to the values of the uncoupled specimens. This means that in this brine the Cu-Ni alloys are cathodically protected by the carbon steel.

4. ELECTROCHEMICAL CORROSION STUDIES AND SURFACE ANALYTICAL INVESTIGATIONS ON CU, NI, CU–NI ALLOYS AND TSTE355 CARBON STEEL IN SALT BRINES (WP 1.5) (GNF/IUT)

In order to get more information on the corrosion mechanisms, besides the long-term immersion experiments (session 3.4), the corrosion behaviour of Cu, Ni, Cu-Ni alloys (Cu-Ni 90-10, Cu-Ni 70-30) and TStE355 carbon steel as well as the galvanic corrosion of the material pairs Cu/carbon steel, Ni/carbon steel and Cu-Ni/carbon steel was studied by using electrochemical and surface analytical methods. The corrosion media used were, as in the long-term immersion experiments, the $MgCl_2$-rich brine (Q-brine) and an NaCl-rich brine. The composition and the pH values of the brines are given in session 3.1.1. The test temperatures were 25°C and 80°C.

The methods applied were electrochemical procedures (potentiodynamic and potentiostatic measurements) and the surface analysis methods EPMA/EDX (electron probe microanalysis in the energy dispersive mode) and SEM (scanning electron microscopy). Applying the two different methods, being independent from each other, it was able to cope with the problems they were confronted with. Correspondent results received by using the two methods, demonstrate the accuracy of the experiments performed.

The corrosion rates were mostly obtained from the determination of the mass loss of the materials. In some cases, ICP-MS and TXRF (total X-ray reflection fluorescence analysis) were applied. The radioisotope method (RIM) which was used in previous investigations [20-24] was not used in these studies due to the lack of adequate facilities. It is important to mention that the electrochemical measurements deliver only information on the starting time period of the corrosion process, and they determine the initial corrosion rate. The final corrosion rate and the long-term corrosion behaviour of the container materials was determined by the long-term immersion experiments (see sessions 3.3 and 3.4). The longest time interval spent for the electrochemical investigations was approximately 100 hours. An extrapolation of the relevant results to a time period of one year was only made in order to be able to compare the electrochemical results obtained under different conditions, and, therefore, to determine the influence of various parameters on the corrosion behaviour of the investigated materials.

4.1 Experimental details of electrochemical measurements

Potentiodynamic and potentiostatic measurements were carried out on Ni, Cu, Ni-Cu alloys and TStE355 carbon steel in Q-brine and NaCl-rich brine at 25°C and 80°C by use of double walled electrolytic cells made of glass in order to be able to perform the

experiments at different temperatures. The cells were equipped with holders made of Teflon to locate the electrodes made of the relevant materials under investigation in definite positions. Besides the working electrode, each cell contained an Ag/AgCl reference electrode filled with 3M KCl solution to reduce the diffusion potential due to the equal ionic mobilities of K^+ and Cl^- (Figure 4.1). In some cases the reference electrode was filled with the same electrolyte solution (Q-brine or NaCl-rich brine), which the electrochemical experiments were performed in. The potentials between the working electrode and the reference electrode were either measured by use of a digital voltmeter or a computer connected with the software Winlab.

In addition the potentiodynamic and the potential vs time measurements were carried out by applying the potentiostats constructed by the Free University of Berlin (FUB) and by the Humboldt University of Berlin (HUB), respectively.

The surface of the electrodes used are 0,5 cm². The relevant densities of the materials which must be known for calculating the corrosion rates are:
σ (carbon steel) = 7.59 g/cm^3 , σ (Ni) = 8.91 g/cm^3 and σ (Cu) 8.92 g/cm^3.

For investigating the Cu-Ni galvanic corrosion the usual set-up was changed by locating the two different metals in separate half cells connected with a salt bridge.

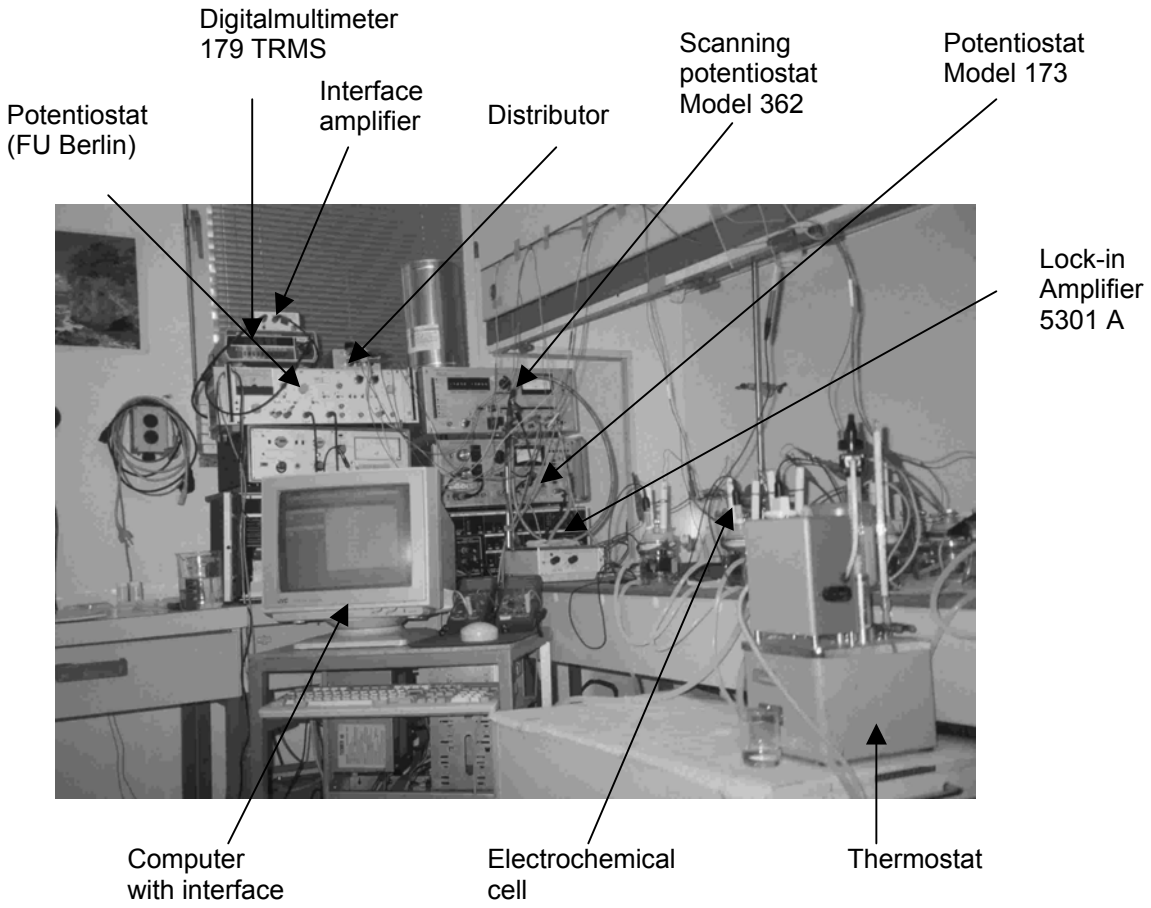

Figure 4.1: General experimental setup

The relevant potentials were measured with individual reference electrodes, equipped with a Luggin capillary each (Figure 4.2). This setup represents a cell with transference [25, 26]. A variety of different measurements can be performed with this experimental set-up. Filling, i.e., the salt bridge with Q-brine or NaCl-rich brine respectively, and closing the short-cut, this new set-up equals the old one but with two reference electrodes instead of one. Removing the salt bridge or opening the short-cut, the rest potentials of the relevant materials can be determined.

If one fills the salt bridge with highly diluted brine, the inner resistance R_i will be increased, which influences the character of contact potentials as will be outlined in the theoretical part of this report (session 4.9).

It has to be mentioned that all the experiments, carried out within the frame of this work were mostly performed under aerobic conditions. Only a few one were carried out in argon atmosphere.

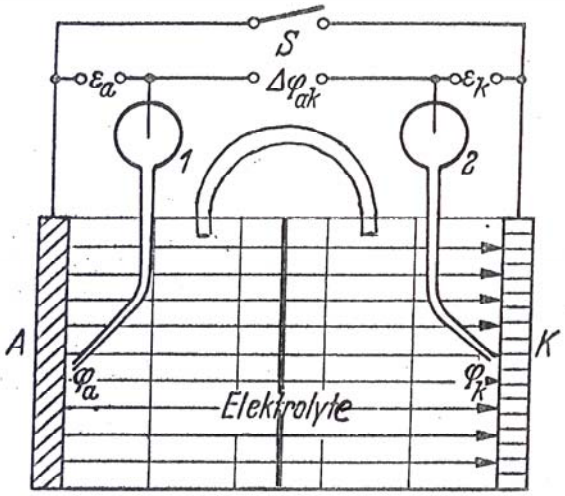

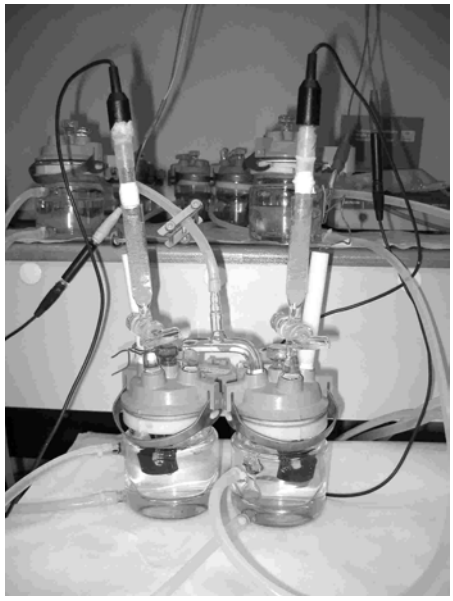

Figure 4.2: Two half cells with a salt bridge
a) Scheme [6] b) View

4.2 Experimental details of surface analysis

The investigation of the element composition of the surfaces of the relevant materials and the morphology of the electrodes applied at the electrochemical experiments were carried out by means of two combined devices, namely scanning electron microscope/electron probe microanalyser of the types Philips XL 30 ESEM as well as TESLA BS 343, both equipped with an energydispersive X-ray analyser RÖNTEC EDR 288 (voltage U=15-20 kV, magnification up to 7500). The electrodes used for the electrochemical measurements were cleaned afterwards with distilled water, dried and stored in a desiccator. The corrosion was investigated vs the material of the electrode or the electrode couples, the electrolyte, the temperature and the time.

4.3 Corrosion results of potentiodynamic measurements

4.3.1 Corrosion of Ni in brines (passive range)

From the cyclovoltammograms can be seen that for Ni both in Q-brine and in NaCl-rich brine, a passive range exists from -700 mV up to + 100 mV (SHE), the potentials being referred to SHE (Figure 4.3). These results are in accordance with the assumption that an amorphous NiO layer is formed [25].

The relevant current densities are a little bit higher for the systems under argon influence than for those in presence of oxygen or air (Figure 4.4), which results from the fact, that the current density i represents the sum of the positive and negative partial current densities, the latter being higher in presence of oxygen due to its being reduced to OH^- or H_2O on a larger scale.

Stirring increases the current density due to prohibiting areas of depletion near to the electrode. In the transpassive range the corrosion rate is doubled by 300 rpmin and it is sixfold by 600 rpmin (Figure 4.5).

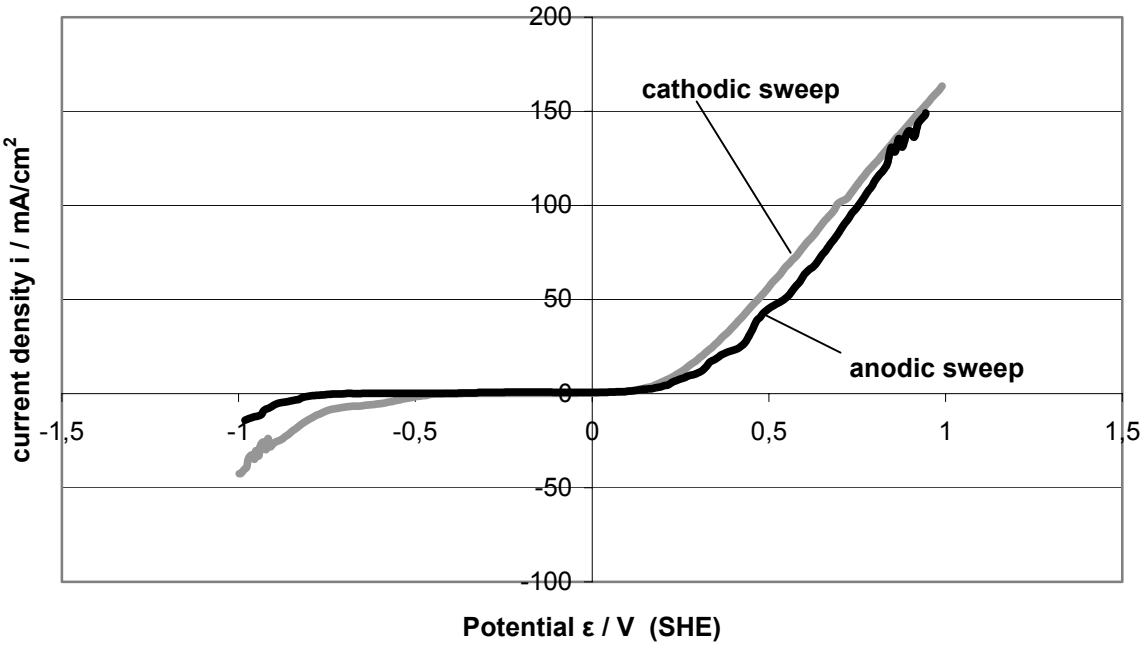

Figure 4.3: Cyclovoltammogram of Ni in Q-brine at 10 mV/s and 25°C, aerobic conditions

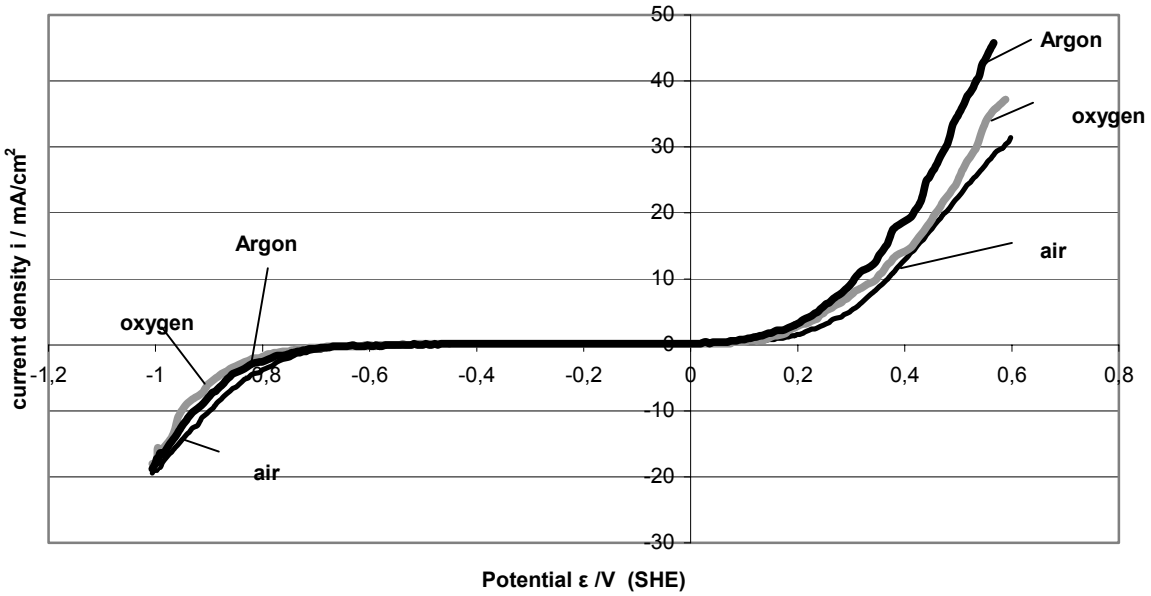

Figure 4.4: Influence of gas atmosphere on cathodic sweeps of Ni in Q-brineat 25°C, 10 mV/s and a stirring rate of 300 rpm

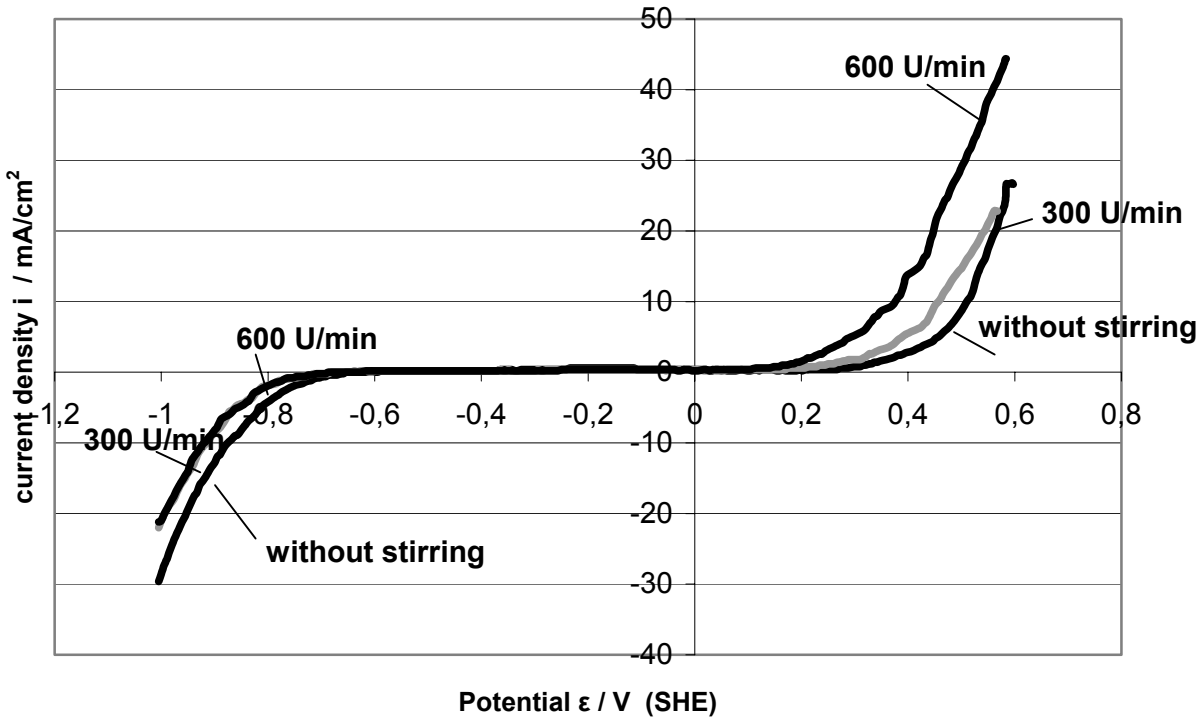

Figure 4.5: Influence of stirring on the anodic sweeps of Ni in Q-brine at 10 mV/s and 25°C, aerobic conditions

4.3.2 Influence of temperature on the current density

The influence of temperature on the relevant current densities (Figure 4.6) is demonstrated by the fact, that the current densities increased at higher temperature. Moreover, it can be seen, that a passive range of Ni even exists at 80°C, although it is shortened at this comparatively high temperature. At higher temperatures the current densities are higher in aerobic atmosphere than under Ar, which proves the partial anodic current density to become dominant. Although the influence of temperature on the passive range cannot be denied it must be emphasized that the passive range was not significant changed under aerobic or anaerobic conditions, neither it could be effected by stirring. But a partial break down of the passivating NiO layer must occur at higher temperature.

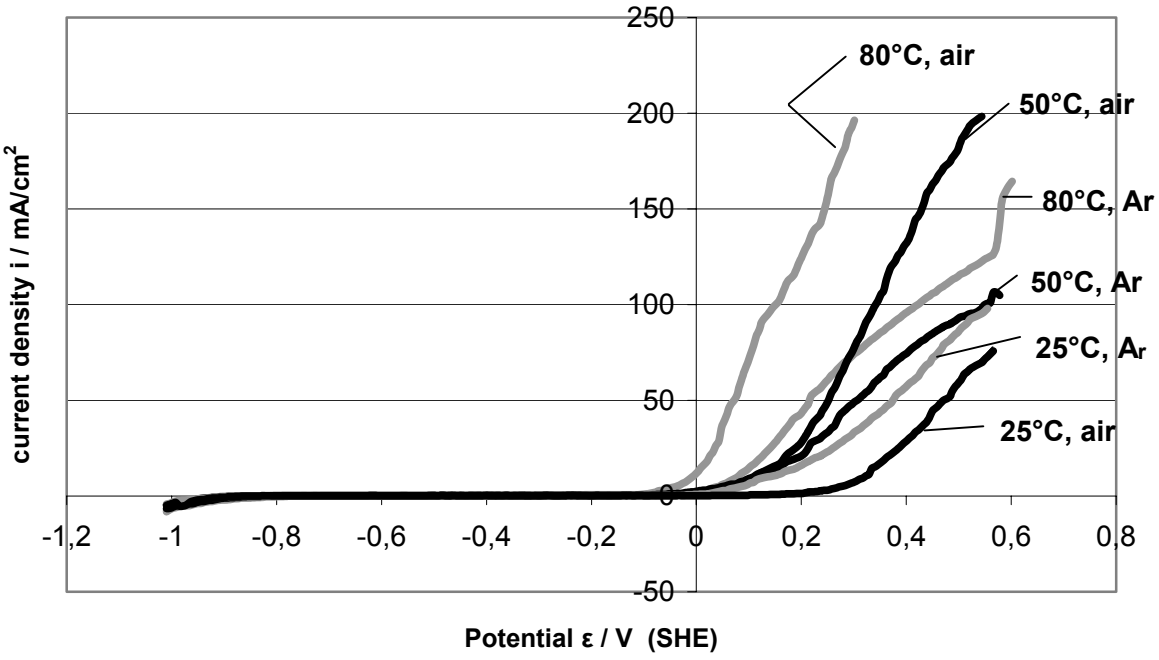

Figure 4.6: Influence of temperature on the anodic sweeps of Ni in NaCl-rich brine at 10 mV/s

4.3.3 Corrosion of Cu in brines

The results obtained from the potentiodynamic measurements on 99.9 Cu in brines demonstrate that at 25°C there is a passive range from -1100 mV up to -100 mV (SHE) in Q-brine (Figure 4.7) and from –1300 mV up to –100 mV in NaCl-rich brine. From experiments carried out with a potential rate of 10 mV/s, the valence change Cu to Cu^+ can be seen from the existence of a peak in the diagramme. Using a potential rate of 1 mV/s this peak disappears in the voltammogram, a phenomenon to be understood by assuming Cu^+ to be oxidized to Cu^{2+}. From the practical point of view there is no corrosion of 99.9 Cu to be seen in the passive range. In the transpassive range, on the other hand, high corrosion rates of several mm/a were determined, which should be caused by the oxidation of the stabilizing $[CuCl_2]^-$ complex to Cu^{2+}.

The corrosion rates obtained from Faradays law coincide with those obtained from the gravimetric determination on condition that z = +1 was taken into account, which proves the assumption that the first electrochemical step is Cu to Cu^+.

4.3.4 Corrosion of Cu-Ni alloys in brines

Figure 4.8 shows a cyclovoltammogram of the Cu-Ni 70-30 alloy in NaCl-rich brine at 25°C under aerobic conditions. The comparison of Figures 4.7 and 4.8 with each other demonstrates the dominant behaviour of Cu in the Cu-Ni 70-30 alloy. Without stirring the limiting current density is reached at +500 mV, the sweep proving that Cu corrodes to the monovalent state, to be oxidized to Cu^{2+} under aerobic conditions.

The reduction from Cu^{2+} to Cu^+ can definitely be seen from the cathodic sweep. The still existing passive range can be compared with that of Ni (Figure 4.4), although it is shifted a little bit more to the negative range and is definitely shorter, especially in Q-brine. Also in this case the corrosion will be increased by temperature, although the characteristics of the voltammograms are not changed (Figure 4.9). The cyclovoltammograms of the Cu-Ni 90-10 alloy are very similar.

In general it must be remarked that copper hinders the formation of an oxide layer on the Cu-Ni alloys which is urgently needed to prevent against corrosion.

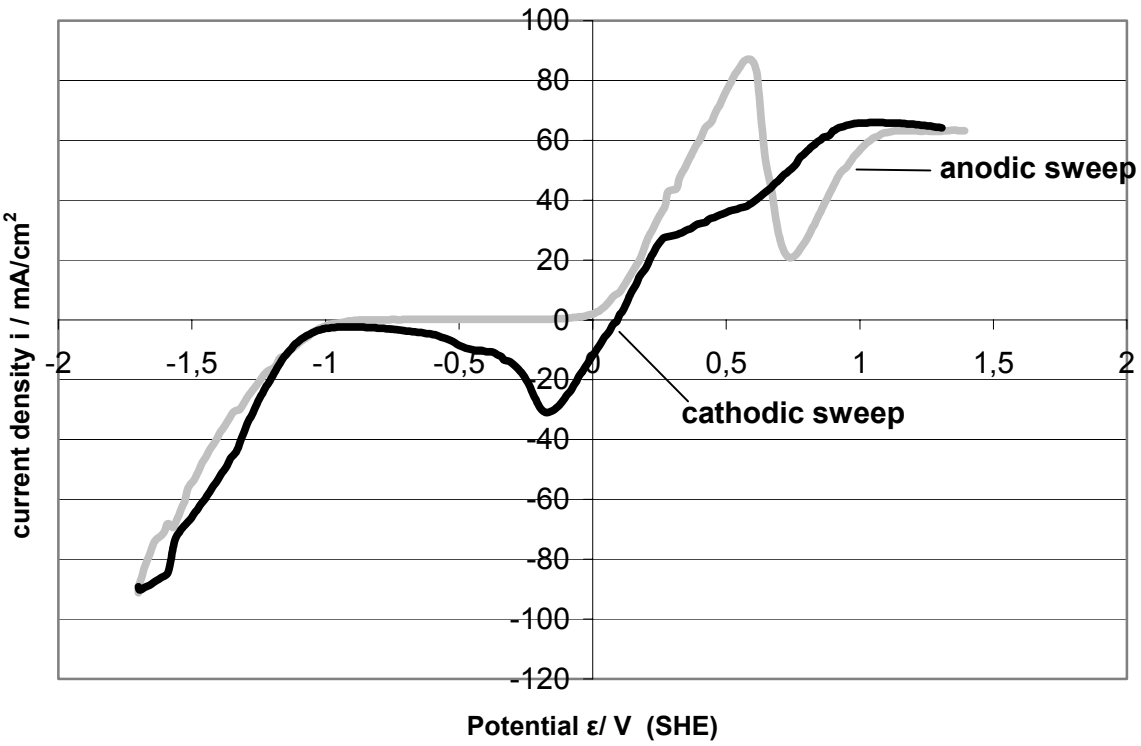

Figure 4.7: Cyclovoltammogram of Cu in Q-brine at 25°C and 10 mV/s, aerobic conditions

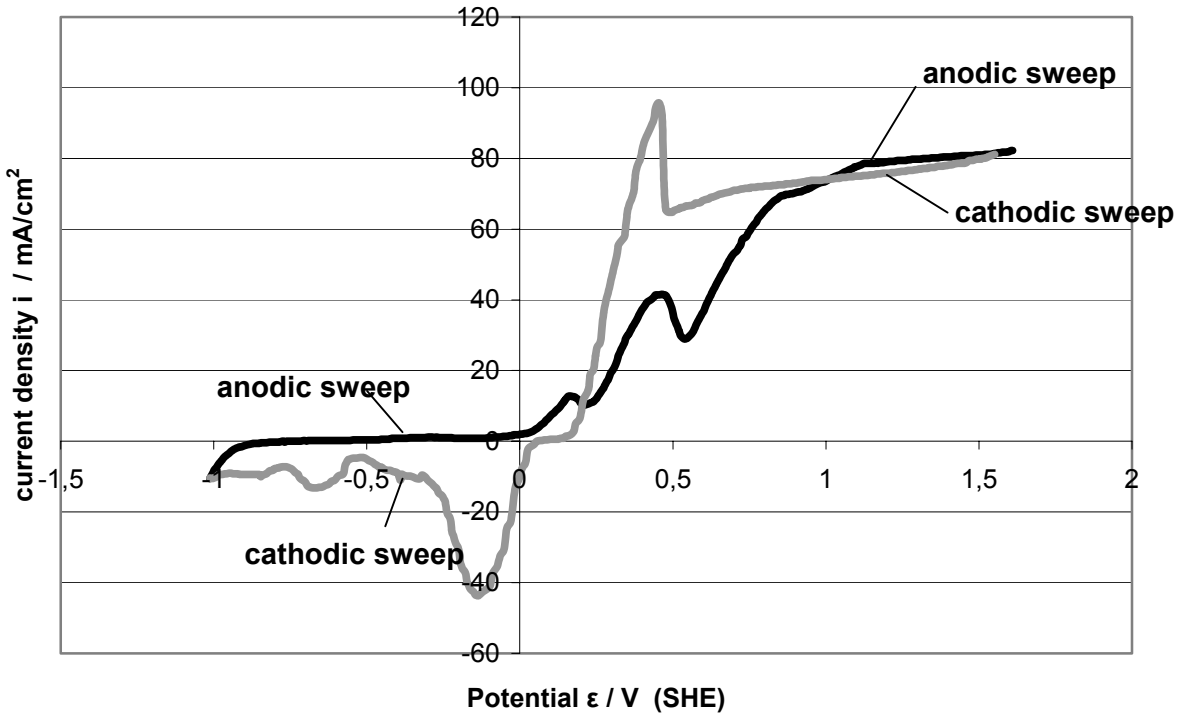

Figure 4.8: Cyclovoltammogram of CuNi 70-30 in NaCl-richbrine at 25°C and 10 mV/s, aerobic conditions, without stirring

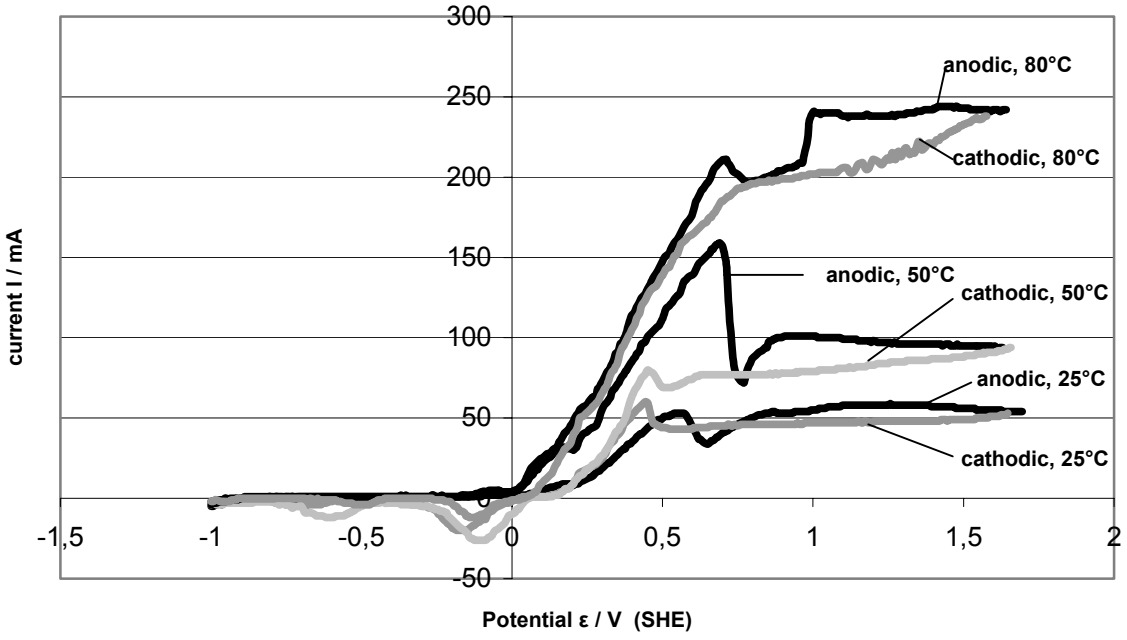

Figure 4.9: Cyclovoltammograms showing influence of temperature on corrosion of the Cu-Ni 70-30 alloy in NaCl-rich brine at 10 mV/s, aerobic conditions

4.4 Corrosion results at rest potentials in brines at 25°C

The corrosion rates of the materials in the two brines at rest potentials at 25°C are listed up in Table 4.1.The data indicate that in both brines the corrosion rates of Ni are smaller (9 µm/a) than those of Cu (24 µm/a). Furthermore, the corrosion rates of Cu are slightly higher in Q-brine (24 µm/a) than in NaCl-rich brine (18 µm/a). The corrosion rate of TStE355 carbon steel is also higher in Q-brine (22 µm/a) than in NaCl-rich brine (14 µm/a), as in the case of Cu. Furthermore, it must be outlined that the corrosion rates of the Cu-Ni alloys are higher in Q-brine (31 µm/a) than in NaCl-rich brine (14 µm/a). Comparing the corrosion rates of Cu-Ni 70-30 with Cu-Ni 90-10 it can be demonstrated that the corrosion rates of the alloy with the higher Cu content are higher (31 µm/a) than those with the lower Cu content (17 µm/a), and are nearly identical with those of carbon steel in the relevant brine system (22 µm/a). Winding up the results it must be stated emphatically that from the electrochemical point of view Ni and a higher Ni content of Ni-Cu alloys increase the resistance of the material towards corrosion under the conditions the experiments were performed.

4.5 Corrosion results at rest potentials in brines at 80°C

At the higher temperature of 80°C, the corrosion rates of all materials in the brines are significant higher than those obtained at 25°C (Table 4.2). Moreover, Table 4.2 shows that the corrosion rates of the materials, except those for Ni, are higher in Q-brine than in NaCl-rich brine. The higher corrosivity of the Q-brine (pH=4.6) compared to the NaCl-rich brine (pH=6.5) is attributed to its higher Cl^- concentration and Mg^{2+} content, as discussed in session 3.1.3, and to the lower pH of the Q-brine due to the hydrolysis ot the high $MgCl_2$ content. The lower pH effects especially the corrosion of carbon steel, because its oxidant is H_3O^+ to be reduced to H_2. At higher temperatures the hydrolysis is increased on account of the fact that the hydrolysis constant depends on temperature in form of an e-function (Van't Hoff) [26].

Table 4.1: Corrosion rates of the materials investigated under aerobic conditions in the test brines at rest potential at 25°C

Material	Electrolyte	Rest potential ε_R/mV (SHE)	Mass loss Δm (mg)	Time T (h)	Corrosion rate R (µm/a)
Ni	Q-brine	-50 +/- 5	0.1	230	8.6
Ni	NaCl-rich	-106 +/- 8	0.05	70	14
Cu	Q-brine	-124 +/- 5	0.24	193	24
Cu	Q-brine	-120 +/- 5	0.09	78	23
Cu	NaCl-rich	-106 +/- 5	0.17	193	17
Cu	NaCl-rich	-100 +/- 5	0.18	193	18
TStE355 steel	Q-brine	-445 +/- 5	-	155	-
TStE355 steel	Q-brine	-435 +/- 5	0.21	220	22
TStE355 steel	NaCl-rich	-410 +/- 5	-	166	-
TStE355 steel	NaCl-rich	-440 +/- 8	0.13	220	14
Cu-Ni 70-30	Q-brine	-94 +/- 5	0.14	210	13
Cu-Ni 70-30	Q-brine	-130 +/- 5	0.20	225	17
Cu-Ni 70-30	NaCl-rich	-27 +/- 4	0.05	180	5.5
Cu-Ni 90-10	Q-brine	-123 +/- 4	0.15	96	31
Cu-Ni 90-10	NaCl-rich	-126 +/- 4	0.05	70	14

Table 4.2: Corrosion rates of the materials investigated under aerobic conditions in the test brines at rest potential at 80°C

Material	Electrolyte	Rest potential ε_R/mV (SHE)	Mass loss Δm (mg)	Time t (h)	Corrosion rate R (µm/a)[1]
Ni	Q-brine	-115 +/-10	0,58	77,0	148
Ni	Solution 3	-130 +/- 8	0,84	77,0	215
Cu	Q-brine	-180 +/- 8	0,45	77,0	115
Cu	Solution 3	-160 +/- 10	0,41	77,0	105
Carbon steel	Q-brine	-375 +/- 5	0,73	101,5	166
Carbon steel	Solution 3	-440 +/-10	0,34	100,0	78
Cu/Ni=70:30	Q-brine	-156 +/- 5	0,37	80,2	91
Cu/Ni=70:30	Solution 3	-100 +/- 10	0,31	80,2	76
Cu/Ni=90:10	Q-brine	-160 +/- 8	0,26	80,2	64

In general the increase of corrosion by rising temperature can also be understood from the corrosion current I_{corr} depending on temperature, which can be described by the Stern-Geary equation [7].

$$I_{corr} = \frac{b_a \cdot b_c}{(b_a + b_c) R_p} = \frac{B}{R_p} \quad \text{with} \quad b_a = \frac{R \cdot T}{\alpha_a \cdot z_a \cdot F} \quad \text{and} \quad b_c = \frac{R \cdot T}{\alpha_c \cdot z_c \cdot F} \tag{1}$$

In this equation R_p is the polarization resistance, R the universal gas constant, F the Faraday constant, T the absolute temperature, z_a and z_c the number of electrons exchanged at anode and cathode, respectively, by the redox reaction and α_a and α_c the relevant transfer coefficients.

The first deviation of (1) leads to (2)

$$\frac{\partial I_{corr}}{\partial T} = \frac{\partial B}{\partial T} \cdot \frac{1}{R_p} = \frac{R}{F R_p \left[\alpha_a \cdot z_a + (1 - \alpha_a) \cdot |z_c|\right]} \tag{2}$$

on condition that R_p is assumed to be constant.
In case of $\alpha_a = \alpha_c = 0{,}5$ and $z_a = |z_c| = 1$ it follows

$$\frac{\partial I_{corr}}{\partial T} = \frac{1}{R_p} \cdot \frac{\partial B}{\partial T} = \frac{1}{R_p} \cdot 0{,}08 \frac{mV}{K} \tag{3}$$

4.6 Results of galvanic corrosion of the material pairs Cu/TStE355 steel, Ni/TStE355 steel and Cu-Ni/TStE355 steel

The galvanic corrosion of the material pairs Cu/TStE355 carbon steel, Ni/carbon steel and Cu-Ni alloys/carbon steel was studied in Q-brine and in NaCl-rich brine at 25°C and at 80°C by applying electrochemical methods The results obtained are compiled in the Table 4.3. The data demonstrate that TStE355 carbon steel is the anode acting as cathode protector with respect to Ni, Cu or Cu-Ni alloys. In both brines at 25°C the corrosion of Ni and Cu galvanic coupled with carbon steel are

below the detection limit (0.01 µm). For Cu in Q-brine the corrosion rate amounts only 5 µm/a at the maximum.

The corrosion rates of the Cu-Ni alloys coupled with carbon steel are higher (33-37 µm/a) in both brines than the values of Cu and Ni. The corrosion rates of the carbon steel coupled with Cu or Ni are 33 up to 45 µm/a in these media at 25°C, those in contact with the relevant Cu-Ni alloys 58-89 µm/a. Higher temperature enhances the galvanic corrosion of the investigated materials. At 80°C the corrosion rates of Ni and Cu coupled with carbon steel are 4-19 µm/a in NaCl-rich and Q-brine. Those of the Cu-Ni alloys in contact with carbon steel are 27-35 µm/a in NaCl-rich and Q-brine (Table 4.3), not differing significantly from the data obtained at 25°C. But the relevant corrosion rates of carbon steel in contact with the materials aforementioned are drastical higher at 80°C than at 25°C. In NaCl-rich brine at 80°C they are in the range of 300 µm/a, in Q-brine even up to 600 µm/a. In general it can be stated that the corrosion rate of carbon steel is higher in Q-brine than in NaCl-rich brine.

Table 4.3: Galvanic potentials and corrosion rates of carbon steel, Cu, Ni and Cu-Ni-alloys in brines at 25°C at 80°C

Galvanic coupled Materials/ Brine [1)]	Me [2)] (80°C) Corrosion rate (µm/a)	Steel (80°C) Corrosion rate (µm/a)	Me (25°C) Corrosion rate (µm/a)	Steel (25°C) Corrosion rate (µm/a)	Galvanic potential. (80°C) mV (SHE)	Galvanic potential (25°C) mV (SHE)
Ni/Steel-Q	11 (Ni)	510	*	42	-380	-428
Ni/Steel-NaCl-rich	4 (Ni)	315	*	45	-438	-448
Cu/Steel-Q	13 (Cu)	342	5	33	-385	-427
Cu/Steel-NaCl-rich	19 (Cu)	253	*	42	-420	-449
Cu-Ni 70-30/Steel Q	12 (Cu-Ni 70-30)	598	37	61	-382	-428
Cu-Ni 70-30/Steel NaCl-rich	27 (Cu-Ni 70-30)	276		89	-438	-446
Cu-Ni 90-10/Steel Q	31 (Cu-Ni 90-10)	429	36	73	-395	-419
Cu-Ni 90-10/Steel NaCl-rich	35 (Cu-Ni 90-10)	333	33	58	-425	-442
	Corrosion rate Cu (80°C) (µm/a)	Corrosion rate Ni (80°C) (µm/a)	Corrosion rate Cu (25°C) (µm/a)	Corrosion rate Ni (25°C) (µm/a)	Contact potential Cu/Ni (80°C) mV (SHE)	Contact potential Cu/Ni (25°C) mV (SHE)
Cu/Ni-Q	154	76	43	*	-165	-111
Cu/Ni-NaCl-rich	189	24	49	*	-110	-107

*) no detected (below the detection limit)
[1)] Q-brine = $MgCl_2$-rich brine; [2)] Me = Ni, Cu, Cu-Ni 90-10, Cu-Ni 70-30, respectively

In general it can be stated that the experimental determined corrosion behaviour of the materials is in accordance with the galvanic potentials measured, which will be outlined in the following chapter from the theoretical point of view. From Figure 4.10 it can be seen, that an experimental time of at least 100 hours will be needed, until the galvanic potential becomes constant.

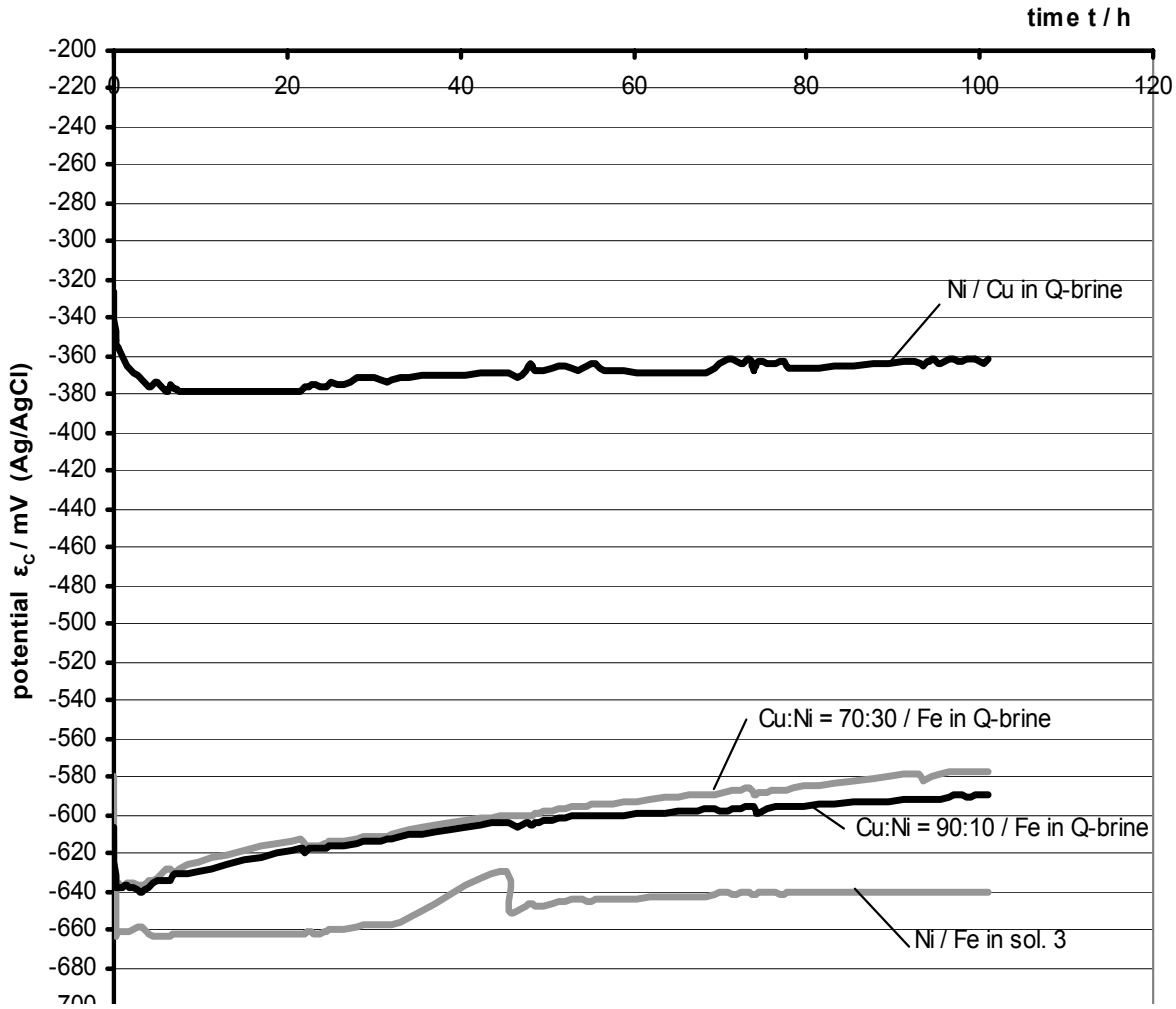

Figure 4.10: Contact potentials of the material pairs Ni/carbon steel, Cu-Ni/carbon steel and Cu/Ni at 80°C

4.7 Theoretical aspects of galvanic potentials with Fe

The physics of galvanic potentials can be understood by studying Figure 4.11. As can be seen from this Figure there are two galvanic potentials to be obtained in general, the anodic galvanic potential at ε_a and the cathodic potential at ε_k, their difference being caused by the inner resistance R_i of the relevant medium, which the electrochemical process is occurring in.

But in the case of Q-brine and NaCl-rich brine, R_i is so small, that ε_a coincides with ε_k. The sum of the current densities is i_s. The cathodic rest potential $(\varepsilon_k)_R$ with the relevant anodic rest current density i_3 must be more positive than ε_k. The anodic rest potential $(\varepsilon_a)_R$ with the relevant anodic rest current density i_1 on the other hand must be more negative than ε_a.

For galvanic corrosion the most important quantities are i_2, the partial anodic density at ε_a, and i_4, the partial anodic current density at ε_k. It is $i_2 > i_1$; $i_2 > i_S$; $i_4 < i_S$; $i_4 < i_3$ As it is easily to be seen, these relations explain the cathodic protecting effect of the anode towards the cathode.

i_S can be calculated from electrochemical measurements by use of the well-known equation (4):

$$i_s = \frac{\Delta\varepsilon_R}{I/q + (R_\pi)_a + (R_\pi)_k} \qquad (4)$$

In (4) $(R_\pi)_a$ and $(R_\pi)_k$ is the polarization resistance at the anode and cathode, respectively, q the conductivity of the medium and l the distance of the electrodes. The important partial current densities i_2 and i_4 representing the corrosion rate of the anode and cathode can be obtained from analytical procedures only.

In Q-brine (pH = 4,5) the equilibrium potential is: $\varepsilon_{eq.}$ (H^+/H_2)= -266 mV, in NaCl-rich brine (pH=6,5) ε_{eq}= -383 mV. The standard potential of Fe is ε_0 (Fe/Fe^{2+}) = -400 mV. Due to Nernst equation its equilibrium potential must be even more negative, because the Fe^{2+} concentration is smaller than 1 mol/l. Therefore for galvanic coupled materials (contact pairs) with carbon steel in Q-brine and NaCl-rich brine, the prevailing oxidant is H_3O^+ to be reduced to H_2. The higher corrosion rate of carbon steel in Q-brine than in NaCl-rich brine shifts the galvanic potential to more positive values, due to the higher i_2 (Figure 4.11) resulting from a higher i_4 These facts are verified experimentally (Table 4.3).

4.8 Results of galvanic corrosion of the material pair Cu/Ni in brines

In order to get a deeper insight into the galvanic corrosion, the corrosion of the contact pair Ni/Cu was studied in Q-brine and NaCl-rich at 25°C and 80°C. For these investigations the experimental set-up was changed by locating Ni and Cu in separate half cells connected by a salt bridge (Figure 4.12).

If the salt bridge was filled with highly diluted Q-brine, R_i would have a higher value and two contact potentials would be measured as can be seen on Figure 4.12. It is demonstrated that Cu is the anode which protects the cathode Ni, its contact potential nearly equaling its rest potential (ε_R= -124 mV; ε_c = -111 mV).

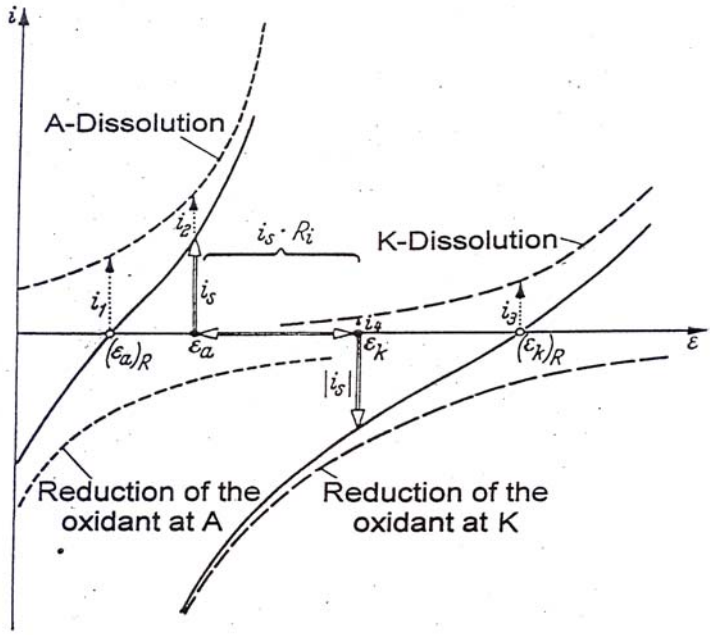

Figure: 4.11: Schematic diagram of contact potentials

Connecting the two half cells with an outer resistance of R_0 = 500 kΩ and a salt bridge filled with Q-brine a Cu/Ni-element is set up, Cu being the anode and Ni the cathode. The Ni cathode is passivated by a surface layer of NiO [6] which is constantly disrupted and rebuilt. Its quality seems to get improved a little bit when time passes on and the relevant potential constantly increases. The corrosion rate of Ni at 25°C is below the detection limit, that of Cu is 43 µm/a in Q-brine and 49 µm/a in NaCl-rich brine (Table 4.3). Cu seems to corrode uniformly (Figure 4.13).

At 80°C the relevant corrosion rates are higher than at 25°C, for Ni 24 µm/a in NaCl-rich brine and 76 µm/a in Q-brine, for Cu 189 µm/a in NaCl-rich brine and 154 µm/a in Q-brine. The relevant galvanic potentials are more negative at 80°C than at 25°C (Table 4.3). This fact can be explained from the theoretical point of view.

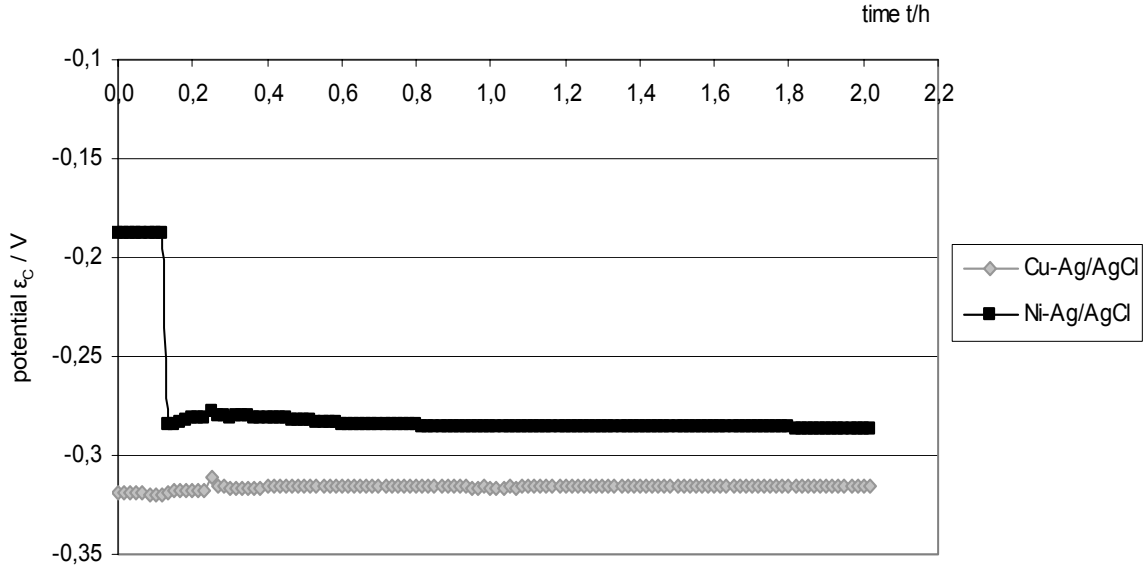

Figure 4.12: Ni/Cu contact potentials vs time in highly diluted Q-brine

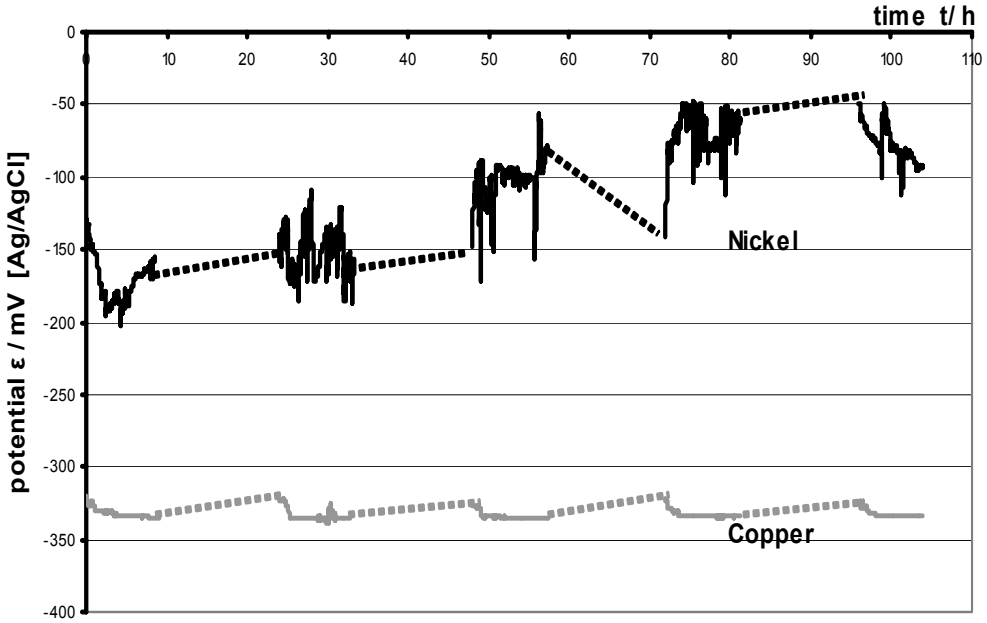

Figure 4.13: Potentials of Ni and Cu connected with 500 kΩ resistance vs time in Q-brine at 28 °C

4.9 Theoretical aspects of galvanic corrosion of Cu/Ni

Although the standard potential of Cu is more positive than that of Ni, E^0 (Cu/Cu^{2+}) = +337 mV, E^0 (Cu/Cu^{+}) = +521 mV, E^0 (Ni/Ni^{2+}) = -250 mV, the equilibrium potential $\varepsilon_{eq.}$ (Cu/Cu^{+}) is shifted to the negative range in the relevant brines, due to the formation of the linear $[Cu/Cl_2]^-$ complex with monovalent Cu, which is the prevailing ionic species in concentrated copper chloride solutions [27]. This strong negatively charged complex decreases the concentration of Cu^+ ions so drastically, that the equilibrium potential $\varepsilon_{eq.}$ (Cu/Cu^{+}) is found to be in the negative range. $\varepsilon_{eq.}$ (Cu/Cu^{+}) must be more negative than the relevant rest potential, which is E_R (Cu) = -124 mV in Q-brine at 25°C (Table 4.1). But $\varepsilon_{eq.}$ (Cu/Cu^{+}) is not sufficiently negative to reduce H_3O^+ to H_2 (ε (H_2/H^+) = -266 mV; pH=4,5; T=25°C). So the prevailing oxidant is O_2 to be reduced to H_2O in this case. The partial cathodic current density of O_2 on the other hand is diffusion controlled (Figure 4.14) [25].

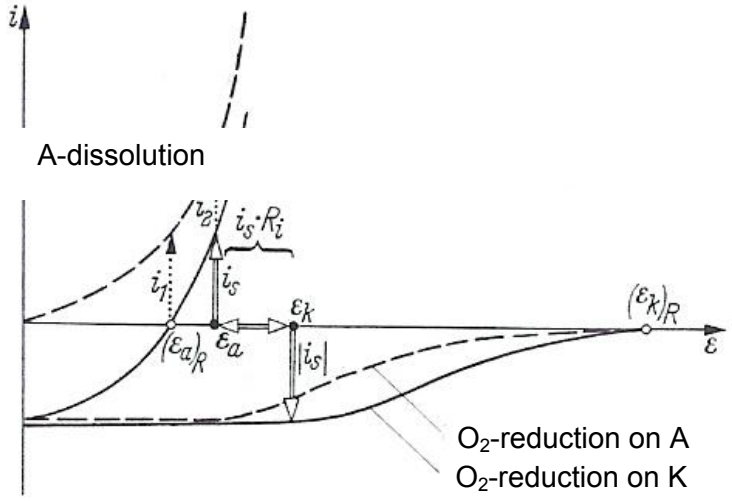

Figure 4.14: Schematic current density-potential diagram in case of contact potentials in NaCl-brine under aerobic conditions [6]

Therefore, the partial anodic current density at the anodic contact potential, which represents the anodic corrosion rate, is

$$i_a = 2i_{O_2}^D \tag{5}$$

It equals the double limiting diffusion current density on condition that anode and cathode are of the same size and the corrosion rate of the cathode is zero, the cathode only acting as O_2 electrode [25].

This seems to be the case with the Ni electrode in brines at 25°C, being passivated by the NiO surface layer. It explains the relative high corrosion rate of Cu which is due to the high partial anodic current density, compensating not only the partial cathodic current density at the Cu anode but also that of the Ni cathode.

The limiting diffusion current density [25] is:

$$i_{O_2}^D = n \cdot F \cdot D \cdot \left(c_{sol}^{O_2}\right) / \partial_N \tag{6}$$

with n being the number of electrodes exchanged, D the diffusion coefficient, F the Faraday constant $c_{sol}^{O_2}$ the O_2 concentration in the solution and ∂_N the thickness of the diffusion layer. $c_{sol}^{O_2}$ is smaller at higher temperatures. Then $i_{O_2}^D$ is smaller making i_{O_2} become smaller too.
A smaller $i_{O_2}^D$ makes i_a decreasing and shifts the contact potential to more negative values. This has been observed (Table 4.3).

4.10 Calculations of thermodynamic data

The Free Reaction Enthalpy ($\Delta_R G$), the Reaction Enthalpy ($\Delta_R H$), and the Reaction Entropy ($\Delta_R S$) of the prevailing reaction

$$2H_2O + 4Cu + 8Cl^- + O_2 \rightarrow 4OH^- + 4\left[CuCl_2\right]^-$$

are of great importance for NaCl-rich and Q-brine.

For calculating one has to start with the Gibbs-Helmholtz equation

$$\Delta_R G = \Delta_R H - T \cdot \Delta_R S \tag{7}$$

The first partial deviation to T gives:

$$\frac{\partial \Delta_R G}{\partial T} = \frac{\partial \Delta_R H}{\partial T} - \Delta_R S - T\frac{\partial \Delta_R S}{\partial T} = -\Delta_R S \tag{8}$$

Arranging will lead to:

$$\frac{\partial \Delta_R H}{\partial T} = T\frac{\partial \Delta_R S}{\partial T} = 0 = \frac{\partial \Delta_R S}{\partial T} \tag{9}$$

if $\Delta_R H$ is assumed to be independent from T within the temperature interval considered.

$\Delta_R S$ can be calculated from

$$-\frac{\partial \Delta_R G}{\partial T} = \Delta_R S = n \cdot F \cdot \frac{\partial \left|\Delta \varepsilon_{eq}\right|}{\partial T} \approx n \cdot F \cdot \frac{\Delta\left(\left|\Delta \varepsilon_R\right|\right)}{\Delta T} \tag{10}$$

if it is assumed that I $\Delta\varepsilon_{eq}$ I ≈ I $\Delta\varepsilon_R$ I, $\Delta\ \varepsilon_{eq}$ being the difference of the relevant equivalent potential and $\Delta\varepsilon_R$ that of the rest potential

$\Delta_R G$ is available from

$$\Delta_R G = -n \cdot F \cdot \left|\Delta \varepsilon_{eq}\right| \approx -n \cdot F \cdot \left|\Delta \varepsilon_R\right| \tag{11}$$

and $\Delta_R H$ from Gibbs-Helmholtz (7).

From these calculation one has also to take into account, that in the test brines it is

$$\left|\Delta \varepsilon_R\right| = \left|\varepsilon_{eq}\left(O_2\right) - \varepsilon_R\left(Cu\right)\right| \tag{12}$$

Moreover it is

$$\varepsilon_{eq}\left(O_2\right) = \varepsilon^0 + \frac{RT}{4F} \cdot \ln \cdot\, p\left(O_2\right) - \frac{RT}{F} \cdot \ln \cdot\, a\left(OH^-\right) \tag{13}$$

p (O_2) being the partial pressure of O_2 and a (OH^-) the activity of OH^- ions. The standard potential ε^0, depending only on temperature and pressure, must be calculated for 25°C and 80°C and for the two test brines.This is possible by using the well-known equations

$$\Delta_R G^0 = -RT \cdot \ln \cdot K \tag{14}$$

$$\frac{\partial \ln K}{\partial T} = \frac{\Delta_R H}{RT^2} \tag{15}$$

and combining them with (11).

K is the equilibrium constant and $\Delta_R G^0$ the standard Free Reaction Enthalpy.
The relevant data obtained for Q-brine and NaCl-rich brine are compiled in Table 4.4

Table 4.4: Thermodynamic data for the Cu -O_2-reaction

Brines	T(K)	$\Delta_R G$ (kJ/mol)	$\Delta_R H$ (kJ/mol)	$\Delta_R S$ (J/mol·K)	ε_{eq} (O_2)/V	ε_R^{Cu}(V)
Q-brine	298	-413	-494	-273	0,951	-0,120
Q-brine	353	-398	-494	-274	0,852	-0,180
Sol. 3	298	-363	-509	-491	0,836	-0,106
Sol. 3	353	-336	-509	-491	0,712	-0,160

The $\Delta_R H$ values verify that $\Delta_R H$ is independent from the temperature T. In general, the data confirm the dominant role, played by the $[CuCl_2]^-$ complex, which causes the abnormal electrochemical behaviour of Cu in these special electrolytes of high practical importance. All the theoretical conclusions are only made from the pure electrochemical point of view without taking any surface layer formation into account but Ni forming the well-known NiO surface layer. These data represent one of the few thermodynamic data which have been calculated for brines uptil now.

Surface investigations by means of SEM/EPMA carried out in addition to these electrochemical studies, and are reported in the following chapters.

4.11 Results of surface analysis of corroded specimens

The element composition and the morphology of the surfaces of Cu, Ni and TStE355 carbon steel electrodes corroded during the foregoing electrochemical measurements were investigated by means of the scanning electron microscopy (SEM) and the electron probe microanalysis (EPMA) in the energy dispersive mode (EDX), respectively. In Table 4.5 the results obtained from the surface analytical experiments as well as those from the electrochemical ones are compiled together with the relevant experimental parameters. A series of selected Cu, Ni, steel electrodes and electrode couples was investigated (Table 4.5, column 1-3). The electrochemical measurements (column 4) were carried out mainly in an electrolytical cell with Ag-AgCl reference electrodes (Figure 4.15) and in two cases in two half cells conected with each other by a salt bridge (Figure 4.16). The electrolyte used was Q-brine (Mg^{2+}, Na^{+}, Cl^{-}, SO_4^{2-}) or NaCl-rich brine (Table 4.5, column 5). The measurements were performed at 26°C as well as at 80°C (column 6). A single measurement lasted up to t=104h (Table 4.5, column 7). Column 8 shows the measured corrosion and galvanic potentials, respectively. The mass loss Δm of an electrode was obtained by weighing (column 9), hence it follows the corrosion rate R by a formal calculation (column 10). The morphology of the surface, i.e, the corrosion degree, is qualitatively estimated by means of SEM is listed in column 11.

Table 4.5: Electrochemical and surface analytical investigations into the corrosion of Cu, Ni and steel electrodes
Electrolyte: Q-brine (Mg^{2+}, Na^{+}, Cl^{-}, SO_4^{2-}) and NaCl-rich brine

n. d. = not detectable

No	Material		Electrochemical measurements							Surface analysis	
			Electrolytical cell (c) with Ag-AgCl reference electrode (specimen no. 1-17) or two half cells (hc) with a salt bridge (no. 18,19)							Scanning electron microscopy (SEM)	Electron probe microanalysis (EPMA) in the energy-dispersive mode (EDX)
1	Electrode couple 2	Electrode 3	Cell or 2 half cells 4	Electrolyte 5	Temperature T(°C) 6	Time t(h) 7	Corrosion or contact potential E(mV) 8	Mass loss Δm(mg) 9	Corrosion rate R(μm/a) 10	Corrosion degree (=morphology of the surface) 11	Superficial element composition 12
1		Cu	c	Q	26	1	- 328			not detectable	
2		Cu	c	Q	26	8	- 339			very weak	
3		Cu	c	Q	26	77	- 330	0.10	25	strong	Cu, some CuO
4	Cu/steel	Cu	c	Q	26	77	- 624	n. d.	0	insignificant	Cu, Fe(Ni,Si), Mg, O, S
5	(Mn,Ni,Si)	steel	c	Q	26	77		0.23	69	very strong	Fe(Mn,Ni,Si), Mg, O, Cl, S
6	Cu/Ni	Cu	c	Q	26	77	- 317	0.23	58	strong	Cu, some CuO
7		Ni	c	Q	26	77		n. d.	0	insignificant	Ni, some NiO
8	Ni/steel	Ni	c	Q	26	77	- 626	n. d.	0	insignificant	Ni, Fe, Mg, O, Cl, S
9	(Mn,Ni,Si)	steel	c	Q	26	77		0.12	36	strong	Fe(Mn,Ni,Si), Mg, O, Cl, S
10	Cu/steel	Cu	c	Q	80	100	- 585	1.53	342	thick layer of Ag	Cu, Ag, Mg, O
11	(Mn,Ni,Si)	steel	c	Q	80	100		0.07	13.4	strong	Fe, Mg, O, Cl, (Ag?)
12	Ni/steel	Ni	c	Q	80	100	- 580	0.06	11.5	insignificant	Ni, some NiO
13	(Mn,Ni,Si)	steel	c	Q	80	100		2.28	510	strong	Fe(Mn,Si), Ni, Ag, Mg, O, Cl, S
14	Cu/Ni	Cu	c	Q	80	100	- 365	0.79	154	layer of Ag	Cu, Ni, Ag, Mg, O, Cl, S
15		Ni	c	Q	80	100		0.39	76	insignificant	Ni, some NiO, some Ag
16	Cu/Ni	Cu	c	NaCl	80	100	- 310	0.97	189	strong	Cu, some CuO, Ag
17		Ni	c	NaCl	80	100		0.12	24	weak	Ni, some NiO, some Ag
18	Cu/Ni	Cu	hc	Q	26	104	- 334	0.17	43	strong	Cu, some CuO
19		Ni	hc	Q	26	104	- 93	0.02	6	insignificant	Ni, some NiO

The element composition of the specimen surface, identified by EPMA/EDX spectra is shown in Table 4.5, column 12, the corresponding quantitative data can be seen from the spectra (e. g. Figure. 4.16b). Characteristic examples of corroded electrodes are shown in the Figures 4.15-4.22. Figure 4.15a (specimen no. 3 in Table 4.5) shows the strongly corroded surface of a Cu electrode in Q-brine after 77h at 26°C; the corresponding mass loss is Δm = 0.10 mg and the corrosion rate R=25 µm/a. The X-ray spectrum (Figure 4.15b) shows Cu and some CuO.

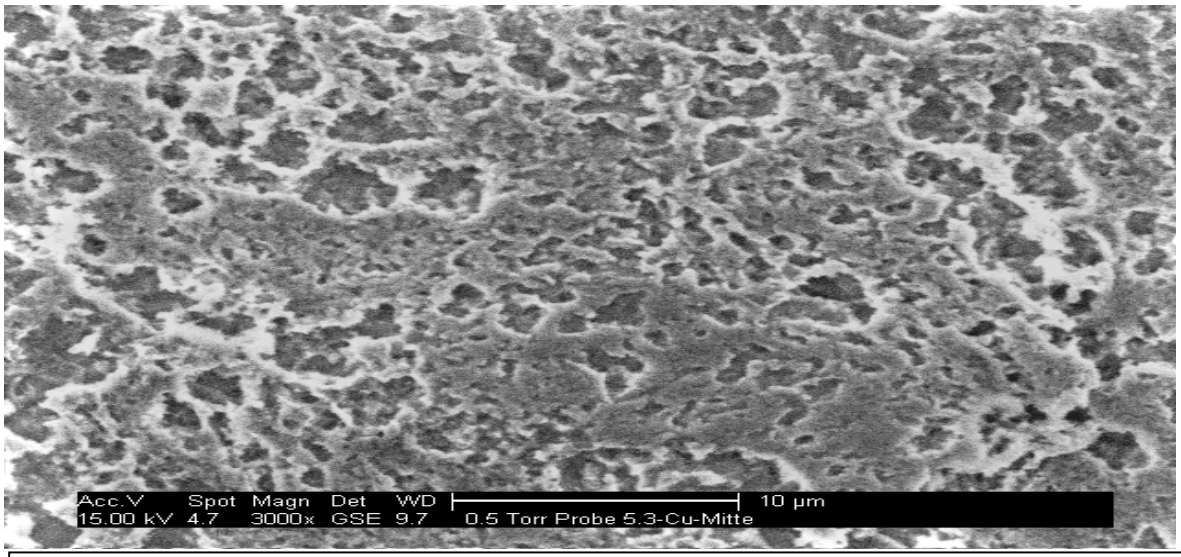

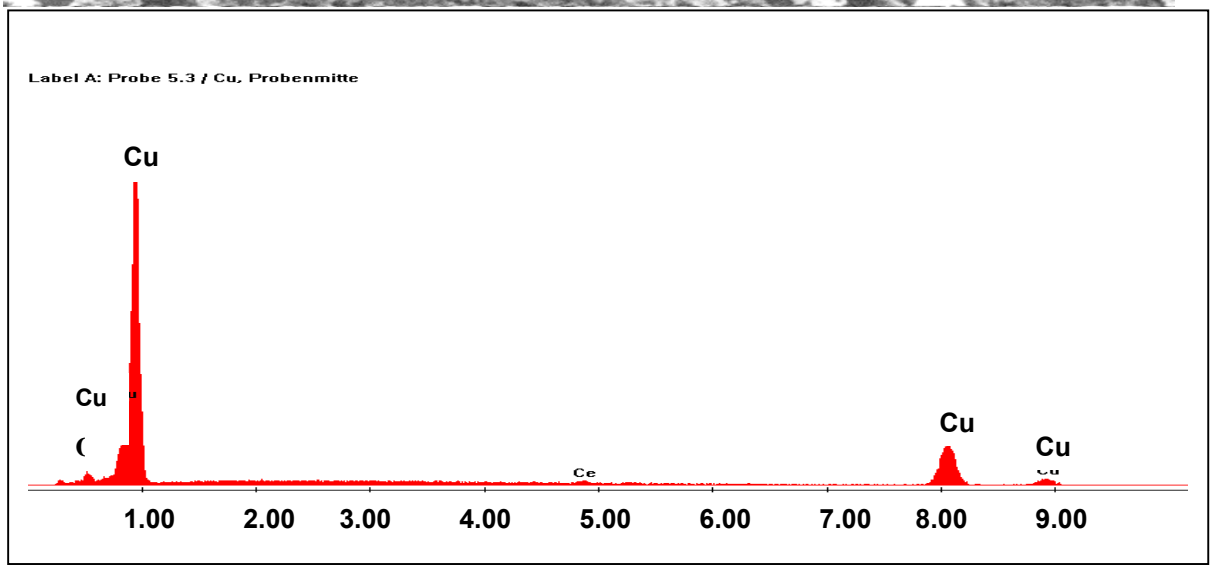

Fig. 4.15: Cu electrode surface (Table 4.6, specimen no. 3) after the electrochemical measurement: Q-brine, T=26 °C, t=77 h, Δm=0,10 mg, R=25 µm·a^{-1}, E_c=-330 mV
Figure 4.15a. (above) SEM micrograph: strong corrosion
Figure 4.15b. (below) EDX spectrum: Cu, some O

In the case of the electrode couple Cu/steel (Table 4.5: no. 4/5) the corrosion of the Cu surface is insignificant (Figure 4.16a, specimen no. 4), whereas the steel surface is very strongly corroded (Figure 4.16b; no. 5). In the steel surface the elements Fe (Mn, Ni, Si), Mg, O, Cl and S were detected (Figure 4.16c); the surface represents a thick layer (µm-range) consisting of crystallites of Cl 3,71 %, Mg 15,23 %, S 1,22 %, Si 2,36 % (Fe/Mg)-oxides, -hydroxides and –chlorides. On the Cu surface small deposited particles were found consisting of Fe(Ni, Si), Mg, O, S.

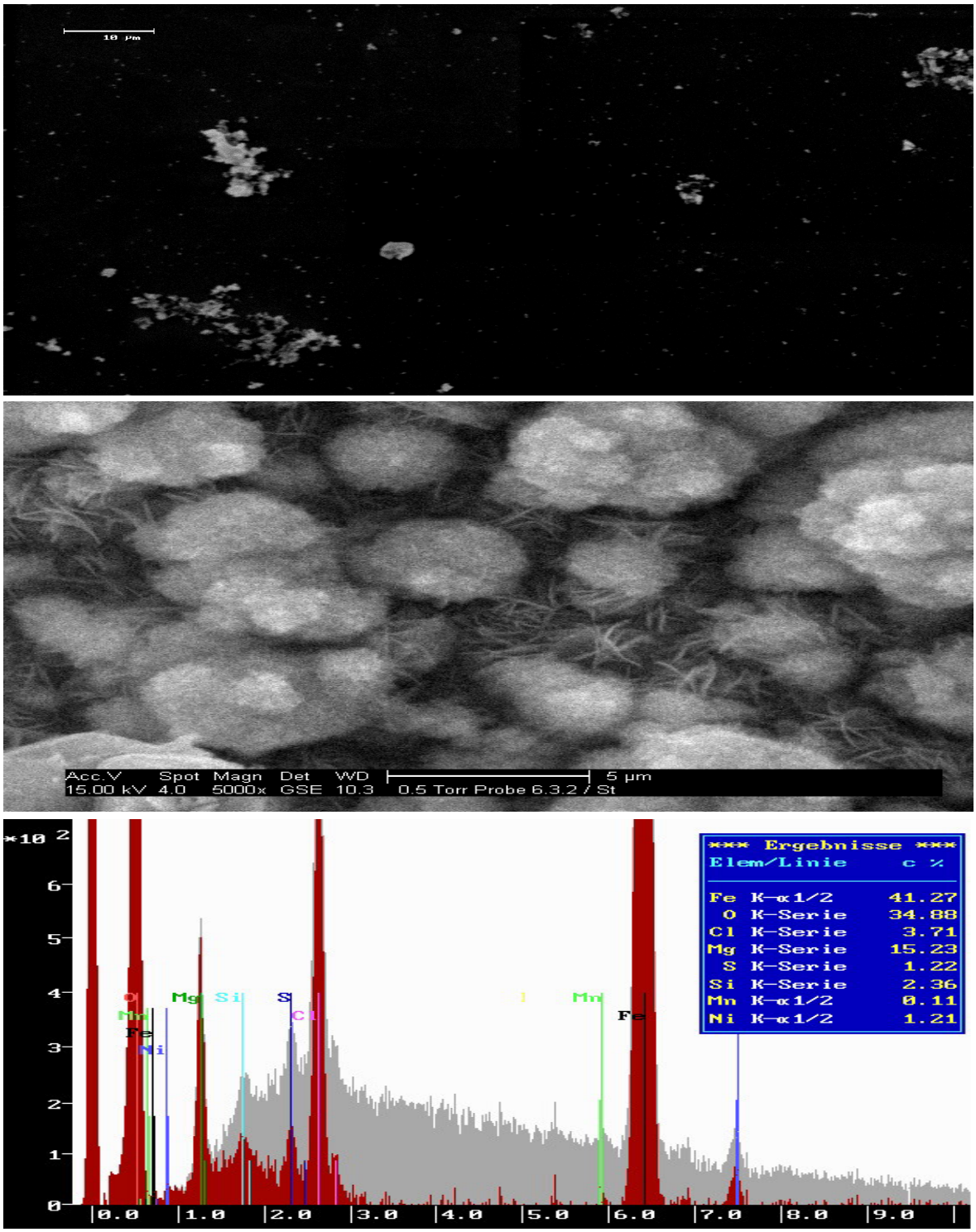

Figure 4.16: Electrode couple Cu/steel (Table 4.5, no. 4/5) after the electrochemical measurement: Q-brine, T=26°C, t=77 h, E_c=-624 mV

4.16a. (above) SEM micrograph of the surface of the Cu electrode: insignificant corrosion; small deposited particles

4.16b. (mid) SEM micrograph of the surface of the steel electrode: strong corrosion, thick corrosion layer, consisting of (Fe,Mg,S)-oxides, -hydroxides, -chlorides; Δm=0,23 mg, R=69 µm/a

4.16c. (below) EDX spectrum of the steel surface: Fe 41,27 %, O 34,88 %,

The same behaviour was found for the couple Ni/steel (Table 4.5, no. 8, 9). The very strong corrosion of steel is in conformity with the measured high mass losses ∆m and the from them resulting corrosion rates R of the steel electrode: ∆m = 0.23 mg, R = 69 µm/a (Cu/steel couple) and ∆m = 0.12 mg, R = 36 µm/a (Ni/steel couple).

In the case of the couple Cu/Ni in Q-brine at 26 °C (Figure 4.17; no. 6/7), the corrosion of the copper surface is very strong whereas the corrosion of Ni can be neglected due to its strong passivation by an oxide/hydroxide layer (session 4.9).

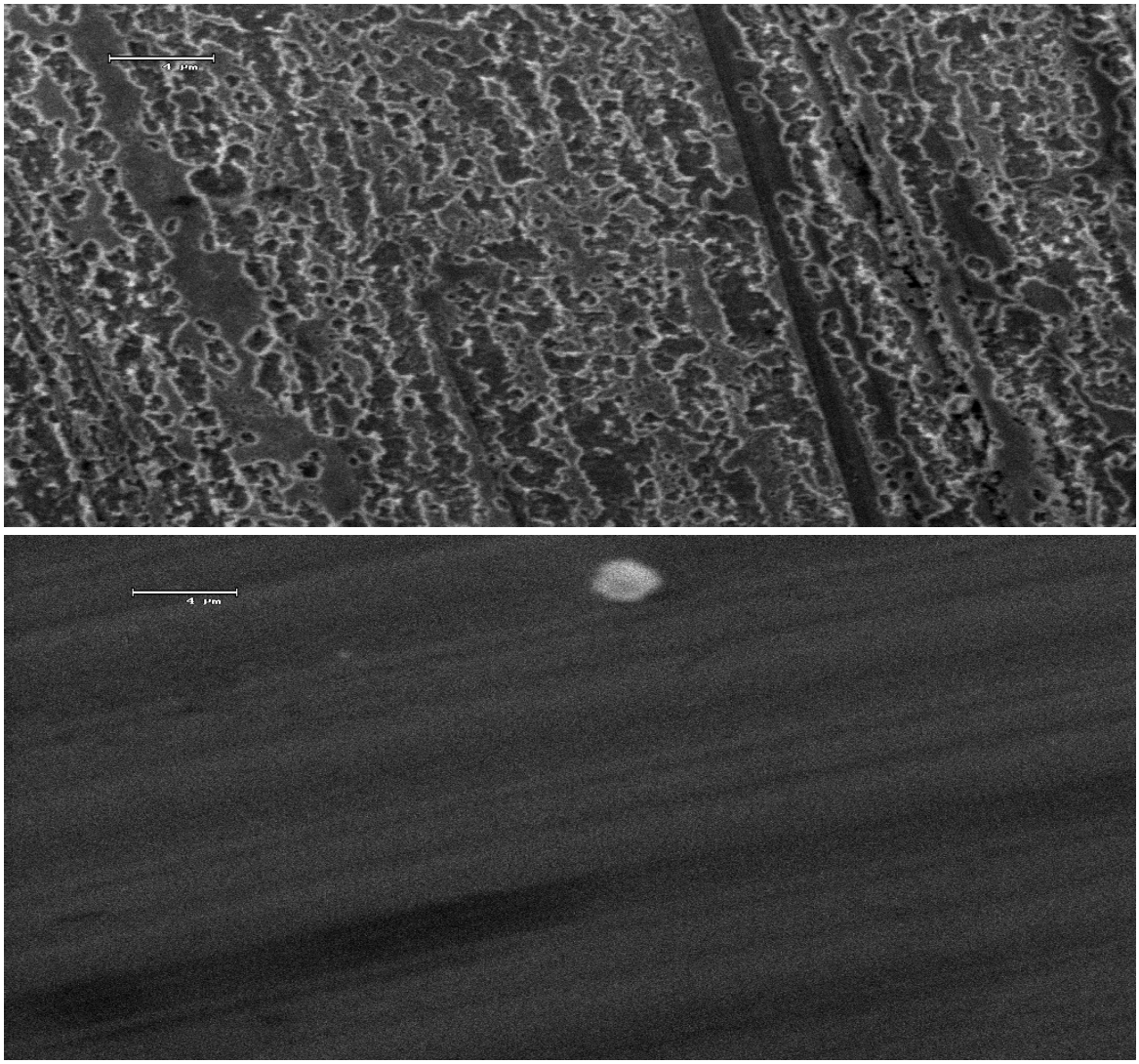

Figure 4.17: SEM micrographs of the electrode surfaces of the couple Cu/Ni (no. 6/7); Q-brine, T=26°C, t=77 h, E_c=-317 mV
4.17a. (above) Cu electrode surface: strong corrosion; ∆m=0,23 mg, R=58 µm/a
4.17b. (below) Ni electrode surface: insignificant corrosion

As expected, at 80°C the corrosion effects are more pronounced as at 26 °C. In the case of the contact pair Cu/Ni in Q-brine (Table 4.5, no. 14/15) Ni is deposited on the Cu electrode (Figure 4.18a, b). Besides Ni, a layer of Ag is deposited like in some other experiments carried out at 80°C. The Ag deposition on the more negative metal, especially on Cu (Table 4.5, no. 10, 14, 16), is due to the complex formation of

$[AgCl_2]^-$, which happens to the AgCl of the reference electrode in concentrated NaCl-solution.

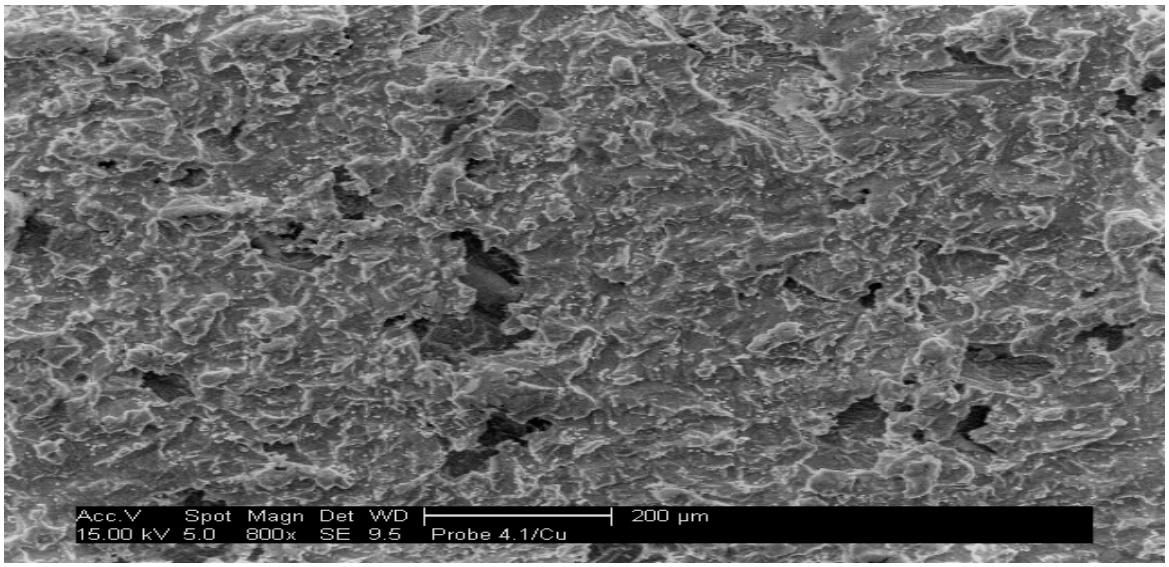

Fig. 4.18a: SEM micrograph of the Cu electrode surface of the couple Cu/Ni (Table 4.5, no. 14/15): strong corrosion, deposited layer and particles; Q-brine, T=80°C, t=100 h, Δm=0,79 mg, R=154 µm/a, E_c=-365 mV

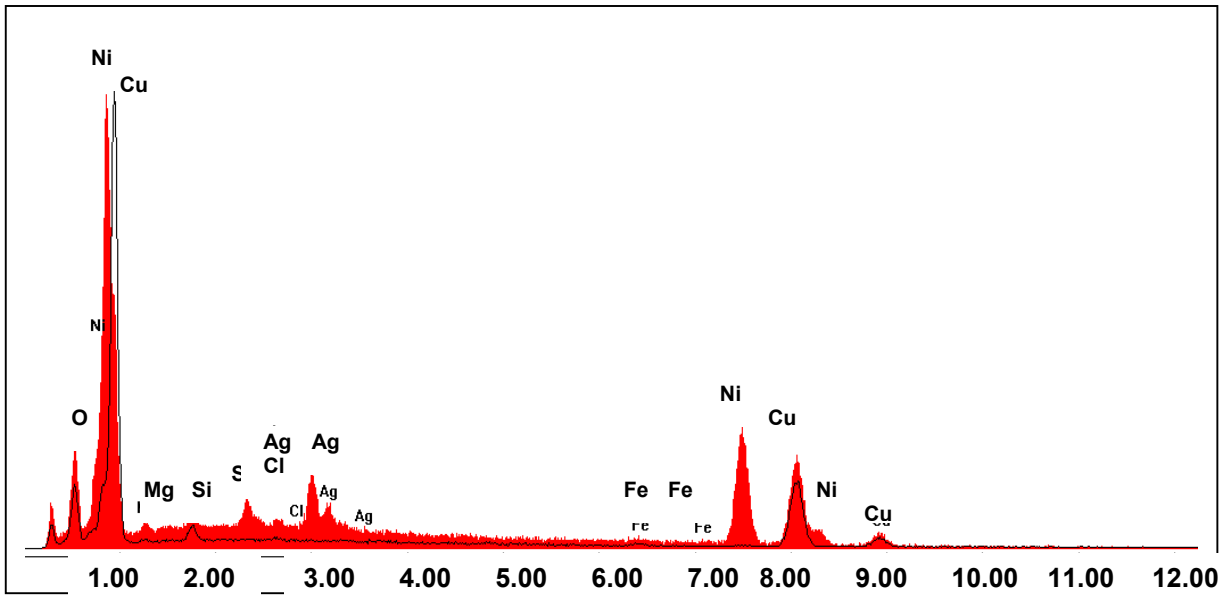

Figure 4.18b: EDX spectrum of the Cu electrode surface before (edged in black) and after (unedged) the electrochemical measurements

The results obtained from the surfaces analyses are in accordance with those from the electrochemical procedures performed at rest and at galvanic potentials. Especially, they confirm that under the experimemntal conditions applied, the Ni electrode is the positive partner and the Cu electrode the negative one. The surface

analysis results represent an addition and an enrichment to the electrochemical ones.

4.12 Conclusions

All the electrochemical and surface analytical investigations prove that the Cu-base materials exhitit a higher corrosion resistance than the TStE355 carbon steel in Q-brine and NaCl rich brine. In the case of galvanic corrosion, carbon steel is always the anode with respect to the Cu-base materials being the cathode.This means that the Cu-base materials will be cathodically corrosion protected by the carbon steel.

If Cu-Ni alloys will be selected as container materials, it must be taken into consideration that at lower temperature (25°C) Ni is more resistant to corrosion than Cu and its alloys due to the formation of a NiO passive layer and due to the relative negative potential of the Cu-base materials, because Cu forms a $[CuCl_2]^-$ -complex in Q-brine and NaCl-rich brine. At higher temperature (≥ 80°C) the opposite is true, because the NiO layer is destroyed, which drastically shortens the Ni passive range, the Ni potential being found in the transpassive range.

In general, the electrochemical experiments demonstrate that, especially, the corrosion of carbon steel is higher in Q-brine (pH = 4.6) than in NaCl-rich brine (pH = 6.5), because H_3O^+ is the dominant oxidant for carbon steel. On the other hand O_2 is the oxidant for the Cu-base materials, because the equivalent potential of H_3O^+/H_2 is shifted more to negative values due to Nernst. The Q-brine, therefore, is more aggressive than NaCl-rich brine.

But for all conclusions made it always must be kept in mind that electrochemistry describes corrosion only for the starting period of the corrosion process, and determines the initial corrosion rate. For the determination of the long-term corrosion behaviour and the final corrosion rate on the container materials long-term corrosion experiments are necessary, as were performed in this study.

The results from the investigation of the element composition and the morphology of corroded Cu, Ni and steel electrode surfaces by means of EPMA / EDX and SEM prove to be a confirmation of those obtained from electrochemical measurement.

5. LONG-TERM CORROSION STUDIES (IMMERSION EXPERIMENTS) IN GRANITIC ENVIRONMENTS (WP 2.1) (FZK.INE)

5.1 Materials and experimental

The long-term corrosion behaviour of the preselected TStE355 carbon steel and three Cu-base materials was investigated in disposal relevant granitic environments by using immersion experiments. The materials were examined in the hot-rolled and annealed condition and had the following composition in wt.%:

Steel: 0.17% C, 0.44% Si, 1.49% Mn, bal. Fe.
Cu: 99.9995 Cu; O: 0.0005
Cu-Ni 90-10: 88.5 Cu; 9.9 Ni; 1.3 Fe; Rest: C, Mn, P, S
Cu-Ni 70-30: 69.3 Cu; 29.3 Ni; 0.6 Fe; Rest: C, Mn, P, S

For the investigations, flat specimens having the dimensions 40 mm by 20 mm by 4 mm were used. All materials were examined in a granitic water having a moderate Cl^-

content of 98 mg/L and a pH value of 9.1 at 22°C (granitic water 1). This medium is typical for granitic formations in France, and is one of the reference media for the performance of corrosion studies on waste packages in the frame of European research programmes. In order to examine the influence of the Cl^- content of granitic water on the steel corrosion, this material was additionally investigated in a granitic water which was in contact with bentonite and had a very high Cl^- content of 6260 mg/L (granitic water 2). This medium is typical for granitic formations in Spain. The chemical composition of the two granitic waters is given in Tables 5.1 and 5.2.

Table 5.1: Composition of granitic water 1 (low Cl^- concentration) used in the long-term corrosion experiments (CEA reference water)

Ion	Concentration (mg/L)
Na^+	97.20
Ca^{2+}	2.30
K^+	4.60
Al^{3+}	1.40
Li^+	0.10
B^{3+}	0.08
Cl^-	98.10
HCO_3^-	25.60
$H_3SiO_4^-$	39.40
F^-	4.90

pH(22°C)=9.1

Table 5.2: Composition of granitic water 2 (high Cl^- concentration) used in the long-term corrosion experiments (CIEMAT reference water)

Ion	Concentration (mg/L)
Na^+	3883.0
Ca^{2+}	151.9
Mg^{2+}	577.7
K^+	20.8
Si	3.4
Cl^-	6258.5
SO_4^{2-}	1304.7
HCO_3^-	34.0
NO_3^-	111.4
Br^-	15.0

pH(22°C)=7.3

The specimens were investigated in the two granitic waters for up to 15 months at a temperature of 90°C which corresponds to the maximum surface temperature of the containers according to the disposal concepts in a granitic formation. For the experiments, stainless steels pressure vessels with corrosion-resistant polytetrafluorethylene (PTFE) inserts of 210 ml volume were used to avoid

evaporation of the granitic waters at the test temperature. Each PTFE insert contained 160 ml of corrosion medium and four specimens of 80 cm^2 total surface. The specimens were suspended by PTFE threads, which were fixed below the lid of the insert. After tightly closing the inserts, the vessels were stored in heated chambers at the test temperature of 90°C.

With these experimental equipment, the initial test conditions were oxidizing. The total amount of oxygen available in the system was about 16 mg, corresponding to 0.2 mg O_2/cm^2 specimen. It consisted of the oxygen content in the 50 ml of air space (15 mg O_2) above the granitic water and the dissolved oxygen (1 mg) in the 160 ml of granitic water. The latter was measured in the autoclaves before starting the experiments by a polarographic method using an O_2 sensor. The value determined at 25°C (6 mg of O_2/l) corresponds to the saturation value in air obtained by the Winkler method. In case of the steel, this oxygen amount was consumed very fast by reactions with Fe so that after a few days reducing conditions were established. In the experiments on the Cu-base materials the oxygen amount available in the autoclaves was slowly consumed by reactions with Cu and Ni that after about eight months test dutation reducing conditions were established. With these selected experimental conditions, an initial oxidizing disposal phase and a subsequent reducing disposal phase were simulated. Evaluation of the specimens regarding general and local corrosion was carried out by gravimetry, measurements of pit depth, surface profilometry and metallography.

5.2 Results on carbon steel

The general corrosion of the TStE355 carbon steel in the granitic waters 1 and 2 was determined from the weight losses of the specimens and the material density. Figures 5.1 and 5.2 show the time-dependence of the general corrosion of the steel, expressed as the integral thickness reduction of the specimens, in the granitic waters at 90°C. The data indicate that the general corrosion of the steel in both test media increases linearly with the exposure time over the test duration of the study. The linear corrosion rates of the steel in the granitic waters, calculated from the slope of the curve, and the results of the local corrosion determined by surface profilometry and metallography are compiled in Table 5.3. It is evident from Table 5.3 that the linear corrosion rate of the TStE355 carbon steel in both granitic waters is low (21.1 µm/a and 22.6 µm/a, respectively). The reason for the small general corrosion rates of the steel in both corrosion media is the formation of a tight protecting corrosion layer on the specimens surface. This black corrosion layer was identified by X-Ray Diffraction (XRD) analysis as Fe_3O_4 (magnetite). However, in the granitic water with a high Cl^- concentration of 6260 mg/L (granitic water 2) the corrosion surface layer broke down locally, resulting to severe pitting corrosion with a maximum depth of up to 1200 µm after 300 days test duration. On the contrary, in the granitic water with a low Cl^- concentration of 98 mg/L (granitic water 1), a very few small pits of about only 60 µm at the maximum were detected after 300 days exposure to the medium.

On the base of the results obtained in this study it can be stated that the TStE355 carbon steel is a potential HLW container material only for granitic formations in which the groundwater has a low Cl^- content. Furthermore, it can be stated that the corrosion behaviour of the steel in granitic environments with high Cl^- content is

different as that in high concentrated salt brines, in which only non-uniform corrosion and not pitting corrosion was obtained [4].

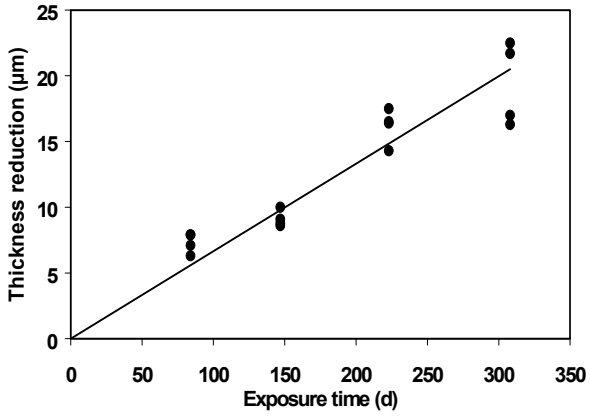

Figure 5.1: Time-dependence of the thickness reduction of the TStE 355 carbon steel in granitic water 1 at 90°C (98 mg/L Cl^-)

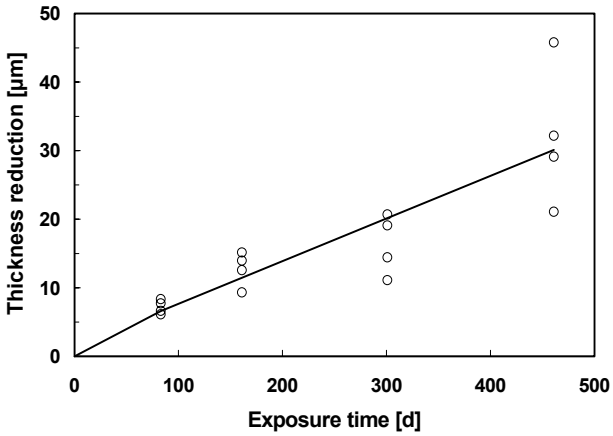

Figure 5.2: Time-dependence of the thickness reduction of the TStE355 carbon steel in granitic water 2 at 90°C (6260 mg/L Cl^-)

Table 5.3: Corrosion results obtained for the TStE355 carbon steel in granitic waters at 90°C (V/S = 2ml/cm^2)

Granitic water 1 (98 mg/L Cl^-)			Granitic water 2 (6260 mg/L Cl^-)		
Exposure time (d)	Linear corrosion rate (µm/a)	Max. pit depth (µm)	Exposure time (d)	Linear corrosion rate (µm/a)	Max. pit depth (µm)
84	21.1±2.1	25	83	22.6±3.6	250
147		50	161		900
223		60	300		1200
308		60	460		1300

5.3 Results on Cu-base materials

Up to about 240 days test duration the measured redox potentials (Eh) at 40°C were +150 to +170 mV which indicates that up to this time oxidizing conditions were available in the experimental system. After longer test duration reducing conditions were established and the measured redox potentials amounted -80 to -100 mV. After the conclusion of the corrosion experiments (maximal test duration 430 days), the measured pH values of the granitic water at 21°C were 9.8-10.2, and, therefore, higher than the initial value of 9.1.

The general corrosion of the three Cu-base materials in the granitic water was determined from the weight losses of the specimens and the material densities. Figures 5.3- 5.5 show the time-dependence of the general corrosion of the individual materials, expressed as the integral thickness reduction of the specimens, in the granitic water at 90°C. The slope of the curves indicates that up to 240 days exposure to granitic water the corrosion rates are relatively high. After longer exposure time, the corrosion rates decrease and reach low values. The decrease in the corrosion rates of the Cu-base materials after longer test duration is attributed to the establishment of reducing corrosion conditions, to the increase of pH value of the corrosion medium, and to the formation of tighter corrosion protecting oxide layers on the specimens surface.The computation of the Eh-pH diagramme for Cu in the granitic water used in these experiments shows that under the long-term conditions established in this study (Eh=-80 to –100, pH=9.8-10.2), the Cu-oxide Cuprite (Cu_2O) is formed. The Eh-pH diagramme was computed by “The Geochemist’s Workbench” software [28] applying the “com.V8.R6” database of EQ3/6 [29].

The integral corrosion rates of the materials in the granitic water, calculated from the integral thickness reduction of the specimens and the exposure time to the corrosion medium (Figs. 5.3-5.5), are compiled in Table 5.4. The data indicate that the corrosion rates are very low (1.1 µm/a-6.4 µm/a). The reasons for this are Eh, pH, and the formation of corrosion protecting surface layers, as discussed above. However, after longer test duration the corrosion surface layer of pure Cu broke down locally. This did not result in a noticeable increase in the integral weight losses (general corrosion) of the Cu-specimens, as shows the low integral corrosion rate. However, it resulted to severe pitting and intergranular corrosion with a maximum depth of up to 600 µm after 430 days test duration. For the alloys Cu-Ni 90-10 and Cu-Ni 70-30 only small pits were odserved which after longer test duration grew together resulting in a non-uniform general corrosion of only 40-50 µm depth after 430 days test duration.

In general it can be stated that under the test conditions applied the alloys Cu-Ni 90-10 and Cu-Ni70-30 exhibit a higher resistance to pitting and intergranular corrosion in the test granitic water than pure Cu.

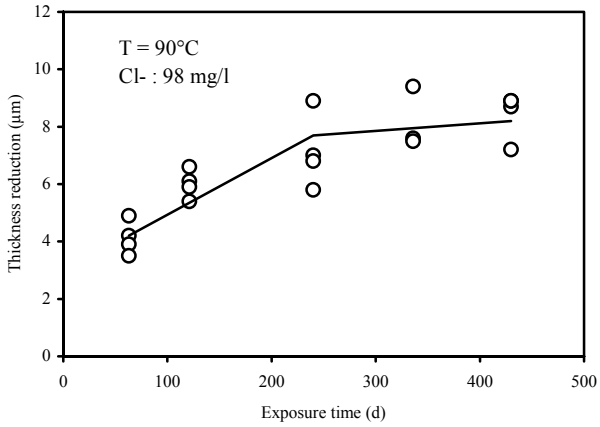

Figure 5.3: General corrosion of Cu in granitic water at 90°C

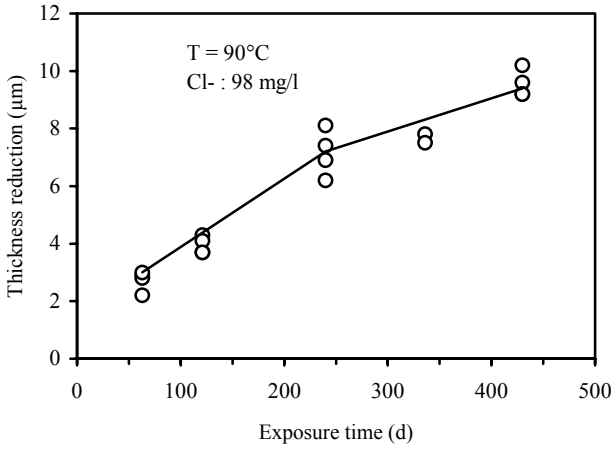

Figure 5.4: General corrosion of Cu-Ni 90-10 in granitic water at 90°C

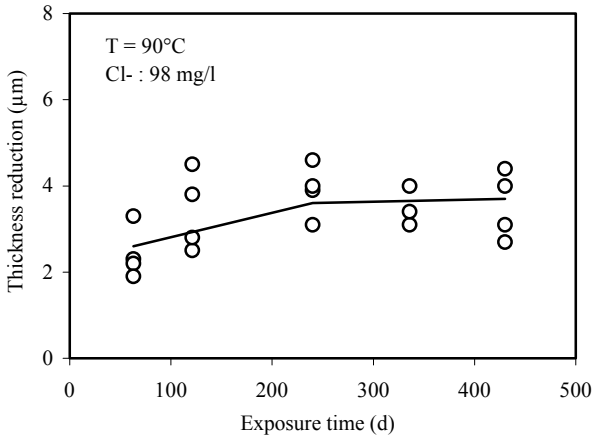

Figure 5.5: General corrosion of Cu-Ni 70-30 in granitic water at 90°C

Table 5.4: Corrosion rates of Cu-base materials in granitic water (Cl^-: 98mg/L) at 90°C

Material	Test time (d)	Integral corrosion rate (µm/a)
Cu	430	4.3 ± 0.5
Cu-Ni 90-10		6.4 ± 0.4
Cu-Ni 70-30		1.1 ± 0.5

5.4 Conclusions

The corrosion results obtained from the long-term immersion experiments in synthetic granitic waters at 90°C (initial oxidizing conditions) can be concluded as follows:

- In the granitic water having the low Cl^- content (98 mg/L) and pH=9.1, the TStE355 carbon steel performs well as HLW/Spent Fuel container material. Under the test conditions applied it is resistant to pitting corrosion and its general corrosion rate is small.

- In the granitic water having the high Cl^- content (6258 mg/L) and pH=7.3, the steel suffers from severe pitting corrosion.

- The general corrosion rates of Cu, Cu-Ni 90-10 and Cu-Ni 70-30 in the test granitic water (98 mg/L Cl^-, pH=9.1) are small (1-7 µm/a). Furthermore, the alloys Cu-Ni 90-10 and Cu-Ni 70-30 are resistant to localized corrosion. However, Cu is susceptible to pitting and intergranular corrosion.

6. STRESS CORROSION CRACKING, ELECTROCHEMICAL AND CREVICE CORROSION STUDIES IN GRANITIC ENVIRONMENTS (WP 2.2 AND WP 2.3) (ENRESA/INASMET)

In the Spanish reference disposal concept in a granitic formation the containers will be surrounded by a clay barrier constructed of compacted bentonite blocks. Under these disposal conditions, general and localized corrosion can occur.

In these studies, the susceptibility of three candidate container materials to certain localized corrosion modes in a simulated granitic-bentonite water has been assessed. The studied localized corrosion phenomena are Stress Corrosion Cracking (SCC), pitting, crevice corrosion and Microbiologically Induced corrosion (MIC). The container materials investigated are the higher corrosion resistant nickel base material Hastelloy C-22 (HC-22) and the intermediate corrosion resistant Cu-OF and Cu30Ni (cuprinickel alloy Cu-Ni 70-30). Besides the parent metal, welded specimens provided with possible container closure techniques were examined.

The materials were investigated under conditions of temperature and water chemistry relevant to the repository setting. The SCC resistance has been evaluated by means of the Slow Strain Rate Testing (SSRT) technique. Potentiodynamic polarization has been applied as electrochemical technique in order to obtain information on the corrosion rate, pitting susceptibility and passivity of the studied alloys in the granitic-bentonite medium. Electrochemical tests with Sulphate Reducing Bacteria (SRB) have been performed in order to determine the MIC resistance of the materials. The crevice corrosion behaviour has been evaluated creating artificial crevice assemblies on test specimens. Finally, the effects of chloride ion concentration and temperature have also been investigated.

6.1 Materials characterization

The three investigated materials were delivered in the hot rolled and normalized condition as plates (13-15 mm thickness) and bars (30 mm diameter). The materials were characterized by means of tension testing and hardness tests, chemical analysis and metallographic examinations. The chemical composition and the mechanical properties of the materials are given in Tables 6.1 and 6.2 The chemical composition slightly varies for different product forms of the same alloy.

The metallographic examinations show for the HC22 alloy an austenitic structure with maclas formation (Figure 6.1). CuOF and Cu30Ni show a recrystalized equiaxic structure with some maclas. In the case of the pure copper, significant differences in the grain size are seen between the plate and the bar condition, Figure 6.2.

Besides the parent metal, Electron Beam Welding (EBW) and Gas Tungsten Arc Welding (GTAW) procedures were considered for the three candidate materials. Figure 6.3 shows a GTA welded joint performed for the HC22 alloy.

Vickers microhardness tests performed along the welded joints indicate a coherent slight increase in the hardness value measured in the Heat Affected Zone (HAZ) and in the weld bead, in comparison with the values obtained for the base material.

Table 6.1: Chemical composition of the materials studied

Weight Composition (%)	HC22 (UNS N06022)		CuOF (UNS C10200)		Cu30Ni (UNS C71500)	
	Plate	Bar	Plate	Bar	Plate	Bar
Ni	*Base*	*Base*	<0.01	<0.01	30.2	30.0
Cr	21.8	21.6				
Mo	13.3	13.0				
W	3.0	3.0				
Fe	2.8	2.9	<0.01	<0.01	0.65	0.73
Cu	0.03	0.08	*Base*	*Base*	*Base*	*Base*
Co	0.38	0.95				
Al	0.22	0.19			<0.01	<0.01
V	0.16	0.14				
C	0.014	0.003			0.005	0.020
Mn	0.22	0.26	<0.01	<0.01	0.69	0.68
P	0.01	<0.01	<0.01	<0.01	<0.01	0.01
O			0.019	0.027	0.006	0.005

Table 6.2: Mechanical properties of the materias studied. Test specimens were taken from plate Longitudinal(L) andTransversal(T)

Alloy		Yield Strength (MPa)	Max. load (MPa)	Elongation (%)	Hardness (HV 10Kg)
CuOF	L	261	266	24	97
	T	268	283	25	
Cu30Ni	L	138	367	49	86
	T	121	362	49	
HC22	L	370	755	76	181
	T	381	730	73	

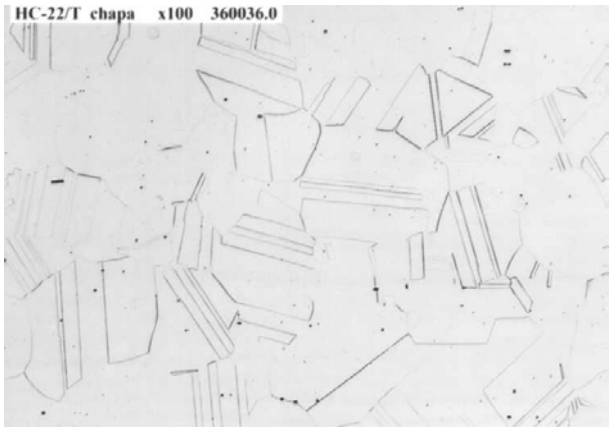

Figure 6.1: Optical micrograph of transversal section
of HC22 specimen taken from plate.

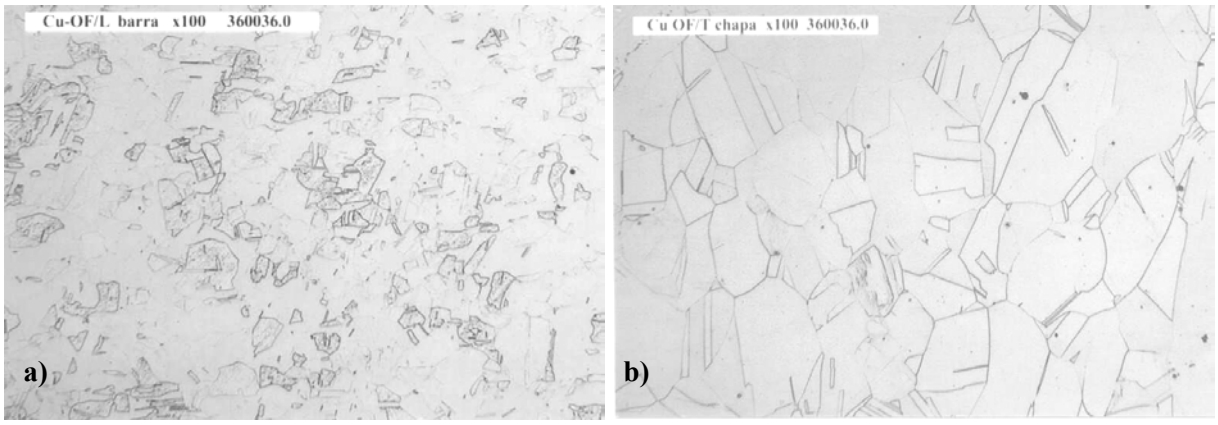

Figure 6.2: a) Optical micrograph of a longitudinal section of CuOF specimen taken from bar.
b) optical micrograph of transversal section of CuOF specimen taken from plate.

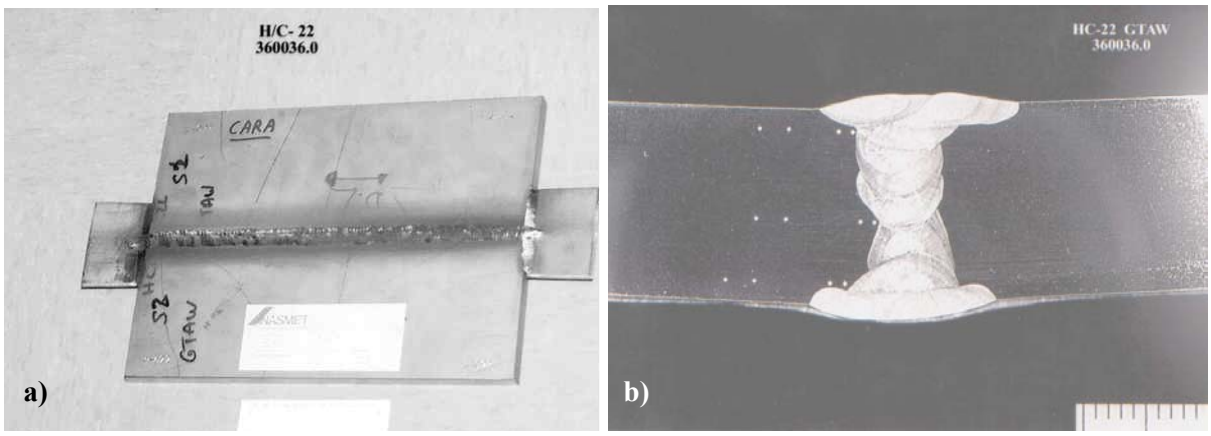

Figure 6.3: a) GTA welded joint in HC22 plate, b) cross section of the former HC22 GTA welded joint after polishing and metallographic etching.
Several Vickers microhardness chains are seen along the welded joint.

6.2 Corrosion environment

The composition of the synthetic granitic-bentonite water used for the experiments is given in Table 6.3. This water results from granitic groundwater diffusion through the clay bentonite barrier [30,31]. Different chloride concentrations ranging from 6500 to 50000 mg/L Cl^- were used, in order to investigate the effect of chloride on the corrosion resistance of the materials. When evaluating the MIC-resistance of the materials, anaerobic SRB were inoculated to the granitic-bentonite medium. SRB are commonly present in Spanish bentonite [31]. The tests were performed at 90ºC, except of the electrochemical corrosion studies, in which also the effect of a lower temperature of 25ºC, was evaluated. Both in the electrochemical and SSR tests, deaereated granitic water was used as corrosion medium. Only in the crevice corrosion experiments a limited amount of oxygen was present.

Table 6.3: Composition of simulated granitic-bentonite water.

Parameter	Composition (mg/L)
Cl^-	6550 – 50000
NO_3^-	110
SO_4^{2-}	1500
HCO_3^-	27
SiO_2	8.3
Br^-	15
Ca^{2+}	135
K^+	20
Mg^{2+}	600
Na^+	3750
pH (25ºC)	7.3

6.3 Experimental setup

6.3.1 Stress corrosion cracking studies

This localized corrosion mode requires the simultaneous action of a corrodent and a sustained tensile stress (applied or residual stress). In these studies, the susceptibility to SCC was studied by means of the Slow Strain Rate Technique (SSRT). A tensile specimen, in contact with a specific environment, is continuously strained in tension until fracture. Tests are conducted according to the requirements described in ISO 7539-7 [32] and ASTM G 129 [33].

The testing equipment consisted of constant extension rate tensile testing machines of 50 KN capacity and selectable crosshead speed within the range of 0.1 to 10^{-6} mm/s. Round tensile specimens of 6 mm diameter and 30 mm gauge length were

machined. In the case of welded joints, specimens were taken in the transverse sense.

The specimens were tested in deaerated granitic-bentonite water at 90ºC and strain rates ranging from 10^{-5} to $2x10^{-7}$ s^{-1}. In order to be able to interpret the results obtained in tha granitic environment, additional comparative investigations were also carried out in argon as inert reference medium. Choosing an appropriate strain rate is of a great importance because at sufficiently high and/or low strain rates SCC could not be observed. For steels, copper and nickel alloys strain rates between 10^{-5} to 10^{-7} are considered the most suitable ones [34]. After each test, the elongation, reduction of area, maximum load and true stress at fracture were measured in order to assess the ductility and mechanical strength of the materials. This was complemented by metallographic studies performed by optical microscopy in order to identify secondary cracks, and fractographic analysis with the aim of evaluating the morphology of cracking. Ductility parameters, secondary cracks and failure mode provide relative measures of the susceptibility to stress corrosion cracking.

6.3.2 Electrochemical corrosion studies

Potentiodynamic polarization is the electrochemical technique used in order to obtain information on the corrosion rate, pitting susceptibility and passivity of the investigated materials. The potentiodynamic tests were conducted according to ASTM G-59 standard [35], and ISO/CD 17475 Test Method [36], in a electrochemical glass cell which contained both the metal to be investigated, and the environment in which the polarization scan was going to be performed (Figure 6.4). The corrosion cell had ports through which the working electrode (test specimen), the platinum counter and a salt bridge connected to a Saturated Calomel reference Electrode (SCE) were inserted. An external heater was used to maintain the desired temperature. During the test, argon was continuously bubbled into the solution in order to create a deaerated solution. The test specimens measuring 15 mm in diameter and 2 mm thickness, with a 600 grit finish, were mounted in a Teflon holder, leaving a final area of $1cm^2$. The tests were performed in the granitic-bentonite water having chloride concentrations of 6,500, 15,000 and 50,000 mg/L, at 25°C and 90°C.

To control the potential and to measure the current, a potentiostat was used. Prior to the start of each test the E_{corr} of the specimen was measured. The potential scan started from a potential -200 mV below E_{corr} and was increased at a rate of 0.167 mV/s. Once the current density reached a value of 10 mA/cm^2 or 2 V, the direction of the potential scan was reversed at the same scan rate. The results were plotted as a polarization curve of potential (V) vs. current density (Amp/cm^2). From this curve the corrosion potential E_{corr}, and the pitting potential E_{pit}, can be obtained. The value of E_{pit} denoted the electrochemical potential at which the applied current rapidly increased indicating the possibility of pit initiation. The general corrosion rates were calculated with the Lineal Polarization Resistance (LPR) method according to specifications provided in ASTM G-102 [37]. The tested specimens were inspected using lens amplification in order to evaluate the corrosion damage.

Electrochemical tests with bacteria were also conducted in electrochemical glass cells (Figure 6.5). Two different media were used: 1) "*Sterile"* deaerated granitic water and 2) deaerated granitc water with inoculation of sulphate-reducing bacteria

(SRB). In both media, the chloride content was 6,500 mg/L. Because anaerobic SRB have a survival range between 10°C and 50°C [38] the tests were conducted at 25°C- 27°C. Potentiodynamic tests, according to ASTM G-59 standard, were performed in both media after 35 and 60 days exposure. The general corrosion rates were calculated with the LPR method. The tested specimens were analyzed by optical and Scanning Electron Microscopy (SEM). In addition, an analysis of the biofilm and corrosion products was performed by Energy Dispersive X-Ray (EDS.

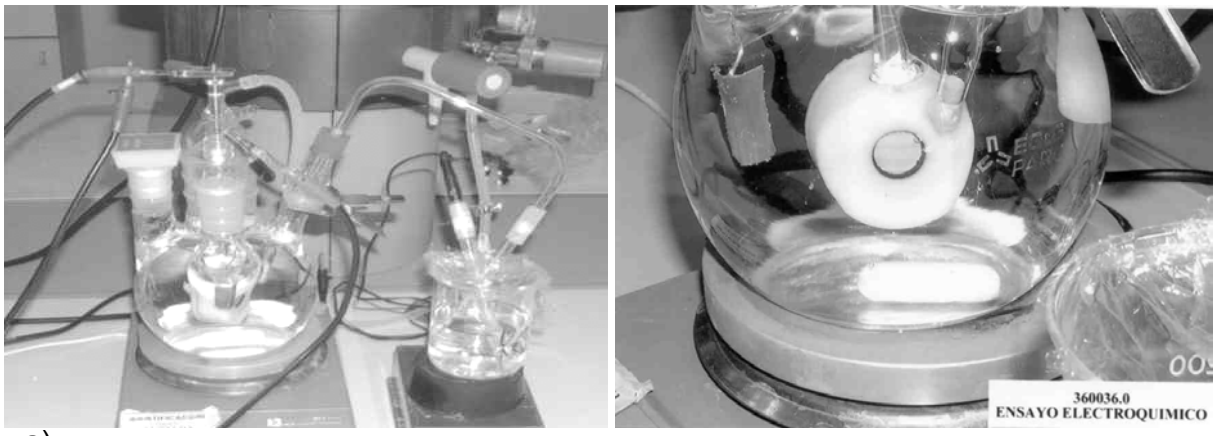

a) b)

Figure 6.4: a) Configuration of corrosion cell, b) detail of working electrode.

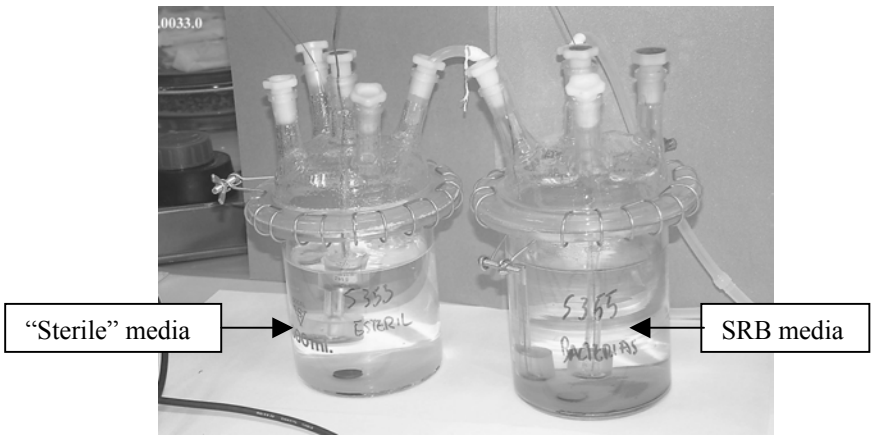

Figure 6.5. Corrosion cell configuration in the electrochemical tests with bacteria.

6.3.3 Crevice corrosion studies

Crevice corrosion occurs when a portion of a metal surface is blocked in such a way that the shielded portion has limited access to the surrounding environment. This results in the establishment of an oxygen (aeration) differential cell, in which the freely exposed area becomes cathodic in relation to the anodic occluded area. Once the differential aeration cell starts, the electrolyte inside the damper, becomes increasingly more acidic due to water dissociation, and enriched in chlorides. Chlorides migrate inside the crevice in order to maintain charge neutrality. This accelerates the corrosion or dissolution of the metal in the crevice with respect to the general corrosion observed in "freely" exposed areas.

In order to evaluate the crevice corrosion sensitivity of the materials, “crevice assemblies” were formed by bolting together flat metal test specimens with crevice formers made of Teflon, according to ASTM standard G-78 [39]. Figure 6.6 shows the crevice corrosion assembly and one Teflon gasket used in the tests. The resulting assemblies were immersed in autoclaves containing the granitic-bentonite solution with different chloride contents ranging from 6,500 to 50,000 mg/L. The tests were conducted at 90°C, and the test duration was 1, 6 and 12 months. Welded and unwelded specimens were examined.

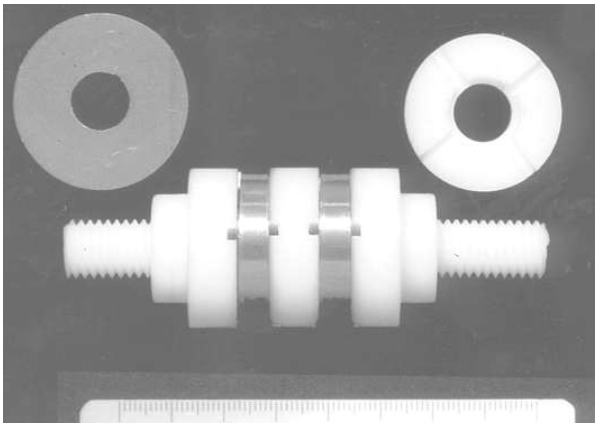

Figure 6.6: Crevice corrosion assembly showing metal specimens and Teflon gaskets

6.4 Results of stress corrosion cracking studies

6.4.1 Hastelloy C-22 (HC22 alloy)

No loss of ductility or mechanical strength was observed for HC22 specimens when tested in the granitic-bentonite environment compared to the results obtained in argon, as it can be seen from the data plotted in Figure 6.7. Furthermore, no secondary cracking was observed at any of the testing conditions both for the parent and welded HC22 alloy, thus indicating no effect of the welding procedure on the excellent resistance of HC22 alloy to stress corrosion cracking (SCC) at the specified test conditions. Figure 6.8a compares two HC22 specimens tested in the granitic and in the reference argon environment. As it can be seen, no differences were detected between the two media.

Fractographic studies on tested specimens show totally ductile fracture surfaces (Figure 6.8b) with dimples formation for the specimens tested in argon and in the granitic water, even at the highest chloride content.

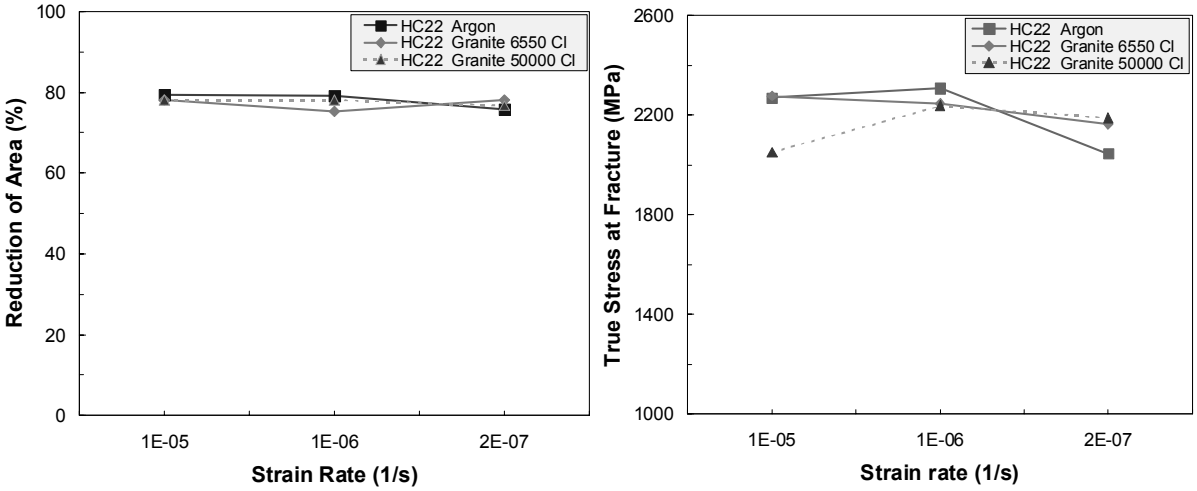

Figure 6.7: Reduction of area and true stress at fracture versus strain rate for the HC22 alloy tested at 90ºC in granitic-bentonite water and in argon.

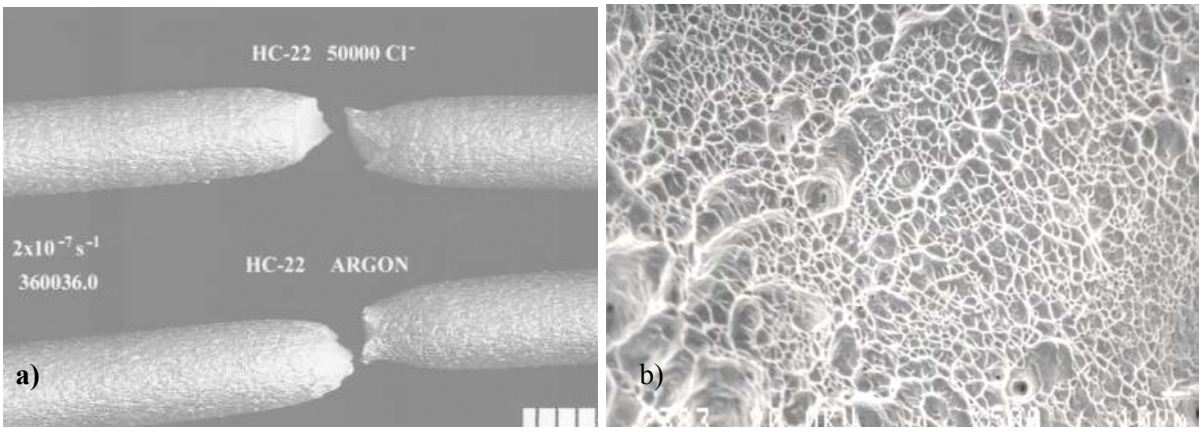

Figure 6.8. a) Macrograph of two HC22 tensile specimens tested at 90ºCand a strain rate of $2x10^{-7}s^{-1}$ in argon and granitic water (50,000 mg/L Cl^-) b) SEM micrograph of the fracture surface of the previous HC22 specimen tested in granitic water.

6.4.2 Copper (CuOF)

The values obtained from the slow strain rate tests carried out in the granitic-bentonite water on CuOF specimens are very close to those in argon, thus indicating no effect of the granitic water on the ductility and strength behaviour of the CuOF specimens. The reduction of area values versus strain rate for CuOF specimens tested in argon and in granitic water are shown in Figure 6.9. The significant drop in the reduction of area, in both environments, with decreasing strain rate, is due to a hardening straining phenomenon mainly attributed to the degree of work hardening, and not to environmental conditions.

No secondary cracks were observed in the metallographic studies at any of the testing conditions(Figure 6.10a). The fractographic examinations show an increase in the brittle feature of the specimens tested in both media, with decreasing strain rate. At the lowest strain rate, a totally brittle fracture surface was observed for specimens tested both in argon and in the granitic-bentonite environment(Figure 6.10b). Again,

this brittle nature is attributed to the degree of work hardening. Tests carried out on GTA welded CuOF specimens indicate no effect of the welded joint on the corrosion resistance of CuOF to SCC. No secondary cracking and no loss of ductility or mechanical strength was observed for CuOF welded specimens when tested in the granitic environment, with respect to the results obtained in argon.

Additionally, in order to evaluate the effect of the hardness on the SCC resistance, a CuOF alloy with an initial hardness value of 97 HB has been soften by annealing. After the heat treatment (525ºC/6 hours), the CuOF had a final hardness of 49 HB. The results obtained from the SSR tests of this"soften" CuOF indicate no loss of ductility or mechanical strength for specimens tested in granitic-bentonite water with 50,000 mg/L chloride, with respect to values obtained in argon. With respect to hard copper, soften copper shows, consequently, higher ductility and lower mechanical properties, as it is given in Table 6.4. Metallographic examinations of soften CuOF specimens show, both for the argon and the granitic bentonitic medium, a certain kind of crack initiation, which is attributed to the heat treatment performed. Figure 6.11 shows optical micrographs of hard (97HB) and "soften" (49HB) CuOF specimens tested at 90°C and a strain rate of $2x10^{-7}$ s^{-1} in granitic water containing 50,000 mg/L Cl^-.

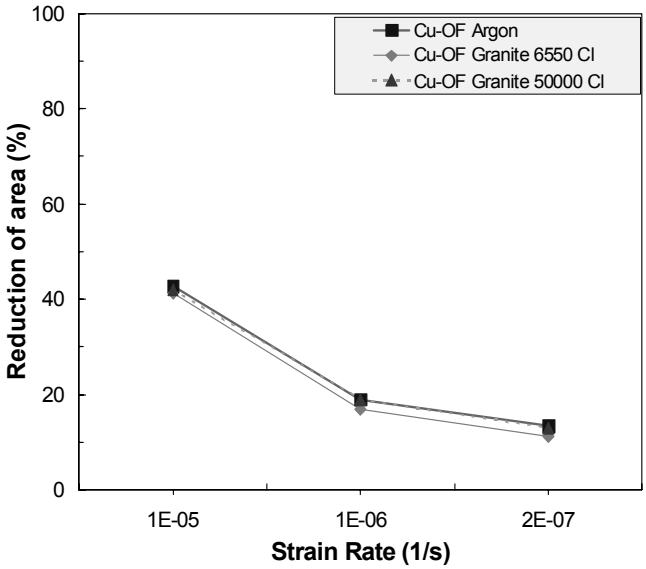

Figure 6.9 Reduction of area values versus strain rate for CuOF specimens tested at 90ºC in argon and in granitic water having different chloride contents.

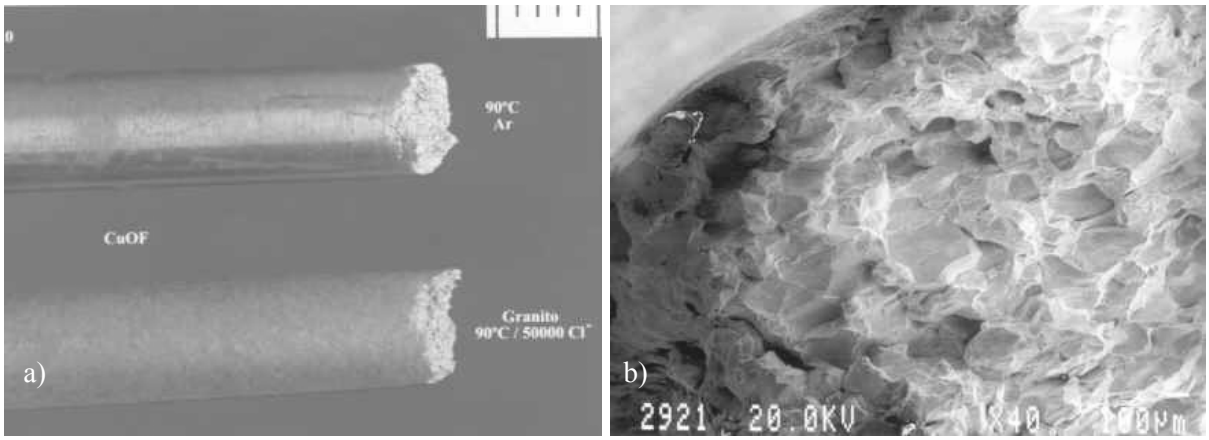

Figure 6.10: a) Macrograph of two CuOF specimens tested at 90ºC and a strain rate of $2x10^{-7}s^{-1}$ in argon and in granitic water having 50,000 mg/L Cl^-
b) SEM micrograph of the fracture surface of the previous CuOF specimen tested in granitic water.

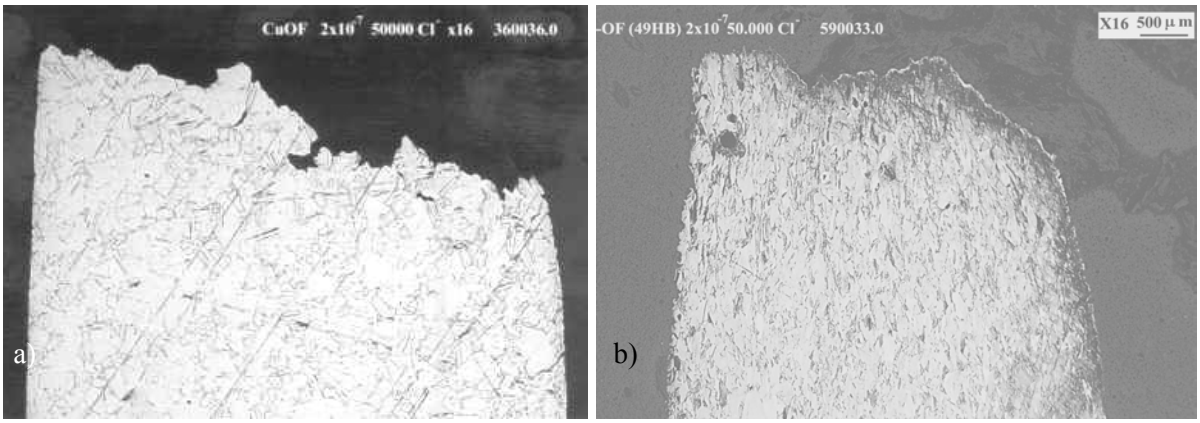

Figure 6.11: Optical micrographs of hard (97HB) and annealed (49HB) CuOF tested at 90ºC and a strain rate of $2x10^{-7}s^{-1}$ in granitic water (50,000 mg/L Cl^-)

Table 6.4: SSRT data for CuOF specimens of different hardness values obtained in granitic water (50,000 mg/L Cl^-) at 90°C and a strain rate of $2x10^{-7}s^{-1}$

	CuOF Half-hard condition (initial)	CuOF annealed (525ºC/ 6 h)
Hardness Brinell (HB)	97	49
Elongation (%)	8.4	46
Reduction of area (%)	13	64
Yield strength (MPa)	186	81
Maximum load (MPa)	220	163
True stress fracture (MPa)	221	330
Time to fracture (h)	130	936
Secondary cracking	None	Shallow cracks
Fracture mode	Brittle	Ductile + Brittle

6.4.3 Cu30Ni alloy

A summary of the results obtained for the Cu30Ni alloy in the SSR tests is given in Table 6.5. Compared to the values in argon, no loss of ductility is noticed for the cupronickel alloy when tested at 90ºC in the chloride containing granitic-bentonite environment.

Table 6.5: Summary of SSRT data obtained for the Cu30Ni alloy at different strain rates and 90ºC in argon and granitic water. D=Ductile, I= Intergranular.

Cu30Ni	Argon $10^{-6}s^{-1}$	6500 Cl^- $10^{-6}s^{-1}$	50000 Cl^- $10^{-6}s^{-1}$	Argon $2x10^{-7}s^{-1}$	6500 Cl^- $2x10^{-7}s^{-1}$	50000 Cl^- $2x10^{-7}s^{-1}$
Elongation (%)	52	49	48	53	54	53
Reduction of area (%)	69	69	70	74	72	69
Yield strength (MPa)	119	110	118	157	145	134
Maximum load (MPa)	307	306	303	344	321	319
True stress at fracture (MPa)	726	716	717	895	782	692
Time to rupture (hr)	155	148	143	795	878	789
Maximum crack penetration (µm)	-	65	120	-	80	120
Fracture mode	D	D + I	D + I	D	D + I	D + I

However, the metallographic studies revealed shallow secondary cracks when tested of strain rates of 10^{-6} and $2x10^{-7}s^{-1}$, thus indicating a slight sensitivity to SCC at very slow strain rates under the test conditions applied. Two representative micrographs are shown in Figure 6.12. In the granitic environment containing 50,000 mg/L chloride, the deepest secondary crack measured on longitudinal sections of the gage length was 120 microns. When testing in granitic water containing 6500 mg/L chloride, the maximum crack depth was 80 microns. For the two above-mentioned strain rates, the crack density and the maximum crack length values were similar.

Fractographic examinations of tested specimens show, in general, a ductile failure mode. In the case of specimens tested in the granitic-bentonite environment, small brittle intergranular areas in the edge of the fracture surface were observed, as it can be seen in Figure 6.13.

Tests carried out on welded Cu30Ni specimens revealed also a slight secondary cracking in the base material when tested in the granitic-bentonite medium at strain rates of $10^{-6}s^{-1}$ and $2x10^{-7}s^{-1}$. The maximum crack length values and the crack density were similar to that obtained for unwelded specimens, thus indicating no effect of the welding procedure on the SCC behaviour of the cupronickel alloy.

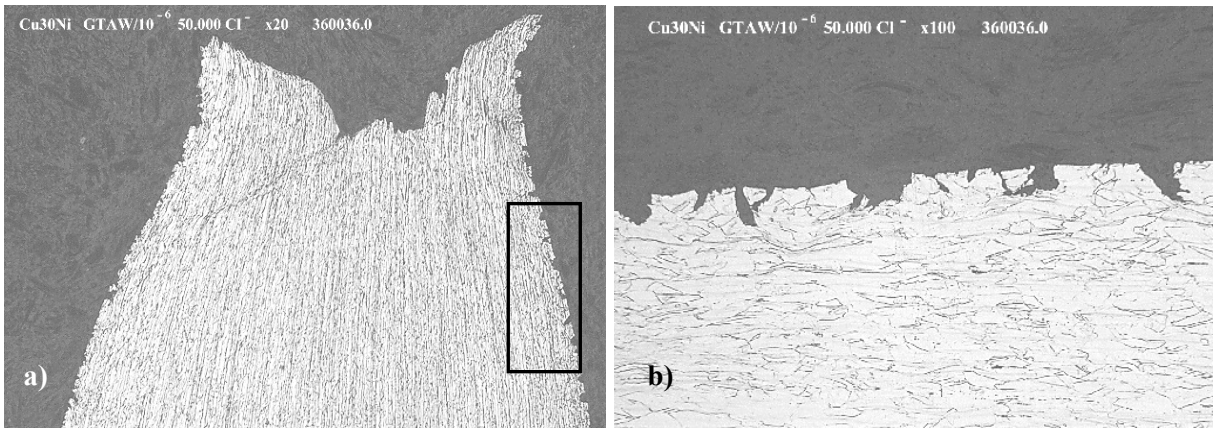

Figure 6.12: Optical micrographs of a GTA welded Cu30Ni specimen tested at 90ºC and a strain rate of 10^{-6} s^{-1} in granitic water containing 50,000 mg/L Cl^-

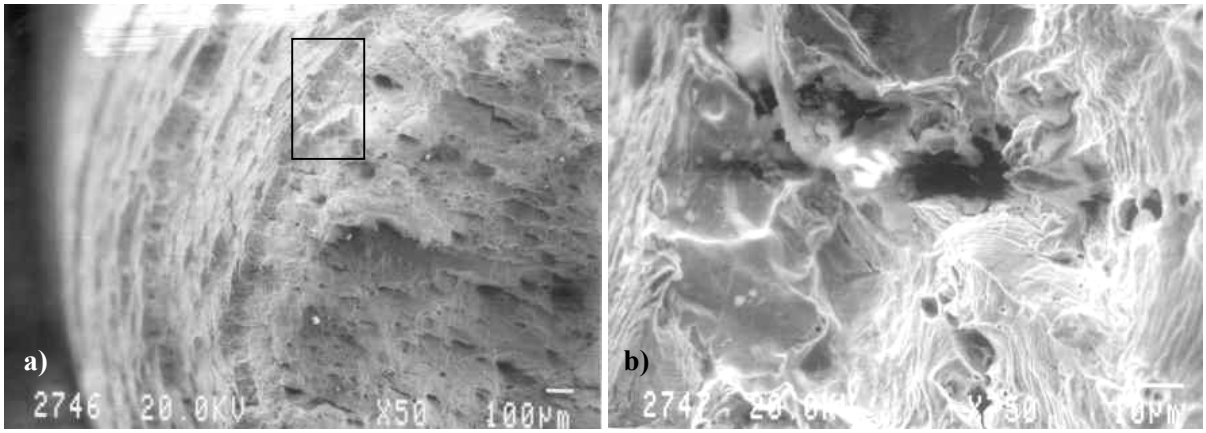

Figure 6.13: SEM micrographs of the fracture surface of a Cu30Ni specimen tested at 90ºC and a strain rate of $2x10^{-7}s^{-1}$ in granitic water (50000 mg/L Cl^-).

6.5 Results of electrochemical corrosion studies

The corrosion data obtained from polarization curves of the three materials in deaerated granitic water at 25°C and 90°C, and chloride contents between 6,500 and 50,000 mg/L are summarized in Table 6.6. For CuOF and Cu30Ni it was observed, in general, that an increase of the chloride concentration increases the general corrosion. It should be noted that in the case of passivation of the material, pitting or some other type of localized corrosion, the estimation of the corrosion rate according to ASTM G-102 is not representative. The calculation of the uniform corrosion rates from electrochemical tests is useful in the case of materials with high or intermediate general corrosion rates.

Table 6.6: Summary of corrosion data obtained from electrochemical polarization tests

MATERIAL	Cl^- (mg/L)	Ecor (V)		Corr.rate (μm/year)		Surface appearance	
		25ºC	90ºC	25ºC	90ºC	25ºC	90ºC
CuOF	6550	-0.28	-0.51	11	13	General corrosion (GC)	
	15000	-0.34	-0.37	14	70	GC	
	50000	-0.32	-0.42	86	140	GC	
CuOF-EBW	50000		-0.37		509	GC	
CuOF-GTAW	50000		-0.36		805	GC	
Cu30Ni	6550	-0.26	-0.33	21	70	Bright / light scale	
	15000	-0.20	-0.38		70	GC/dealloying	light scale/GC
	50000	-0.35	-0.40	65	390	GC/dealloying	light scale/GC
Cu30Ni-EBW	50000		-0.40		87	-	light scale/GC
Cu30Ni-GTAW	50000		-0.39		44	-	light scale/GC
HC22	6550	-0.41	-0.30	<10	15	Bright / slight tarnishing	
	15000	0.37	-0.35	<10	18	Bright / slight tarnishing	
	50000	0.25	-0.33	<10	14	Bright / slight tarnishing	
HC22-EBW	50000		-0.17			Bright / slight tarnishing	
HC22-GTAW	50000		-0.25			Bright / slight tarnishing	

The polarization curves for the three investigated materials, are given in Figures 6.14-6.16. No susceptibility to pitting corrosion was observed for all materials, in their parent and welded state, at any of the tested conditions. Visual and optical examinations of tested specimens, Figures 6.14-6.16 corroborate the results obtained in the potentiodynamic tests. No pits are detected at any testing conditions. Generalized corrosion is observed on the surface of copper alloys. In the case of the Cu30Ni alloy sometimes a slight dealloying corrosion was observed (Figure 6.15b). For the HC22 alloy a very thin passive oxide film or tarnishing was observed. No pitting corrosion was observed on the welded specimens.

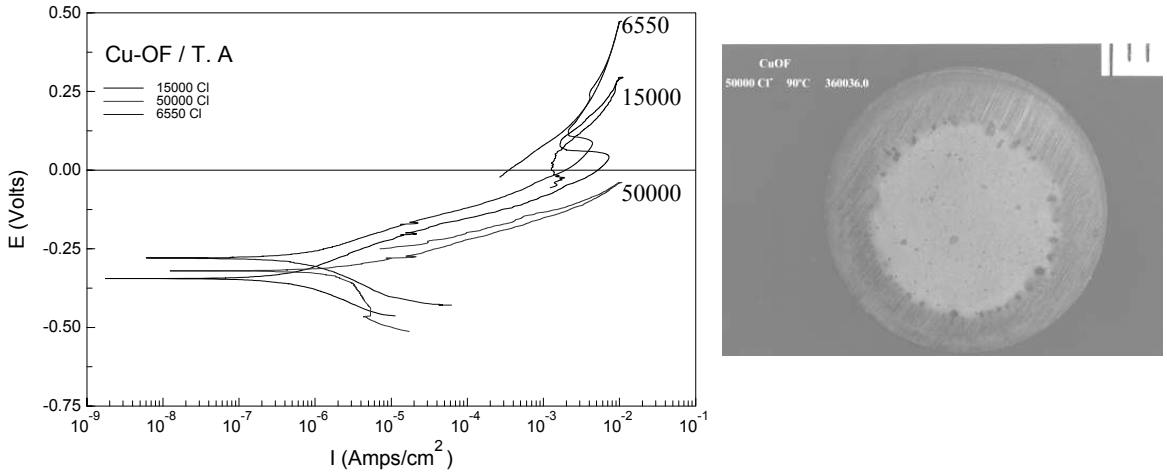

Figure 6.14: (a) left side: Polarization curves for CuOF alloy tested at 25ºC in granitic water with different chloride contents. (b) right side: CuOF specimen after polarization test in granitic water (50000 mg/L Cl^-) at 90ºC.

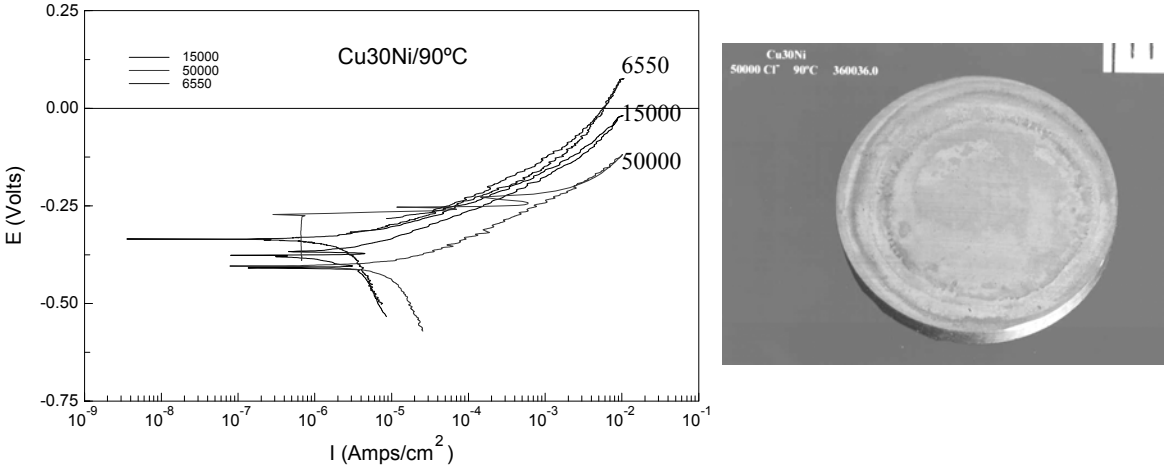

Figure 6.15: (a) left side: Polarization curves for Cu30Ni tested at 90ºC in granitic water having different chloride contents. (b) right side: Cu30Ni specimen after polarization test in granitic water (50000 mg/L Cl^-) at 90ºC

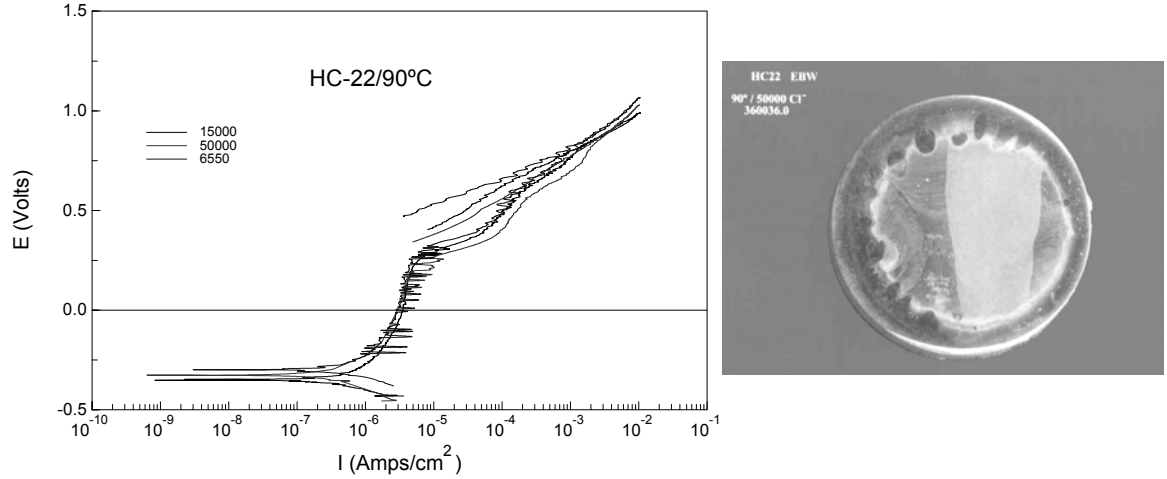

Figure 6.16: (a) left side: Polarization curves for HC22 tested at 90ºC in granitic water having different chloride contents. Right side:EB welded HC22 after polarization test in granitic water (50000 mg/L Cl^-) at 90ºC

The results obtained in the electrochemical tests in granitic water containing bacteria show for the copper materials a significant increase in the amount of corrosion products, with respect to tests performed in the sterile environment (Figure 6.17). The corrosion rates measured by the LPR method are represented in Figure 6.18. They are significantly higher in the presence of SRB cultures.

The results of metallographic studies of corroded specimens show, accordingly, deeper generalized corrosion for the copper materials tested in the inoculated medium (Figure 6.19), with respect to those tested in the sterile one. SEM examinations of corroded specimens reveal a significant biofilm growth on the surface of the copper materials exposed to the bacterial medium. Some of the more representative micrographs obtained in these studies are shown in Figures 6.20 and 6.21. Energy dispersive x-ray (EDS) analysis of this biofilm revealed a significant enrichment in sulphur, thus indicating corrosion activity due to SRB and, therefore, certain evidence of MIC. No sulphur was detected in the EDS analyses of the specimens tested in the sterile medium.

In the case of the HC22 alloy,the corrosion rates in the sterile and inoculated media are very similar and low (below 10 microns per year). No biofilm growth is detected on the surface of specimens tested in the bacterial environment, as it is shown in Figure 6.21, indicating that the alloy does not favor the establishment of SRB colonization, being then less susceptible to MIC. This is mainly attributed to the high molybdenum and chromium content of the HC22 alloy.

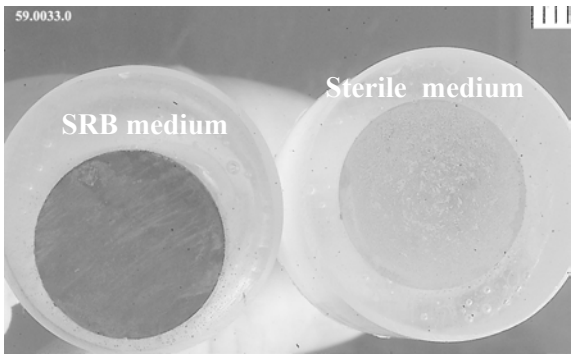

Figure 6.17: Cu30Ni specimens after potentiodynamic polarization test subsequent to 1440 hours exposition at 25ºC to sterile and inoculated granitic water

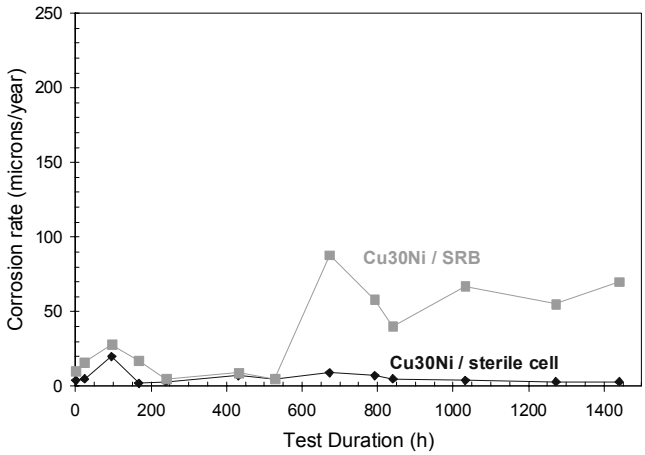

Figure 6.18: Corrosion rates of Cu30Ni in inoculated and sterile granitic water.

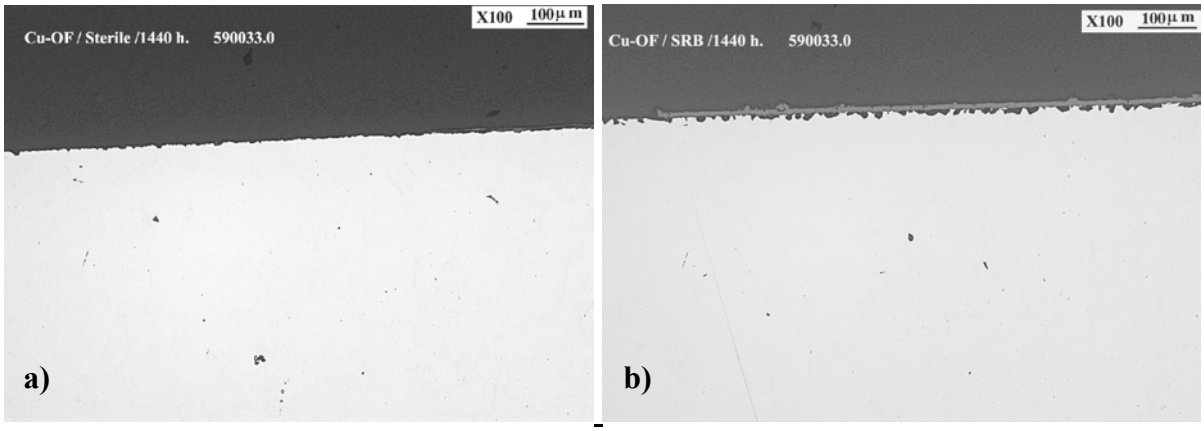

Figure 6.19: Optical micrographs of CuOF specimens after polarization test in a) "sterile" granitic water and b) inoculated granitic water.
The potentiodynamic test was performed after 1440 hours exposure

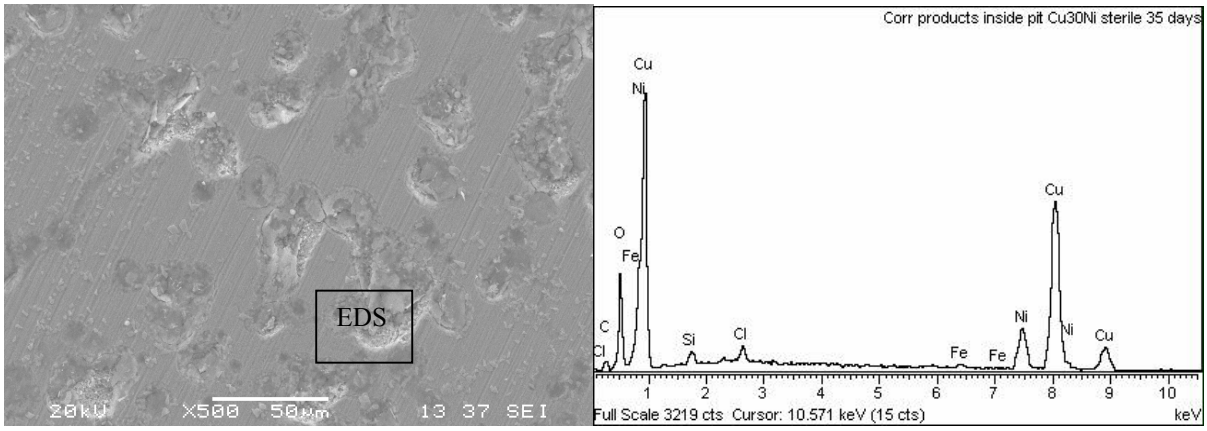

Figure 6.20: SEM micrograph and EDS spectrum of the surface of a Cu30Ni specimen after potentiodynamic test, subsequent to 35 days exposure in "sterile"medium.

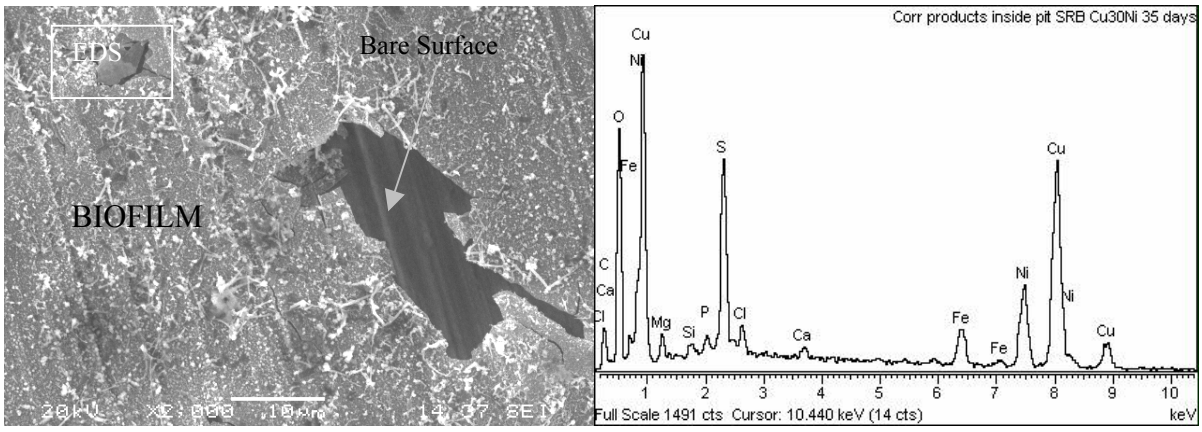

Figure 6.21. SEM micrograph showing biofilm growth on the surface of a Cu30Ni specimen after potentiodynamic test, subsequent to 35 days exposure in SRB inoculated medium. EDS spectrum of former biofilm.

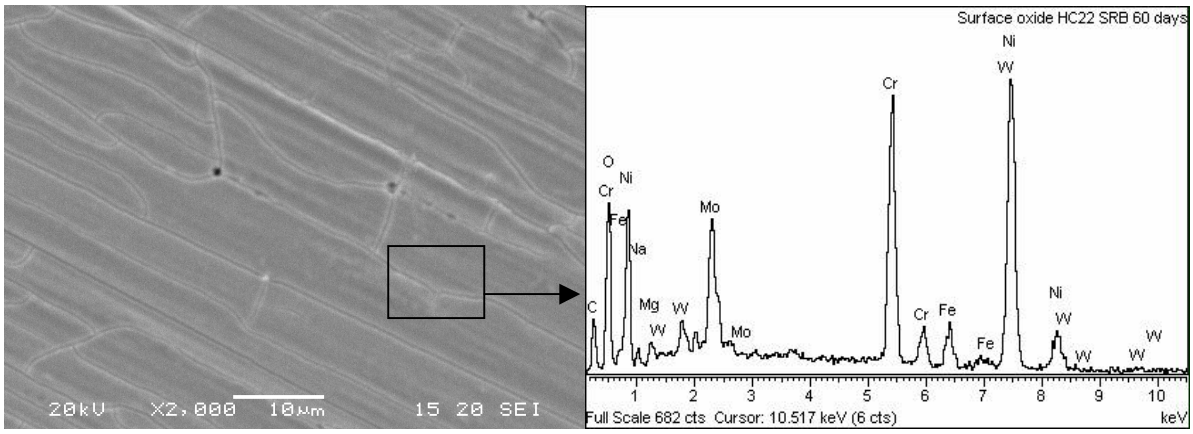

Figure 6.22: SEM micrograph and EDS spectrum of the surface of a HC22 specimen after potentiodynamic test, subsequent to 60 days exposure in the medium inoculated with SRB. No signs of biofilm growth were detected

6.6 Results of crevice corrosion studies

Investigations performed on parent and welded copper and cupronickel specimens in granitic-bentonite water at 90ºC, and chloride contents up to 50000 mg/L indicate no crevice corrosion damage.

The HC22 specimens show after testing the same appearance as berore testing (Figure 6.23). Only in some cases a slight tarnishing due to a very shallow oxide formation was detected.

In the case of the Cu30Ni and CuOF specimens general corrosion was observed in exposed areas (not occluded). No localized attack was observed, however, in areas contacting or bordering the Teflon crevice formers, thus indicating no crevice corrosion sensitivity. Figures 6.24-6.26 show some of the more representative micrographs obtained in the metalographic studies of tested specimens.

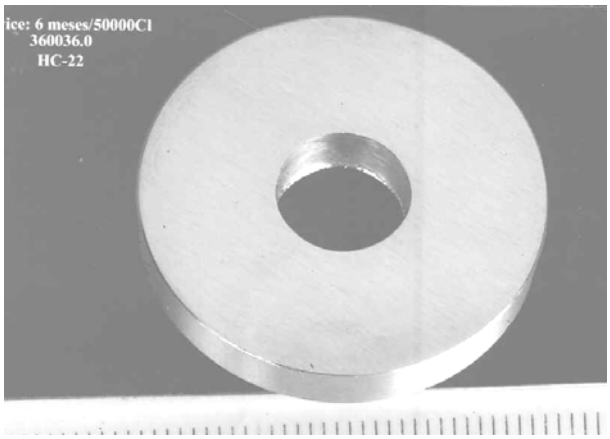

Figure 6.23. HC22 crevice specimen after six months exposure to granitic water (50000 mg/L Cl^-) at 90ºC

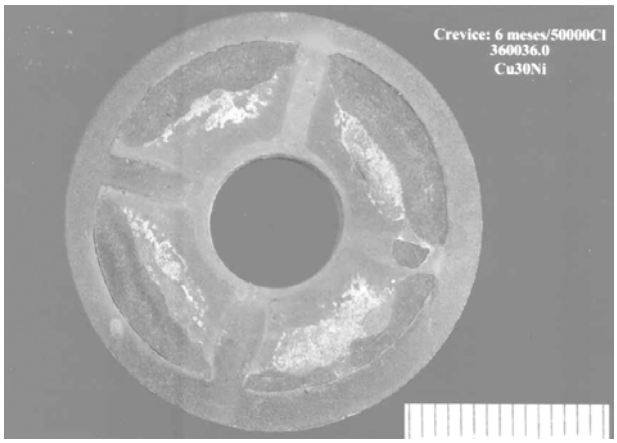

Figure 6.24. HC22 crevice specimen after six months exposure to granitic water (50000 mg/L Cl^-) at 90ºC

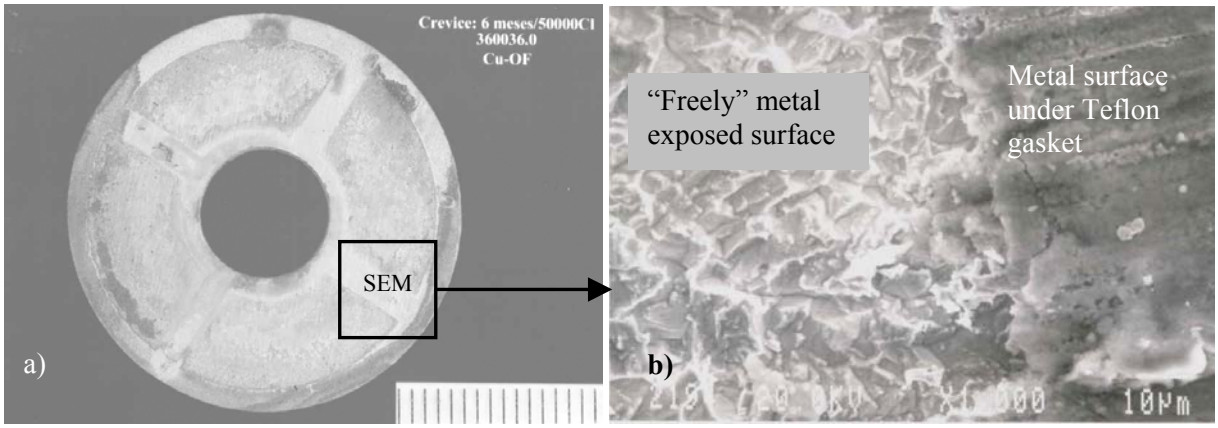

Figure 6.25. a) CuOF crevice specimen after six months exposure to granitic water (50000 mg/L Cl^-) at 90°C
b) SEM micrograph of the previous Cu-OF specimen

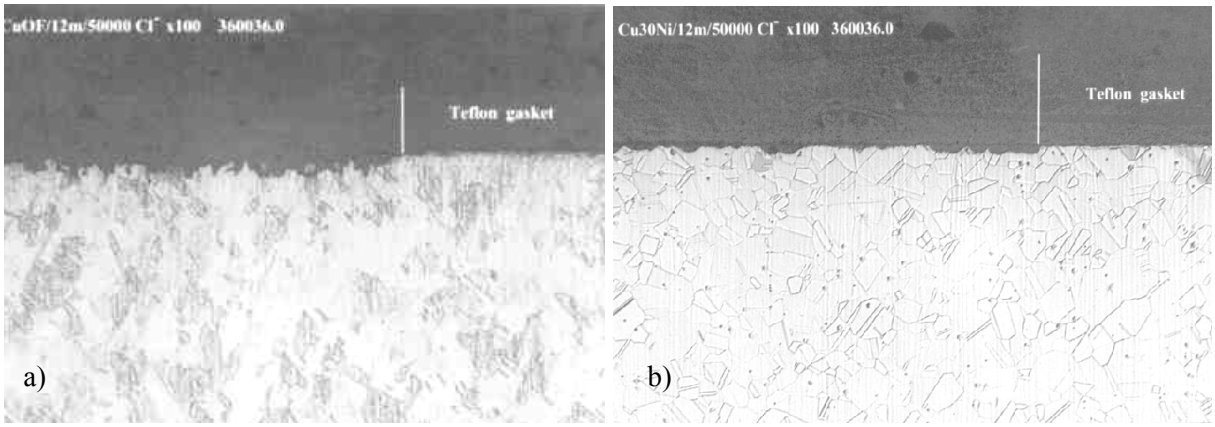

Figure 6.26: Optical micrographs of CuOF (a) and Cu30Ni (b) crevice specimens tested 12 months in granitic water (50,000 mg/L Cl^-) at 90ºC (x100).

6.7 Conclusions

From the results obtained in the studies carried out, the following conclusions can be drawn.

HC22 alloy

- No sensitivity to SCC, crevice or pitting corrosion has been observed for HC22 alloy when tested at 90ºC in the granitic-bentonitic water with chloride contents up to 50000 mg/L.

- There is no effect of the EB and GTA welding procedures in the resistance of the alloy to the above mentioned localized corrosion phenomena.

- No susceptibility to MIC due to SRB has been found for HC22 alloy.

Copper CuOF

- No sensitivity to SCC, no loss of ductility or mechanical strength is noticed for hard and annealed CuOF when tested in the granitic-bentonite environment with respect to the results obtained in argon. With respect to hard copper, soften copper shows, consequently, higher ductility and lower mechanical properties.

- There is no effect of the GTA welding procedures in the resistance of CuOF alloy to SCC.

- No susceptibility to pitting or crevice corrosion is observed for parent and welded CuOF specimens when tested in the granitic-bentonitic water at temperatures up to 90ºC and chloride contents up to 50000 mg/L. In general, an increase in the chloride concentration augments general corrosion rates.

- Significant biofilm growth is detected on the surface of CuOF specimens tested in presence of SRB. In these inoculated media, specimens show higher corrosion rates, with respect to those obtained in sterile conditions, thus indicating certain evidence of MIC due to SRB.

Cu30Ni alloy

- No loss of ductility is noticed for cupronickel alloy when tested in the granitic-bentonite environment. Metallographic studies reveal, however, secondary cracks when tested in the granitic environment with chloride contents up to 6500 mg/L, at the strain rates of 10^{-6} and $2x10^{-7}s^{-1}$, thus indicating a slight sensitivity to SCC under the test conditions applied. Similar maximum crack length values and crack density are obtained in the parent metal of welded Cu30Ni specimens.

- No susceptibility to pitting or crevice corrosion is observed for Cu30Ni specimens, in their parent and welded condition, when tested at 90ºC in the granitic-bentonitic water with chloride contents up to 50000 mg/L. A slight dealloying corrosion is observed in the highly chloride medium.

Electrochemical tests with SRB show a significant biofilm growth on the surface of Cu30Ni specimens. In these inoculated media, specimens show higher corrosion rates, respect to those obtained in sterile conditions, thus indicating certain evidence of MIC due to SRB.

7. CORROSION STUDIES IN CLAY ENVIRONMENTS (WP3) (SCK.CEN)

The aim of the present study is to evaluate the influence of oxygen content, elevated temperature, and radiolysis products on the localized corrosion behaviour of preselected candidate container materials. The experiments into the influence of oxygen on corrosion were performed in a glove box under anaerobic conditions, those into the effect of elevated temperature on corrosion were carried out in autoclaves at 140°C under aerobic conditions.

7.1 Experimental

7.1.1 Materials

The susceptibility to localized corrosion (pitting) of eight candidate container materials was evaluated. These materials are: carbon steel TStE 355, stainless steels AISI 316L, AISI 316Ti, AISI 316L hMo and UHB 904L, nickel alloys Hastelloy C-4 and Hastelloy C-22, and titanium alloy Ti/0.2Pd (Ti99.8-Pd, TiGr-7). The chemical composition of these materials is given in Table 7.1.

Table 7.1: Chemical composition (wt. %) of the candidate container materials.

Material	Chemical composition (wt.%)												
	Fe	Ni	Cr	Mo	Mn	Si	Ti	Cu	Co	C	S	P	Others
Carbon steel													
TStE 355	bal	0.03	0.03	-	1.12	0.344	0.003	-	-	0.180	0.002	0.010	Nb: 0.017; N_2: 0.005
Stainless steels													
AISI 316L	bal	11.00	16.90	2.08	1.54			-	-		0.001	0.032	
AISI 316Ti	bal			2.05	1.08	0.540	-	-	-	0.017	0.009	0.028	
AISI 316L hMo	bal	10.70	16.80	2.84	1.16		0.30	-	-		0.001	0.030	
UHB 904L	bal			4.47	1.48	0.400	-	1.51	-	0.044	0.001	0.019	N_2: 0.080
Ni-alloys		12.53	17.67			0.610	-			0.015			
HASTELLOY C-4	0.98	25.00		15.85	0.04			-	0.01		0.003	0.004	
HASTELLOY C-22	2.80		19.70		0.22	0.190	<0.01	0.03	0.38	0.019	<0.005	0.010	W: 3.0; Al: 0.22; V: 0.16; Nb + Ta: 0.05
				13.30			-						
Ti-alloy	0.04	bal	15.75		-			-	-			-	Pd: 0.16; O_2: 0.13; N_2< 0.01; H_2: 0.001
Ti/0.2Pd (TiGr-7)		bal	21.80	-		0.020	bal			0.003	-		
		-				-				0.014			
			-			-							
										0.010			

7.1.2 Experimental techniques

The experimental approach via electrochemical testing was twofold:

- the susceptibility to localized corrosion (pitting) of the investigated container materials was determined by conducting cyclic potentiodynamic polarization (CPP) measurements. This technique provides three characteristic potentials: (i)

E_{NP}, the critical pit nucleation potential or breakdown potential (i.e. the potential above which new pits nucleate and grow), (ii) E_{PP}, the protection potential or repassivation potential (i.e. the potential above which existing pits can grow, but new pits cannot nucleate; beneath this potential, pits do neither grow nor nucleate), and (iii) OCP, open circuit potential (i.e. the potential that the metal assumes in the studied electrolyte under open circuit conditions).

- The CPP technique was chosen because it provides a reasonable, rapid method for predicting the tendency of an alloy to suffer localised corrosion in the form of pitting. The CPP-curves were recorded with a scan rate of 1 mV/s.

- experiments were also performed to monitor the free corrosion potential, E_{CORR}, as a function of time, in media representative for the underground repository conditions, because the OCP-values derived from the CPP curves do not represent the actual value encountered in the underground environment. E_{CORR} depends on several factors such as the environmental conditions (e.g. oxygen content) and the surface conditions (e.g. mass transport). E_{CORR} has also been known to vary with time, so that an equilibrium cannot be obtained within the limited time span of a CPP measurement [40,41].

A combination of these two techniques is essential in establishing the long-term corrosion behaviour of the candidate overpack materials. This is realized by comparing the 'actual' value of E_{CORR} relative to E_{NP} and E_{PP}, which are determined from the CPP-curves:
- $E_{CORR} \geq E_{NP}$: immediate pitting problems;
- $E_{CORR} << E_{NP}$: no pitting will occur;
- $E_{CORR} < E_{NP}$: if E_{CORR} is close to E_{NP}, pitting can occur if the separation between E_{CORR} and E_{NP} is reduced, *e.g.* by changing the oxidizing power of the solution, at MnS inclusions (i.e. a local site with a higher potential), *etc.*;
- $E_{CORR} << E_{NP}$ and $E_{CORR} > E_{PP}$: the overpack material could suffer long-term corrosion problems because localised attack, once initiated, will not be able to repassivate;
- $E_{CORR} << E_{PP}$: pits can neither grow nor nucleate;

7.1.3 Experimental setup

The experimental setup to perform CPP-measurements consists of a potentiostat/galvanostat, a computer, and a three-electrode corrosion cell, *viz.* a working electrode (i.e. a sample of the investigated material), a counter electrode (Pt), and a reference electrode (Ag/AgCl).

The electrochemical laboratory setup used to perform the CPP-experiments under anaerobic conditions is identical to the setup used under aerobic conditions during the previous EC-programme [5]. To perform the experiments under anaerobic conditions, the double-walled glass corrosion cell, which was developed for more efficient and precise temperature control, was implanted in a glove box, which provides an enclosed compartment operating under a controlled and inert Ar-atmosphere. The setup is illustrated in Figure 7.1. All test solutions were degassed, using a 4-channel On-Line Vacuum Degassing System (Alltech Associates, Inc.), and purged with nitrogen until an oxygen level below 10 ppb was reached. The dissolved

oxygen content in the test solutions was continuously measured by means of an oxygen analyser Process Unit 73 O_2-2 (Knick).

The experiments at 140°C (aerobic conditions) were performed in an autoclave. As reference electrode, an internal Ag/AgCl electrode, completely constructed from Teflon®, was developed in cooperation with the Reactor Materials Department of SCK•CEN. The electrode consists of a silver wire onto one end of which a AgCl layer is deposited electrolytically. This wire is placed inside a heat-shrunk Teflon® tube which is filled with 0.1M KCl. A ceramic plug (MgO-ZrO_2) maintains contact between the sensing element of the reference electrode and the test solution. The Teflon® heat shrinkable tubing provides the pressure balance between the internal electrolyte solution and the test solution in the autoclave. A schematic representation of the internal Ag/AgCl reference electrode is shown in Figure 7.2.

Figure 7.1: View of the laboratory setup used to perform pitting experiments under anaerobic conditions.

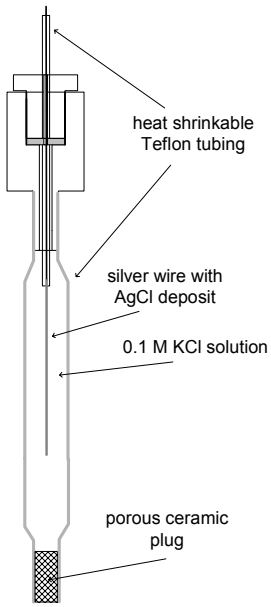

Figure 7.2: Schematic drawing of the internal Ag/AgCl reference electrode used to perform CPP-measurements at 140°C (in an autoclave).

7.1.4 Experimental parameters

The influence of four environmental parameters on the pitting corrosion of the candidate container materials was investigated. These were: the oxygen level, the temperature, the chemical composition of the underground disposal environment (chloride, sulphate, and thiosulphate content), and the presence of the most important radiolytic product (hydrogen peroxide) of the clay water.

The oxygen content reflects the aerobic and anaerobic phases of the disposal. The experiments under aerobic conditions were performed in solutions that were in

equilibrium with air (1 atm.). The experiments under anaerobic conditions were performed in a glove box, which operates under a controlled and inert (Ar) atmosphere. The content of the dissolved oxygen in the test solutions was always kept below 10 ppb. Three different temperatures were considered: 140°C, being the temperature of the near field surrounding the containers in the first phase after disposal, 16°C, being the temperature of the Boom Clay formation at 225 metres below ground level, and 90°C, being an intermediate temperature. In the period 2000-2003, tests were performed at 16°C and 90°C under anaerobic conditions and at 140°C under aerobic conditions. The experimental results will be interpreted in combination with the data gained from the previous EC-programme (experiments under aerobic conditions at 16°C and 90°C) [5].

The CPP-experiments were performed in solutions with varying chloride, sulphate, and thiosulpate concentrations. The chloride concentration was varied up to 50,000 mg/L. The influence of thiosulphate was investigated in the range 20 – 200 mg/L. Experiments were performed in solutions containing 0.2, 216, 1700, and 5400 mg/L SO_4^{2-}, whereby: 0.2 mg/L represents the sulphate content in the undisturbed Boom Clay formation (anaerobic conditions), 216 and 5,400 mg/L SO_4^{2-} are representative for the sulphate content of slightly oxidized and fully oxidized Boom Clay under aerobic conditions, and1700 mg/L represents the sulphate content in the bentonite backfill material.

The interaction of gamma radiation from the waste with the aqueous solutions surrounding the metallic container can result in the production of a range of primary and secondary radiolysis products, such as e^-_{aq}, $H\cdot$, H_2, $\cdot OH$, H_2O_2, O_2^-, HO_2, O_2, H^+, and OH^- [42]. In this study, the influence of hydrogen peroxide (H_2O_2) was investigated. The maximum level of H_2O_2 that can be expected at the surface of a 30 mm thick stainless steel overpack for the Belgian repository concept in Boom Clay was calculated to be 8.10^{-2} mol/L [43]. Therefore, in this study the hydrogen peroxide concentration was varied in the range 8.10^{-3} – 8.10^{-1} mol/L.

7.2 Results

7.2.1 Monitoring of the OCP as a function of time

The time dependency is one of the major factors affecting the accuracy of E_{CORR}. However, this value is essential in evaluating the long-term corrosion behaviour of the candidate container materials (by comparing its value to the E_{NP}- and E_{PP}-data). Therefore, in order to gain a more accurate value for E_{CORR} in the underground repository environment, the open circuit potential of AISI 316L hMo type stainless steel was monitored in solutions/slurries representative for the various phases of the disposal period. The results are summarised in Table 7.2.

Table 7.2: Evolution of E_{CORR} with time in the various environmental conditions.

Identification	Environment	Condition	T [°C]	$\Delta E^{(1)}$ [mV]	$E_{CORR}^{(2)}$ [mV_{SHE}]	Time [days]
SOCW2[(3)]	solution	aerobic	90	280	+320	3
SICW1[(4)]	solution	anaerobic	30	75	-10	6
SL04[(5)]	slurry	aerobic	22	60	+265	120
SL16[(5)]	slurry	anaerobic	30	50	-120	115

(1) potential shift of E_{CORR} over the entire span of the experiment.
(2) potential measured at the end of the experiment.
(3) synthetic oxidized claywater containing 1,000 mg/L Cl^- and 216 mg/L SO_4^{2-}.
(4) synthetic interstitial Boom claywater containing 27 mg/L Cl^- and 0.2 mg/L SO_4^{2-}.
(5) bentonite mixed with deionized water (with a liquid to solid ratio of 30/70).

7.2.2 Results from CPP-measurements

The susceptibility of the various candidate container materials to pitting corrosion was determined by the use of cyclic potentiodynamic polarization (CPP) measurements. For each alloy/solution combination, at least three CPP scans were recorded, and from the obtained polarization curves, average values of the characteristic potentials E_{NP} and E_{PP} were determined. All CPP measurements reported in this report were recorded at a scan rate of 1 mV/s (forward and backward scan) and the scan was reversed when the current density reached a value of 1 mA/cm².

The specimens were wet-ground to a 600-grit finish (SiC-paper). After grinding, the specimens were cleaned with ethanol, rinsed in deionized water and dried in hot air. The surface exposed to the test solutions was about 2 cm². The electrolytes used in all the measurements were prepared from analytical-grade chemicals and deionized water. The test solutions were deaerated with purified nitrogen for 15 minutes prior to each experiment.

7.2.2.1 Experiments under anaerobic conditions

The results of the CPP-measurements at 16°C and 90°C under anaerobic conditions are represented in Table 7.3 and Table 7.4, respectively.

7.2.2.2 Experiments at elevated temperature

The results of the CPP-measurments at 140°C under aerobic conditions are represented in Table 7.5.

7.2.2.3 *Experiments under aerobic conditions at 90°C in solutions containing the radiolysis product H_2O_2*

The results of the CPP-measurements under aerobic conditions (90°C) to investigate the influence of the main radiolysis product H_2O_2 are represented in Table 7.6.

Table 7.3: Data from the CPP-measurements under anaerobic conditions in clay environments(T=16°C)

Solutions	Chemical composition			C-steel	Stainless steel				Ni-alloy		Ti-alloy
	$[Cl^-]$ (mg/L)	$[SO_4^{2-}]$ (mg/L)	$[S_2O_3^{2-}]$ (mg/L)	TStE 355	316L	316L hMo	316Ti	904L	Hastelloy C-4	Hastelloy C-22	Ti/0.2Pd
SICW1	27	0.2	0	uniform corrosion	no pitting	no pitting	no pitting	no pitting	no pitting	no pitting	no pitting
SICW2	100	0.2	0	uniform corrosion	no pitting	no pitting	no pitting	no pitting	no pitting	no pitting	no pitting
SICW3	1,000	0.2	0	uniform corrosion	**+1199** (+151)	**+1186** (+269)	**+1083** (+48)	no pitting	no pitting	no pitting	no pitting
SICW4	10,000	0.2	0	uniform corrosion	**+759** (+157)	**+1314** (+123)	**+857** (+77)	no pitting	no pitting	no pitting	no pitting
SICW5	20,000	0.2	0	uniform corrosion	**+801** (-15)	**+1136** (+17)	**+769** (-64)	no pitting	no pitting	no pitting	no pitting
SICW6	50,000	0.2	0	uniform corrosion	**+616** (+8)	**+1156** (-3)	**+727** (-31)	no pitting	no pitting	no pitting	no pitting
SICW7	1,000	0.2	20	uniform corrosion	no pitting	no pitting	**+1036** (-22)	no pitting	no pitting	no pitting	no pitting
SICW8	1,000	0.2	50	uniform corrosion	no pitting	no pitting	**+1043** (-16)	no pitting	no pitting	no pitting	no pitting
SICW9	1,000	0.2	100	uniform corrosion	no pitting	no pitting	**+978** (+11)	no pitting	no pitting	no pitting	no pitting
SICW10	1,000	0.2	200	uniform corrosion	no pitting	**+1220** (+18)	**+1184** (-24)	no pitting	no pitting	no pitting	no pitting
SBW1	100	1,700	0	no pitting	no pitting	no pitting	no pitting	no pitting	no pitting	no pitting	no pitting
SBW2	1,000	1,700	0	no pitting	no pitting	no pitting	no pitting	no pitting	no pitting	no pitting	no pitting
SBW3	10,000	1,700	0	no pitting	no pitting	no pitting	no pitting	no pitting	no pitting	no pitting	no pitting
SBW4	20,000	1,700	0	no pitting	no pitting	no pitting	no pitting	no pitting	no pitting	no pitting	no pitting
SBW5	50,000	1,700	0	no pitting	no pitting	no pitting	no pitting	no pitting	no pitting	no pitting	no pitting
SBW6	1,000	1,700	20	uniform corrosion	no pitting	no pitting	no pitting	no pitting	no pitting	no pitting	no pitting
SBW7	1,000	1,700	50	uniform corrosion	no pitting	no pitting	no pitting	no pitting	no pitting	no pitting	no pitting
SBW8	1,000	1,700	100	uniform corrosion	no pitting	no pitting	no pitting	no pitting	no pitting	no pitting	no pitting
SBW9	1,000	1,700	200	uniform corrosion	no pitting	no pitting	no pitting	no pitting	no pitting	no pitting	no pitting
RCW	27	<0.1	0	no pitting	no pitting	no pitting	no pitting	no pitting	no pitting	no pitting	no pitting

SICW: Synthetic Interstitial Boom Clay Water.
SBW: Synthetic Bentonite Water.
RCW: Real Interstitial Boom Clay Water.
The data in bold represent the critical potential for pit nucleation (E_{NP}). The data between brackets represent the protection potential (E_{PP}).

Table 7.4: Data from the CPP-measurements under anaerobic conditions in clay environments (T=90°C)

Solutions	Chemical composition			C-steel	Stainless steel				Ni-alloy		Ti-alloy
	$[Cl^-]$ (mg/L)	$[SO_4^{2-}]$ (mg/L)	$[S_2O_3^{2-}]$ (mg/L)	TStE 355	316L	316L hMo	316Ti	904L	Hastelloy C-4	Hastelloy C-22	Ti/0.2Pd
SICW1	27	0.2	0	uniform corrosion	no pitting	no pitting	no pitting	no pitting	no pitting	no pitting	no pitting
SICW2	100	0.2	0	uniform corrosion	**+914** (+243)	no pitting	**+715** (+120)	no pitting	tarnish	no pitting	no pitting
SICW3	1,000	0.2	0	uniform corrosion	**+844** (+83)	**+645** (+30)	**+684** (+122)	**+798** (+151)	tarnish	tarnish	no pitting
SICW4	10,000	0.2	0	uniform corrosion	**+420** (-50)	**+504** (-7)	**+463** (-49)	**+560** (+116)	tarnish	tarnish	no pitting
SICW5	20,000	0.2	0	uniform corrosion	**+295** (-92)	**+497** (-100)	**+428** (-80)	**+548** (+61)	tarnish	tarnish	no pitting
SICW6	50,000	0.2	0	uniform corrosion	**+223** (-136)	**+401** (-121)	**+312** (-115)	**+420** (-102)	tarnish	tarnish	no pitting
SICW7	1,000	0.2	20	uniform corrosion	**+578** (+31)	**+694** (+39)	**+737** (+88)	**+898** (+161)	no pitting	no pitting	no pitting
SICW8	1,000	0.2	50	uniform corrosion	**+617** (+39)	**+724** (+14)	**+656** (+17)	**+842** (+185)	no pitting	no pitting	no pitting
SICW9	1,000	0.2	100	uniform corrosion	**+738** (-21)	**+805** (-73)	**+691** (+8)	**+891** (+223)	no pitting	no pitting	no pitting
SICW10	1,000	0.2	200	uniform corrosion	**+576** (-103)	**+774** (-73))	**+636** (-146)	**+818** (+195)	no pitting	no pitting	no pitting
SBW1	100	1,700	0	uniform corrosion	no pitting	no pitting	no pitting	no pitting	no pitting	no pitting	no pitting
SBW2	1,000	1,700	0	uniform corrosion	**+722** (-7)	**+681** (-105)	**+431** (-3)	**+980** (+132)	no pitting	no pitting	no pitting
SBW3	10,000	1,700	0	uniform corrosion	**+416** (-109)	**+482** (-130)	**+229** (-79)	**+578** (-66)	no pitting	no pitting	no pitting
SBW4	20,000	1,700	0	uniform corrosion	**+187** (-146)	**+261** (-64)	**+304** (-88)	**+348** (-88)	tarnish	no pitting	no pitting
SBW5	50,000	1,700	0	uniform corrosion	**+213** (-181)	**+343** (-102)	**+342** (-133)	**+407** (-80)	tarnish	no pitting	no pitting
SBW6	1,000	1,700	20	uniform corrosion	**+819** (-64)	**+632** (-49)	**+853** (-52)	**+834** (+34)	no pitting	no pitting	no pitting
SBW7	1,000	1,700	50	uniform corrosion	**+709** (-26)	**+606** (-45)	**+321** (-223)	**+426** (-13)	no pitting	no pitting	no pitting
SBW8	1,000	1,700	100	uniform corrosion	**+776** (-70)	**+879** (+24)	**+609** (-175)	**+875** (+85)	no pitting	no pitting	no pitting
SBW9	1,000	1,700	200	uniform corrosion	**+772** (-13)	**+693** (-154)	**+629** (-126)	**+871** (+122)	no pitting	no pitting	no pitting
RCW	27	<0.1	0	uniform corrosion	no pitting	no pitting	no pitting	no pitting	no pitting	no pitting	no pitting

SICW: Synthetic Interstitial Boom Clay Water.
SBW: Synthetic Bentonite Water.
RCW: Real Interstitial Boom Clay Water.
The data in bold represent the critical potential for pit nucleation (E_{NP}). The data between brackets represent the protection potential (E_{PP}).

Table 7.5: Data from the CPP-measurements under aerobic conditions in clay environments (T=140°C)

Solutions	Chemical composition			C-steel	Stainless steel				Ni-alloy		Ti-alloy
	$[Cl^-]$ (mg/L)	$[SO_4^{2-}]$ (mg/L)	$[S_2O_3^{2-}]$ (mg/L)	TStE 355	316L	316L hMo	316Ti	904L	Hastelloy C-4	Hastelloy C-22	Ti/0.2Pd
SOCW1	100	216	0	uniform corrosion	**+491** (-124)	**+569** (-110)	**+530** (-159)	**+1023** (+10)	no pitting	no pitting	no pitting
SOCW2	1,000	216	0	uniform corrosion	**+214** (-156)	**+266** (-199)	**+265** (-177)	**+511** (-181)	no pitting	no pitting	no pitting
SOCW3	10,000	216	0	uniform corrosion	**+94** (-247)	**+172** (-153)	**+124** (-309)	**326** (-151)	**+363** (-208)	no pitting	no pitting
SOCW4	20,000	216	0	uniform corrosion	**+52** (-226)	**+87** (-284)	**+90** (-336)	**+256** (-191)	**+330** (-222)	no pitting	no pitting
SOCW5	50,000	216	0	uniform corrosion	**-15** (-372)	**-2** (-325)	**+74** (-350)	**+150** (-246)	**+342** (-183)	**+334** (-101)	no pitting
SOCW6	100	5,400	0	uniform corrosion	no pitting	no pitting	no pitting	no pitting	no pitting	no pitting	no pitting
SOCW7	1,000	5,400	0	uniform corrosion	**+555** (-114)	**+680** (-144)	**+549** (-145)	**+581** (-189)	no pitting	no pitting	no pitting
SOCW8	10,000	5,400	0	uniform corrosion	**+121** (-187)	**+147** (-336)	**+218** (-412)	**+425** (-279)	no pitting	no pitting	no pitting
SOCW9	20,000	5,400	0	uniform corrosion	**+62** (-190)	**+136** (-333)	**+141** (-344)	**+347** (-397)	**+401** (-188)	no pitting	no pitting
SOCW10	50,000	5,400	0	uniform corrosion	**-8** (-276)	**+69** (-279)	**+133** (-343)	**+197** (-204)	**+301** (-204)	**+348** (-118)	no pitting
SOCW11	1,000	216	20	uniform corrosion	**+301** (-128)	**+301** (-154)	**+269** (-153)	**+391** (-202)	no pitting	no pitting	no pitting
SOCW12	1,000	216	50	uniform corrosion	**+239** (-145)	**+267** (-213)	**+276** (-180)	**+522** (-134)	no pitting	no pitting	no pitting
SOCW13	1,000	216	100	uniform corrosion	**+74** (-190)	**+282** (-202)	**+285** (-172)	**+475** (-165)	no pitting	no pitting	no pitting
SOCW14	1,000	216	200	uniform corrosion	**+69** (-184)	**+153** (-204)	**+277** (-207)	**+554** (-128)	no pitting	no pitting	no pitting
SOCW15	1,000	5,400	20	uniform corrosion	**+570** (-125)	**+401** (-129)	**+499** (-148)	**+950** (-36)	no pitting	no pitting	no pitting
SOCW16	1,000	5,400	50	uniform corrosion	**+614** (-127)	**+626** (-149)	**+418** (-213)	**+789** (-37)	no pitting	no pitting	no pitting
SOCW17	1,000	5,400	100	uniform corrosion	**+904**[(1)] (-183)	**+686** (-174)	**+683** (-278)	**+714** (-66)	no pitting	no pitting	no pitting
SOCW18	1,000	5,400	200	uniform corrosion	**+589** (-238)	**+391** (-216)	**+374** (-278)	**+671** (-101)	no pitting	no pitting	no pitting
SBW1	100	1,700	0	uniform corrosion	**+876** (-232)	**+854** (-156)	**+810** (-171)	**+847** (-154)	tarnish	no pitting	no pitting
SBW2	1,000	1,700	0	uniform corrosion	**+629** (-278)	**+555** (-239)	**+461** (-251)	**+599** (-198)	tarnish	no pitting	no pitting
SBW3	10,000	1,700	0	uniform corrosion	**+199** (-319)	**+231** (-289)	**+225** (-308)	**+142** (-278)	tarnish	no pitting	no pitting
SBW4	20,000	1,700	0	uniform corrosion	**+59** (-272)	**+161** (-267)	**+114** (-346)	**+96** (-267)	tarnish	no pitting	no pitting
SBW5	50,000	1,700	0	uniform corrosion	**-20** (-388)	**+57** (-302)	**+40** (-321)	**-5** (-359)	tarnish	no pitting	no pitting
SBW6	1,000	1,700	20	uniform corrosion	**+580** (-260)	**+501** (-244)	**+366** (-226)	**+440** (-210)	no pitting	no pitting	no pitting
SBW7	1,000	1,700	50	uniform corrosion	**+675** (-255)	**+646** (-244)	**+399** (-302)	**+467** (-229)	no pitting	no pitting	no pitting
SBW8	1,000	1,700	100	uniform corrosion	**+456** (-240)	**+639** (-266)	**+424** (-285)	**+512** (-233)	no pitting	no pitting	no pitting
SBW9	1,000	1,700	200	uniform corrosion	**+472** (-266)	**+555** (-234)	**+586** (-303)	**+326** (-217)	no pitting	no pitting	no pitting

SOCW: Synthetic Oxidized Boom Clay Water.
SBW: Synthetic Bentonite Water.
The data in bold represent the critical potential for pit nucleation (E_{NP}). The data between brackets represent the protection potential (E_{PP}).
(1) E_{NP} was determined as the potential where I reached a value of 20 µA/cm².

Table 7.6: Data from the CPP-measurements under aerobic conditions (90°C)

Material	Type	Solution	Chemical composition			Characteristic potentials		
			$[Cl^-]$ (mg/L)	$[SO_4^{2-}]$ (mg/L)	$[H_2O_2]$ (mol/L)	OCP (mV_{SHE})	E_{NP} (mV_{SHE})	E_{PP} (mV_{SHE})
C-steel	TStE 355	SOCW2	1,000	216	0	-608	u.c.	u.c.
		SOCW19	1,000	216	0.8	+181	u.c.	u.c.
		SOCW20	1,000	216	0.08	-229	u.c.	u.c.
		SOCW21	1,000	216	0.008	-341	u.c.	u.c.
Stainless steel	AISI 316L	SOCW2	1,000	216	0	-531	473	68
		SOCW19	1,000	216	0.8	+693	742	589
		SOCW20	1,000	216	0.08	+484	579	306
		SOCW21	1,000	216	0.008	+425	528	278
	AISI 316L hMo	SOCW2	1,000	216	0	-489	556	109
		SOCW19	1,000	216	0.8	+673	n.h.	n.h.
		SOCW20	1,000	216	0.08	+539	684	303
		SOCW21	1,000	216	0.008	+393	624	310
	AISI 316Ti	SOCW2	1,000	216	0	-82	590	110
		SOCW19	1,000	216	0.8	+659	819	549
		SOCW20	1,000	216	0.08	+487	640	309
		SOCW21	1,000	216	0.008	+433	571	275
	UHB 904L	SOCW2	1,000	216	0	-74	782	196
		SOCW19	1,000	216	0.8	+643	n.h.	n.h.
		SOCW20	1,000	216	0.08	+524	784	481
		SOCW21	1,000	216	0.008	+359	741	378
Ni-alloy	Hast. C-4	SOCW2	1,000	216	0	-339	n.p.	n.p.
		SOCW19	1,000	216	0.8	+593	n.p.	n.p.
		SOCW20	1,000	216	0.08	+338	n.p.	n.p.
		SOCW21	1,000	216	0.008	+276	n.p.	n.p.
	Hast. C-22	SOCW2	1,000	216	0	-133	n.p.	n.p.
		SOCW19	1,000	216	0.8	+566	n.p.	n.p.
		SOCW20	1,000	216	0.08	+458	n.p.	n.p.
		SOCW21	1,000	216	0.008	+369	n.p.	n.p.
Ti-alloy	Ti/0.2Pd	SOCW2	1,000	216	0	-280	n.p.	n.p.
		SOCW19	1,000	216	0.8	+342	n.p.	n.p.
		SOCW20	1,000	216	0.08	+87	n.p.	n.p.
		SOCW21	1,000	216	0.008	-177	n.p.	n.p.

OCP : Open Circuit Potential (derived from CPP-curves).
u.c. : uniform corrosion.
n.h. : no hysteresis (the CPP-curves did not show a positive hysteresis, which is typical for the presence of pitting corrosion; surface analyses did however reveal signs of pitting).
n.p. : no pitting (neither the CPP-curves nor the surface analyses indicated that pitting had occurred under these conditions).

7.3 Discussion

7.3.1 Determination of ECORR

Table 7.2 shows clearly that the concentration of dissolved oxygen plays an important role on E_{CORR}.

- in Boom Clay water, E_{CORR} decreased from +320 mV_{SHE} to -10 mV_{SHE} when changing the conditions from aerobic to anaerobic.
- in bentonite slurry, the decrease in E_{CORR} is even slightly more pronounced (from +265 mV_{SHE} under aerobic conditions to -120 mV_{SHE} under anaerobic conditions).

These results indicate that the candidate container materials will be less susceptible to localized corrosion under anaerobic conditions, which is consistent with the general findings in the literature.

The E_{CORR}-values were determined for AISI 316L hMo type stainless steel. Care has to be taken when using these values for the interpretation of the E_{NP}- and E_{PP}-data of the other investigated candidate container materials. We assumed that the E_{CORR}-values are only slightly dependent on alloy composition and environmental conditions (chloride content, temperature), so the same approximate value was used for the interpretation of all polarization curves. To facilitate the interpretation, the value of E_{CORR} is indicated as a dotted horizontal line on the curves.

7.3.2 CPP-measurements under anaerobic conditions

7.3.2.1 Experiments at 16°C (Table 7.3)

Ti/0.2Pd, Hastelloy C-4, Hastelloy C-22, and UHB 904L are resistant to pitting in all SICW- and SBW-solutions (even at levels of 50,000 mg/L Cl^-).

The carbon steel TStE 355 exhibits general corrosion in all SICW-solutions. This carbon steel does not show any signs of corrosion attack in SBW-solutions containing up to 50,000 mg/L Cl^-. However, the addition of thiosulphate (even as low as 20 mg/L) caused a general corrosion attack.

The stainless steels AISI 316L, AISI 316L hMo, and AISI 316Ti are resistant to pitting in all SBW-solutions (up to 50,000 mg/L Cl^-). In SICW, these stainless steels are resistant to pitting in solutions containing up to 1,000 mg/L Cl^-. At $[Cl^-] \geq 1{,}000$ mg/L, slight signs of pitting corrosion were observed. However, the E_{NP}-values remained much more positive than the actual E_{CORR} (-10 mV_{SHE}), indicating that these alloys are highly unlikely to suffer immediate pitting problems under these conditions. These alloys could, however, suffer long-term pitting for $[Cl^-] \geq 20{,}000$ mg/L, since E_{PP} dropped below the actual E_{CORR}.

7.3.2.2 Experiments at 90°C (Table 7.4)

Only Ti/0.2Pd remained unaffected in all SICW- and SBW-solutions (even at levels of 50,000 mg/L Cl^-). The carbon steel TStE 355 exhibits general corrosion in all SICW- and SBW-solutions.

For the Ni-alloys (Hastelloy C-4 and C-22), the CPP-curves show a hysteresis, which is typical for pitting corrosion. This can be seen on Figure 7.3 (Hastelloy C-22). However, analysis of the surface by optical microscopy after the experiment only reveals a tarnished surface (yellow-orange spots) without evidences of pitting attack. This is illustrated on Figure 7.4 for Hastelloy C-22. In some occasions, slight signs of intergranular attack were observed on Hastelloy C-22 samples, as can be seen on Figure 7.5. Thus, the hysteresis is probably the result of an alteration of the passive layer. On Figure 7.3, a current peak around 400-500 mV (vs. SHE) can be observed. This peak can probably be attributed to either (i) the Cr (III) to Cr (VI) transformation or (ii) $Ni(OH)_2$ to Ni_3O_4 transformation.

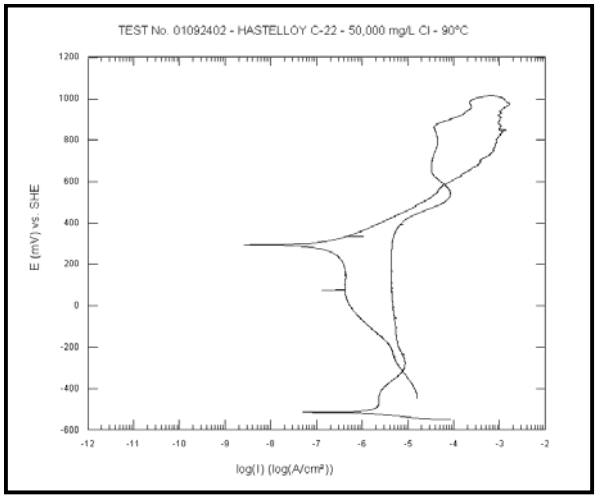

Figure 7.3**:** CPP-curve for HASTELLOY C-22 in SICW containing 0.2 mg/L SO_4^{2-} and 50,000 mg/L Cl^-.

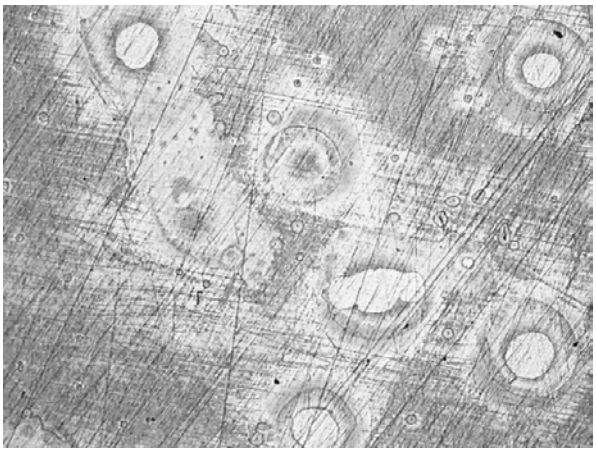

Figure 7.4: Optical micrograph of HC-22 after CPP-test in SICW containing 50,000 mg/L Cl^-, 50×

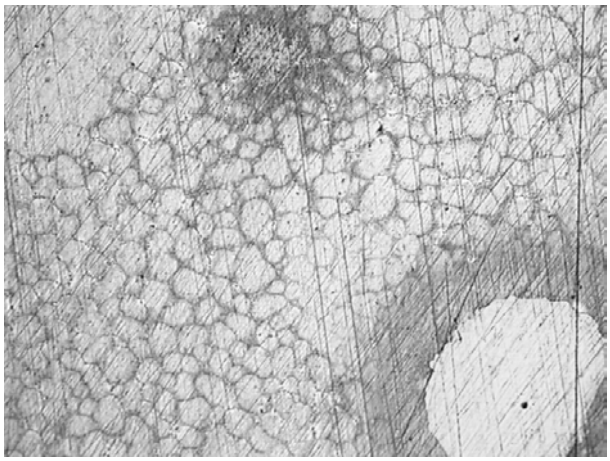

Figure7.5: Optical micrograph of HC-22 after CPP-test in SICW containing 50,000 mg/L Cl^- with slight signs of IGA, 100×

The E_{NP}- and E_{PP}-values of AISI 316L, AISI 316L hMo, AISI 316Ti, and UHB 904L type stainless steel in SICW (0.2 mg/L SO_4^{2-}) and in SBW (1,700 mg/L SO_4^{2-}) at 90°C are presented in Figures 7.6 and 7.7, respectively. The stainless steels are not expected to suffer immediate pitting problems because the E_{NP}-values are situated well above the actual E_{CORR} in all SICW- and SBW-solutions. Long-term pitting problems are only expected to occur in SICW- and SBW-solutions containing at least 10,000 mg/L Cl^- because below 10,000 mg/L Cl^-, E_{PP} is still more positive than the actual corrosion potential. UHB 904L will even remain resistant to long-term pitting up to 50,000 mg/L Cl^-.
The UHB 904L type stainless steel has a slightly higher resistance to pitting than the three 316 grade stainless steels. The pitting resistance decreases with increasing chloride concentration. Thiosulphate does not have any significant effect on the resistance of the stainless steels to pitting corrosion.

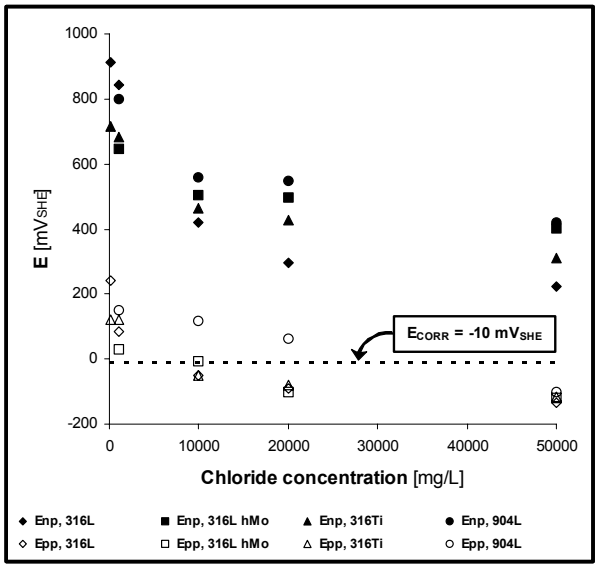

Figure 7.6: Influence of Cl^- on E_{NP} and E_{PP} of 316L, 316L hMo, 316Ti, and UHB 904L type stainless steel in SICW containing 0.2 mg/L SO_4^{2-} (90°C).

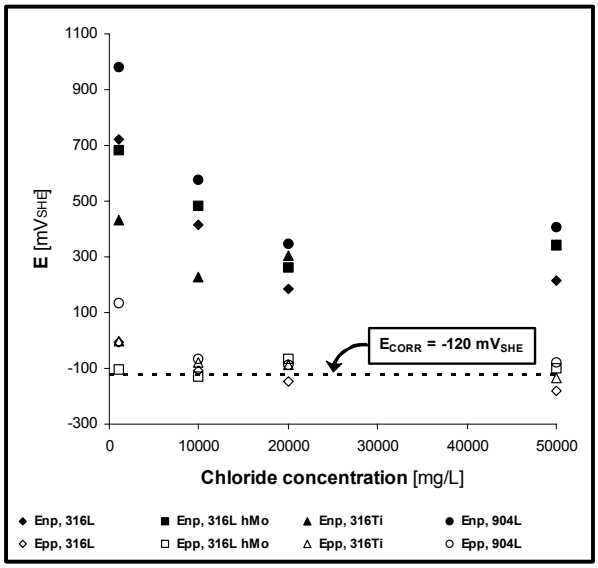

Figure 7.7: Influence of Cl^- on E_{NP} and E_{PP} of 316L, 316L hMo, 316Ti, and UHB 904L type stainless steel in SBW containing 1,700 mg/L SO_4^{2-} (90°C).

7.3.3 CPP-measurements under aerobic conditions at 140°C

Ti/0.2Pd exhibits a high resistance to general and pitting corrosion in all SOCW-solutions (100 - 50,000 mg/L). The carbon steel ist also resistant to pitting corrosion but it is attacked by general corosion in all SOCW-solutions.

The recorded CPP-curves for Hastelloy C-4 and Hastelloy C-22 show the presence of a positive hysteresis in several SOCW-solutions. This shape is generally associated with pitting corrosion. However, surface analyses (Optical Microscopy and Scanning Electron Microscopy) revealed several observations indicating that Hastelloy C-4 and C-22 are not attacked by pitting corrosion. These observations are:

HASTELLOY C-4. In SOCW-solutions up to 20,000 mg/L Cl^-, the surface of the specimens revealed only a tarnished surface, i.e. a yellow-orange discolouration of the surface, without evidences of pitting attack. In SOCW-solutions containing 20,000 mg/L Cl^- and higher, evidence of attack was only observed at the interface between the sample and the mounting resin, as can be seen in Figure 7.8, while the rest of the sample remained unaffected. Therefore, it was concluded that in these high chloride containing solutions, the hysteresis is due to crevice corrosion. EDS-analysis of the attacked zone (Figure 7.8, zone 1, square) revealed the presence of the major alloying elements of HASTELLOY C-4 (Ni, Cr, Mo, Fe). EDS-analysis of the layer (Figure 7.8, zone 2, circle) adjacent to the attacked zone revealed the presence of K, Na, and Cl, indicating that this layer mainly consists of salt deposits of the test solution (NaCl, KCl), together with some of the alloying elements (Ni, Cr, Mo).

HASTELLOY C-22. In SOCW-solutions with a chloride concentration lower than 50,000 mg/L, no hysteresis was found on the CPP-curves and no alteration of the surface (neither tarnishing nor corrosion attack) was observed. Figure 7.9 shows a SEM-micrograph of an uncleaned HASTELLOY C-22 specimen after CPP-testing in SOCW containing 216 mg/L SO_4^{2-} and 50,000 mg/L Cl^-. A thick salt layer was observed near the interface sample/mounting resin. EDS-analysis of this layer (zone 3, rectangle) revealed the presence of remnants of the test solution (K, Na, and Cl) together with some of the alloying elements (Ni, Cr, Mo). However, at the top right of zone 3 (indicated with the arrow) slight signs of crevice corrosion are observed (see the typical circular shaped attack).

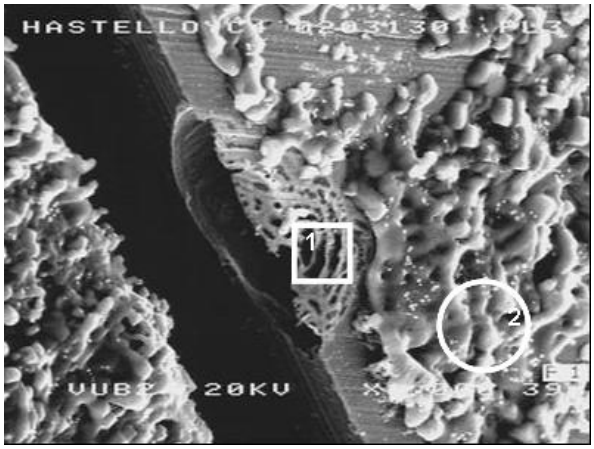

Figure: 7.8 SEM-micrograph of an uncleaned HASTELLOY C-4 specimen after CPP-testing in SOCW containing 216 mg/L SO_4^{2-} and 50,000 mg/L Cl^-.

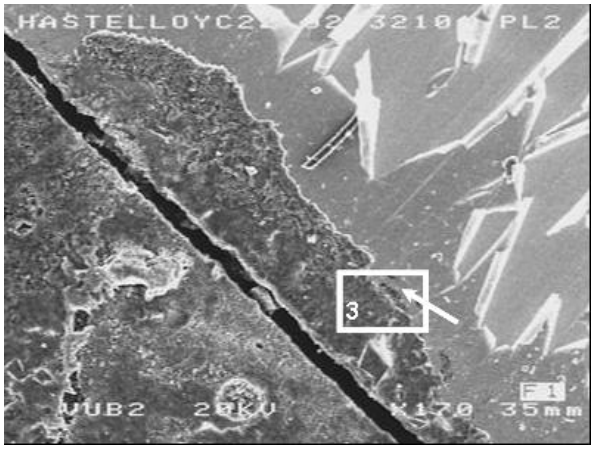

Figure 7.9: SEM-micrograph of an uncleaned HASTELLOY C-22 specimen after CPP-testing in SOCW containing 216 mg/L

7.3.3.1 Influence of alloying elements, chloride, and sulphate concentration on the pitting susceptibility of the tested stainless steels

Influence of alloying elements

UHB 904L has a slightly higher resistance to pitting than the other tested stainless steels: E_{NP} is always more than 200-300 mV more positive for UHB 904L in comparison to the other stainless steels. The three grades of AISI 316 type stainless steel (AISI 316L, AISI 316L hMo, and AISI 316Ti) have comparable pitting characteristics, i.e. the E_{NP}-values usually differ less than 100 mV.

Influence of chloride content

The pitting resistance of all tested stainles steels decreases with increasing chloride concentration: E_{NP} is drastically shifted towards more active potentials with increasing [Cl^-]. Figures 7.10 and 7.11 present the data for E_{NP} as a function of Cl^- for AISI 316L, AISI 316L hMo, AISI 316Ti, and UHB 904L type stainless steels in SOCW containing 216 mg/L SO_4^{2-} and 5,400 mg/L SO_4^{2-}, respectively.

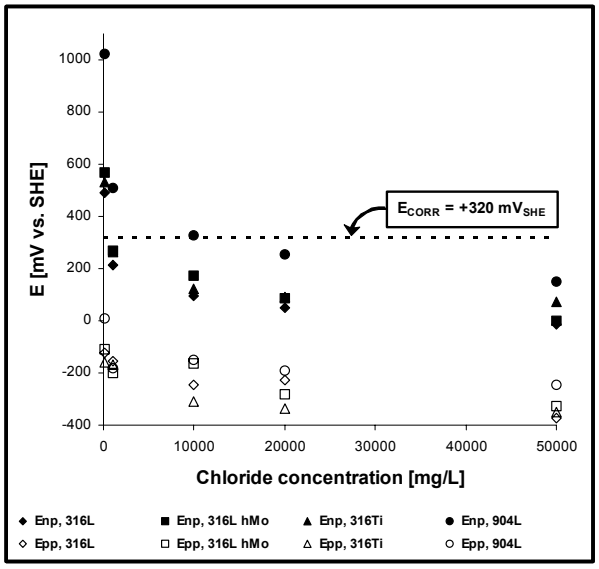

Figure 7.10: Influence of Cl^- on E_{NP} and E_{PP} of 316L, 316L hMo, 316Ti, and UHB 904L type stainless steel in SOCW containing 216 mg/L SO_4^{2-}.

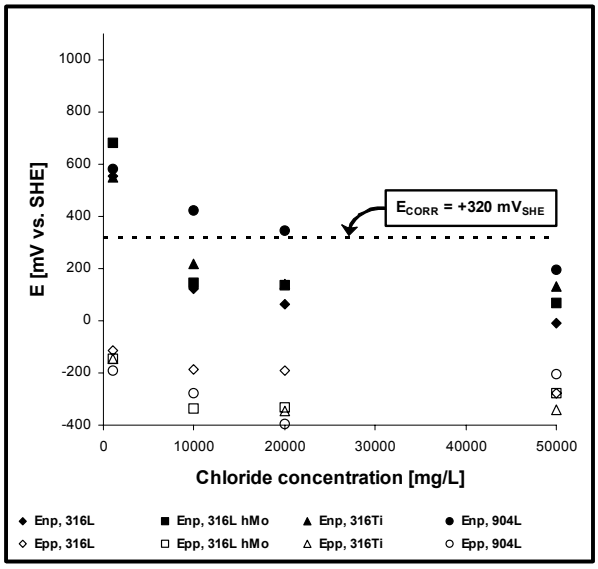

Figure 7.11: Influence of Cl^- on E_{NP} and E_{PP} of 316L, 316L hMo, 316Ti, and UHB 904L type stainless steel in SOCW containing 5,400 mg/L SO_4^{2-}.

In SOCW containing 216 mg/L SO_4^{2-} and 100 mg/L Cl^-, E_{NP} is more than 200 mV more positive than the actual E_{CORR} (+320 mV_{SHE}) for all tested stainless steels. These materials are, therefore, unlikely to suffer pitting immediately after closure of the underground repository under normal disposal conditions in the Boom clay formation (140°C, presence of oxygen, 90 mg/L Cl^-). When [Cl^-] is increased to 1,000 mg/L then only UHB 904L will remain resistant to pitting in SOCW containing 216 mg/L SO_4^{2-} (E_{NP} is still about 200 mV more noble than the actual E_{CORR}). In SOCW containing 5,400 mg/L SO_4^{2-} and 100 mg/L Cl^-, none of the stainless steels show signs of pitting attack. When [Cl^-] is increased to 1,000 mg/L than still all the

stainless steels are resistant to pitting. However, when [Cl^-] is increased even further to 10,000 mg/L then only UHB 904L is resistant to pitting.

In all tested solutions (216 mg/L and 5,400 mg/L SO_4^{2-}), the protection potential is more negative than the actual E_{CORR} for all stainless steels. This implies that once the protectice layer is damaged locally, the environmental conditions are such that it will not be able to repassivate. The value of the protection potential is also found to be rather independent of the chloride concentration.

Influence of sulphate content

The influence of the sulphate content can be studied by combining the data obtained in SOCW (216 mg/L and 5,400 mg/L SO_4^{2-}) and SBW (1,700 mg/L SO_4^{2-}). Under aerobic conditions, the actual E_{CORR} in SOCW and SBW is +320 mV_{SHE} and +265 mV_{SHE}, respectively. A value of +320 mV_{SHE} was used for the interpretation of the polarisation curves because it is the most noble value and ,therefore, it imposes the most stringent condition. This value is indicated on the curves as a horizontal dotted line.

Figure 7.12 shows the influence of the sulphate concentration on E_{NP} for AISI 316L type stainless steel in claywater solutions containing varying chloride concentrations. From Figure 7.12 the inhibitive effect of sulphate on pitting corrosion can clearly be seen, i.e. more chloride is needed to initiate pitting which means that the pitting resistance of the stainless steels increases with increasing sulphate concentration. In claywater solutions containing 100 mg/L Cl^-, E_{NP} is more noble than the actual E_{CORR} for all SO_4^{2-}-concentrations. When the [Cl^-] is increased to 1,000 mg/L, E_{NP} remains above the actual E_{CORR} only when 1,700 mg/L (or higher) SO_4^{2-} is added to the solutions. For the solutions containing 10,000 mg/L Cl^- and higher, all E_{NP}-values drop below the actual E_{CORR}. However, it was found that this inhibitive effect diminishes with increasing chloride concentration, i.e. the E_{NP}-values were independent of [SO_4^{2-}] when 20,000 mg/L Cl^- was added to the solutions. The same observations were made also for the other stainless steels. However, for UHB 904L, the inhibitive effect disappeared at much higher [Cl^-] (50,000 mg/L).

Figure 7.13 presents the influence of sulphate on E_{NP} and E_{PP} for AISI 316L hMo type stainless steel in claywater solutions containing 1,000 mg/L Cl^-. The protection potential is independent of the SO_4^{2-}-concentration. This independence was also observed for the other stainless steels.

The inhibitive effect of sulphate on the pitting behaviour raises the question whether it would not be possible to retard (or even eliminate) the effect of pitting corrosion of the metallic container by altering the near-field composition of the underground repository. It could, therefore, be advisable in future R&D to investigate in which way the backfill material can be modified (by *e.g.* adding various constituents to the backfill material) to avoid pitting corrosion under disposal conditions without adversely influencing other phenomena.

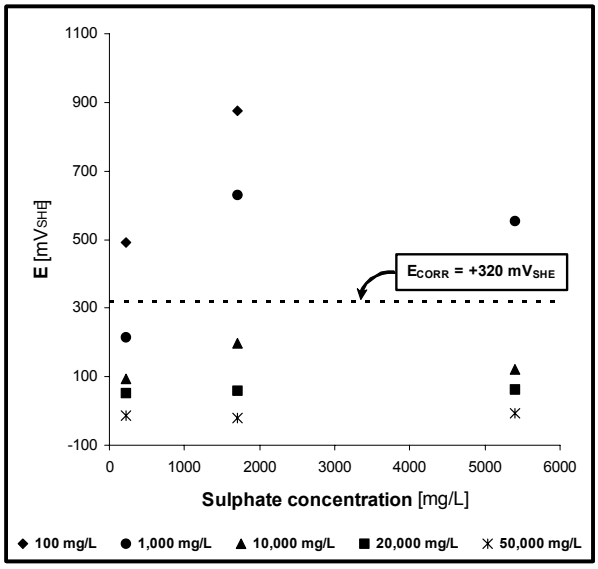

Figure 7.12: Influence of SO_4^{2-} on E_{NP} of 316L type stainless steel in claywater containing varying Cl^- contents (140°C)

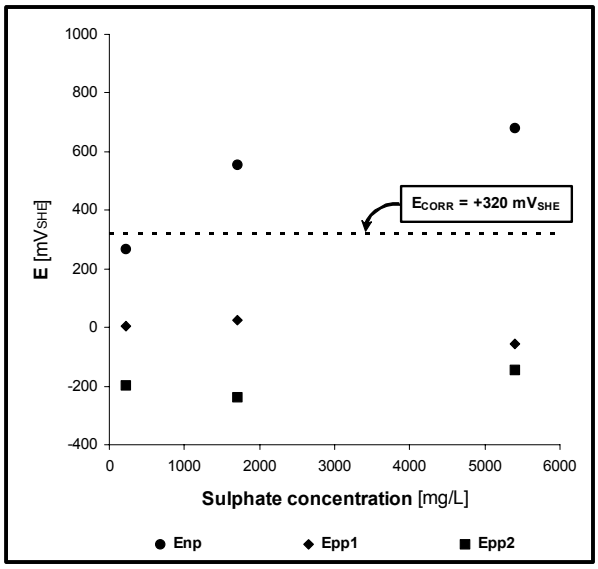

Figure 7.13: Influence of SO_4^{2-} on E_{NP} and E_{PP} of 316L hMo type stainless steel in claywater containing 1,000 mg/L Cl^- (140°C)

7.3.3.2 Influence of temperature on the susceptibility of the stainless steels to pitting

The influence of temperature on the susceptibility of AISI 316L, AISI 316Ti, AISI 316L hMo, and UHB 904L type stainless steel to pitting corrosion in SOCW containing 216 and 5,400 mg/L SO_4^{2-} is presented in Figures 7.14 and 7.15, respectively. The Figures show that increasing the temperature from 90 to 140°C lowers E_{NP} by several hundreds of millivolts. This decrease of E_{NP}, as a consequence of an increasing temperature, becomes smaller with increasing [Cl^-]. Also, the influence of temperature on the values of E_{NP} is less pronounced for UHB 904L. Figures 7.14 and 7.15 also show that AISI 316L, AISI 316Ti, and AISI 316L hMo type stainless steels present rather similar pitting resistance characteristics.

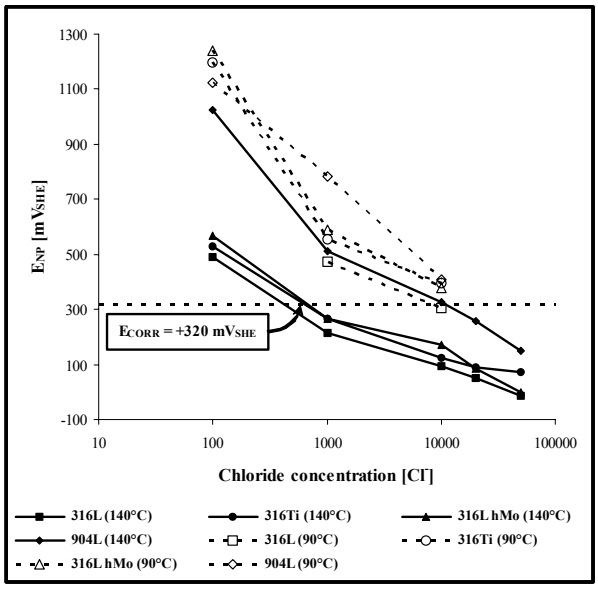

Figure 7.14: Influence of temperature on E_{NP} of 316L, 316L hMo, 316Ti, and UHB 904L type stainless steel in SOCW containing 216 mg/L SO_4^{2-}.

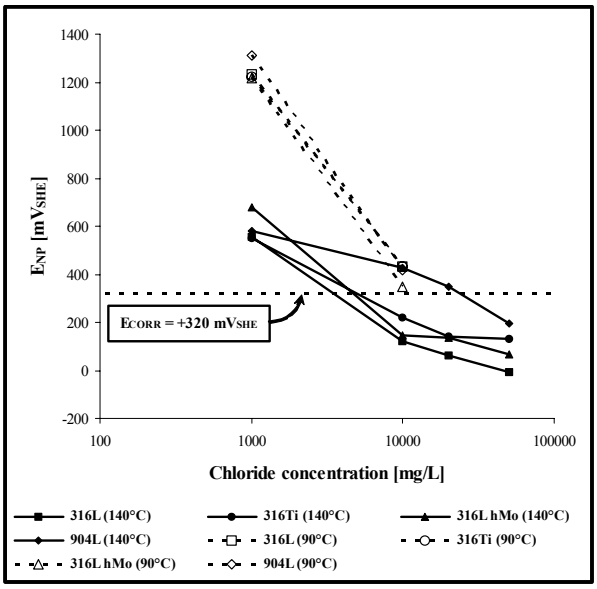

Figure 7.15**:** Influence of temperature on ENP of 316L, 316L hMo, 316Ti, and UHB 904L type stainless steel in SOCW containing 5,400 mg/L SO_4^{2-}.

7.3.4 CPP-measurements under aerobic conditions at 90°C

The maximum H_2O_2-concentration (8.10^{-2} mol/L) that can be expected at the surface of a 30 mm thick stainless steel overpack was calculated according to the kinetic method reported in [5] and based on the present Belgian disposal concept.

Ti/0.2Pd, Hastelloy C-4, and Hastelloy C-22 remain unaffected by the addition of H_2O_2 to the solutions. The carbon steel TStE 355 exhibits general corrosion in all solutions containing hydrogen peroxide (up to 8.10^{-1} mol/L), as in the H_2O_2-free solutions.

The stainless steels AISI 316L, AISI 316L hMo, AISI 316Ti, and UHB 904L show in the presence of H_2O_2 a very similar corrosiopn behaviour. The addition of H_2O_2 has a dual effect:

- on the one hand, H_2O_2 has a beneficial effect on the pitting susceptibility because the E_{NP}- and E_{PP}-values are significantly more positive in the solutions containing H_2O_2. This could suggest that H_2O_2 promotes passivation. It was also observed that the E_{NP}-values increase with increasing H_2O_2-concentration. This is indicative for an inhibiting effect of H_2O_2 on pitting (this effect is however less pronounced than for sulphate).

- on the other hand, H_2O_2 exerts a detrimental effect on the susceptibility to pitting because the addition of H_2O_2 caused a sharp increase of the OCP. Consequently, the potential difference between E_{NP} and the OCP (this can be considered as a parameter that indicates the risk for pitting) is reduced significantly (in some cases the difference was less than 100 mV). Also, the protection potential, E_{PP}, is situated below the OCP when H_2O_2 is present in the solutions. Under these circumstances, a local damage of the passive layer (either due to pitting or mechanically) will probably never be able to repassivate.

7.3.5 The critical chloride content approach

The critical chloride content is defined as the maximum chloride level below which pitting is not expected to occur.

It has been found [44,45] that a linear relationship exists between the critical pit nucleation potential, E_{NP}, and the chloride concentration, $[Cl^-]$, of the type

$$E_{NP} = A - B \cdot \log\left[Cl^-\right] \qquad (1)$$

where B is a constant depending on the alloy composition, supporting electrolyte composition, measurement technique, *etc.*

From equation (1), it is possible to estimate the maximum chloride level below which pitting is not expected to occur immediately in environments relevant for various underground repository conditions (conditions evolving in the course of the disposal period). The maximum chloride level is determined as the intersection between the regression line and the actual value of E_{CORR}.

As an example, the regression lines and the fitting results for AISI 316L, AISI 316L hMo, AISI 316Ti, and UHB 904L type stainless steels in SOCW containing 216 and 5,400 mg/L SO_4^{2-} under aerobic conditions (140°C) are presented in Figures 7.16 and 7.17, respectively. The estimated chloride levels above which pitting is expected to occur immediately in environments relevant for various conditions in clay formations are presented in Table 7.6. The results from the previous EC-Project are added for comparison (SOCW and SBW, aerobic, 90°C).

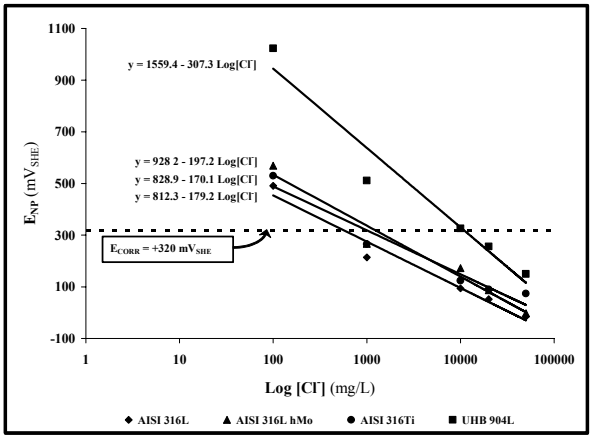

Figure 7.16**:** Linear fitting of (E_{NP}, log[Cl^-]) plots of 316L, 316L hMo, 316Ti, and UHB 904L type stainless steel in SOCW containing 216 mg/L SO_4^{2-} (140°C).

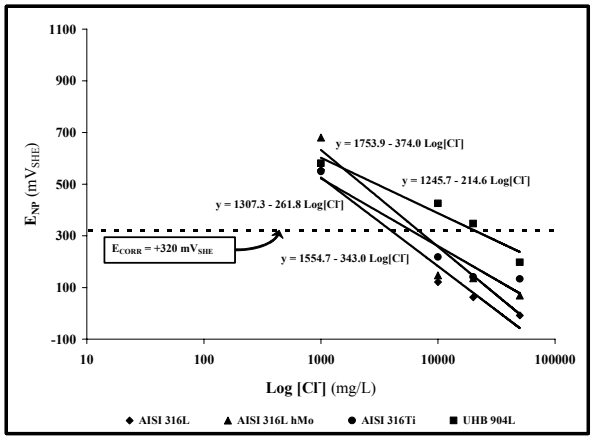

Figure 7.17**:** Linear fitting of (E_{NP}, log[Cl^-]) plots of 316L, 316L hMo, 316Ti, and UHB 904L type stainless steel in SOCW containing 5,400 mg/L SO_4^{2-} (140°C).

The critical chloride content approach yields the following additional information:

- all four of the tested stainless steels seem to be adequately resistant to pitting corrosion in an argillaceous environment. under aerobic conditions. Under the most severe conditions, i.e. a high temperature (140°C) and a low degree of oxidation (216 mg/L SO_4^{2-}), the maximum level of chloride above which pitting is expected to occur for AISI 316L is approximately 560 mg/L, which is more than 6 times higher than the expected chloride content of the near-field environment for the Belgian disposal concept (~90 mg/L Cl^-). The other three stainless steels can even resist environments containing higher amounts of Cl^- ($[Cl^-]_{MAX}$ for AISI 316L, AISI 316Ti and AISI 316L hMo was estimated to be 980, 1220 and 10800 mg/L, respectively).

- as the near-field environment becomes more oxidizing, i.e. the further in the disposal period, the tested stainless steels become more resistant to pitting. In this case the $[Cl^-]_{MAX}$ is increased with a factor of about 6-7 (140°C) when $[SO_4^{2-}]$ increases from 216 to 5,400 mg/L. This effect is most pronounced at 140°C and is almost negligible at 90°C.

- the oxygen level has a significant influence on the pitting resistance. As oxygen will be consumed in the underground repository, the tested stainless steels become much more resistant to pitting. $[Cl^-]_{MAX}$ is increased with a factor of about 25, for AISI 316L hMo and UHB 904L, when the conditions change from aerobic to anaerobic.

- when the temperature is increased from 90 to 140°C, the maximum chloride level above which pitting is expected to occur decreases drastically. $[Cl^-]_{MAX}$ decreases approximately 15, 10, and 8 times (216 mg/L SO_4^{2-}) for AISI 316L, AISI 316Ti, and AISI 316L hMo, respectively. In highly oxidized clay environments (5,400 mg/L SO_4^{2-}), the temperature has a much lower influence on $[Cl^-]_{MAX}$. UHB 904L is less susceptible to temperature.

- the 'critical chloride content approach can be used as a tool to determine the suitability of stainless steels in other argillaceous disposal environments containing Cl^- by estimating the maximum chloride level below which pitting is not expected to occur.

Table 7.6: Estimated chloride levels above which pitting is expected to occur immediately in environments relevant for various disposal conditions in clay formations

Material	**Experimental conditions**	**T** (°C)	**$[SO_4^{2-}]$** (mg/L)	**$[Cl^-]_{max}$** (mg/L)	**Note**
AISI 316L	SOCW AEROBIC	140	216	0.56×10^3	1)
AISI 316Ti		140	216	0.98×10^3	
AISI 316L hMo		140	216	1.22×10^3	
UHB 904L		140	216	10.80×10^3	
AISI 316L	SOCW AEROBIC	140	5,400	4.0×10^3	1)
AISI 316Ti		140	5,400	5.9×10^3	
AISI 316L hMo		140	5,400	6.8×10^3	
UHB 904L		140	5,400	20.6×10^3	
AISI 316L	SBW AEROBIC	140	1,700	6.9×10^3	1)
AISI 316Ti		140	1,700	7.6×10^3	
AISI 316L hMo		140	1,700	9.0×10^3	
UHB 904L		140	1,700	6.5×10^3	
AISI 316L	SOCW AEROBIC	90	216	8.1×10^3	2)
AISI 316Ti		90	216	9.2×10^3	
AISI 316L hMo		90	216	9.6×10^3	
UHB 904L		90	216	18.3×10^3	
AISI 316L	SOCW AEROBIC	90	5,400	13.8×10^3	2)
AISI 316Ti		90	5,400	10.7×10^3	
AISI 316L hMo		90	5,400	13.9×10^3	
UHB 904L		90	5,400	12.8×10^3	
AISI 316L hMo	SBW AEROBIC	90	1,700	80.5×10^3	2)
UHB 904L		90	1,700	22.1×10^3	
AISI 316L	SICW ANAEROBIC	90	0.2	0.27×10^6	1)
AISI 316Ti		90	0.2	1.8×10^6	
AISI 316L hMo		90	0.2	67.8×10^6	
UHB 904L		90	0.2	5.7×10^6	
AISI 316L	SBW ANAEROBIC	90	1,700	0.35×10^6	1)
AISI 316Ti		90	1,700	108.3×10^6	
AISI 316L hMo		90	1,700	1.8×10^6	
UHB 904L		90	1,700	0.62×10^6	

1) experiments performed during the current EC-programme (period : November 2000 – October 2003).
2) experiments performed during the previous EC-programme (period: January 1996 – December 1998).

7.4 Conclusions

Ti/0.2Pd (Ti99.8-Pd, Ti-Gr-7) is the only material that was resistant to pitting corrosion under all experimental conditions.

Under anaerobic conditions at 16°C, the carbon steel TStE 355 remains unaffected in SBW-solutions without thiosulphate. Under all other conditions, TStE 355 is subject to gereral corrosion. The Hastelloy C-4, Hastelloy C-22, and UHB 904L are resistant to pitting. AISI 316L, AISI 316L hMo, and AISI 316Ti are resistant to pitting in all SBW-solutions (up to 50,000 mg/L Cl^-) and in SICW up to 1,000 mg/L Cl^-. Although at $[Cl^-] \geq 1{,}000$ mg/L slight signs of pitting were observed on the stainless steels, the E_{NP}-values remained much more positive than the actual E_{CORR} (-10 mV_{SHE}).

Under anaerobic conditions at 90°C, the carbon steel TStE 355 exhibits general corrosion in all SICW- and SBW-solutions. Hastelloy C-4 and Hastelloy C-22 are resistant to pitting. Although in some conditions, the CPP-curves revealed a hysteresis, it was found that this is probably the result of an alteration of the passive layer. UHB 904L has a slightly higher pitting resistance than the three 316 grade stainless steels. The E_{NP}-values for AISI 316L, AISI 316L hMo, and AISI 316Ti are situated well above the actual E_{CORR} in all SICW- and SBW-solutions. The E_{PP}-values drop below the actual E_{CORR} for $[Cl^-] > 10{,}000$ mg/L.

Under aerobic conditions at 140°C, the carbon steel TStE 355 exhibits general corrosion in all SOCW- and SBW-solutions. Hastelloy C-4 and Hastelloy C-22 are resistant to pitting. However, in SOCW-solutions containing high $[Cl^-]$ (> 20,000 mg/L), the samples show signs of pitting at the interface between the sample and the mounting resin. This indicates that under these severe conditions, Hastelloy C-4 and Hastelloy C-22 could be susceptible to crevice corrosion. UHB 904L has a slightly higher resistance to pitting than the other stainless steels. The three grades of AISI 316 type stainless steels have comparable pitting characteristics. The pitting resistance decreases with increasing chloride concentration. In SOCW, E_{NP} drops below the actual E_{CORR} when the chloride concentration is increased to 1,000 mg/L (except for UHB 904L). In SBW, E_{NP} remains well above the actual E_{CORR} for chloride concentrations up to 10,000 mg/L. E_{PP} is more negative the the actual E_{CORR} in all SOCW- and SBW-solutions. Sulphate has an inhibitive effect on pitting. This means, the higher the sulphate concentration, the more chloride is required to initiate pitting. This inhibitive effect diminishes with increasing $[Cl^-]$. An increase in temperature causes a steep decrease of E_{NP}.

The oxygen level has a significant influence on the pitting resistance. As oxygen will be consumed in the underground repository, the tested stainless steels become much more resistant to pitting: $[Cl^-]_{MAX}$ is increased by a factor of about 25, for AISI 316L hMo and UHB 904L, when the conditions change from aerobic to anaerobic.

The ‘critical chloride content’ approach is a useful tool to determine the suitability of stainless steels in other argillaceous disposal environments containing Cl^- by estimating the maximum chloride level below which pitting is not expected to occur.

8. CONCLUSIONS

8.1 Salt environment

The results obtained in the present studies confirm previous findings that the alloy Ti99.8-Pd is the strongest candidate for the realization of the **corrosion-resistant container concept** in rock salt. This alloy exhibits in the test brines at 150°C both without gamma radiation and in the presence of a gamma radiation field of 10 Gy/h an excellent resistance to general corrosion (corrosion rates only 0.1-0.25 µm/a) and pitting corrosion. Furthermore, it is known from our previous stress corrosion cracking studies (slow strain rate tests in NaCl-rich brine at 170°C) that Ti99.8-Pd is completely resistant to stress corrosion cracking (SCC) in brines and it does not suffer a loss of ductility. A corrosion-resistant container concept could consist of a thick-walled carbon steel container as mechanical support against the rock pressure which is provided with a corrosion protection made of Ti99.8-Pd.

TStE355 carbon steel and copper-base materials such as Cu, Cu-Ni 90-10 and Cu-Ni 70-30 are promising materials for the **corrosion-alowance container concept** in rock salt. Unter the test conditions applied (T=150°C), all these materials are resistant to pitting corrosion in the sense of an active-passive corrosion element, and their general corrosion rates imply corrosion allowances acceptable for thick-walled containers. The Electron Beam (EB) and Tungsten-Inert-Gas (TIG) welding (potential container closure techniques) reduce significantly the resistance of the carbon steel to localized corrosion in $MgCl_2$-rich brine at 150°C. However, localized corrosion problems can be avoid by a stress relief thermal treatment of the welds. The investigations have shown that the thermal treated welded steel is resistant to localized corrosion, as does also the unwelded steel.

An disadvantage by use of carbon steel as container material is its high corrosion rate in brines, especially at high temperatures (150-170°C) in $MgCl_2$-rich brine, which results in the formation of high quantities of hydrogen in the disposal area. A such problem can be avoid by corrosion protection of the thick-walled carbon steel containers by a thin-walled container made by Ti99.8-Pd or a Cu-base material (Cu or Cu-Ni alloys). However, by attack of salt brines and failure of the corrosion protection material a galvanic corrosion between the steel and the corrosion protection material occurs under certain conditions which changes the corrosion behaviour of the individual materials. The results obtained on galvanic coupled specimens indicate that by attack of of $MgCl_2$-rich brine and in the presence of a gamma radiation field of 10 Gy/h (formation of strong oxidizing radiolytic products), galvanic corrosion occurs on the galvanic coupled material pairs steel/Ti99.8-Pd and steel/Cu-base materials, respectively, which results in the case of the less carbon steel to strong localized corrosion and in a significant increase in its general corrosion rate compared to the value of the uncoupled steel. For the galvanic coupled more noble Cu-base materials a clear decrease in the corrosion rate was observed compared to the values of the uncoupled materials. The corrosion rate of the galvanic coupled Ti99.8-Pd is very close to the value of the uncoupled material. In NaCl-rich brine (T=150°C) no galvanic corrosion occurs between the steel and the above-mentioned corrosion protection materials because all materials form in brines stable corrosion protection layers.

The electrochemical and surface analytical investigations indicate that the Cu-base materials have a higher corrosion resistance than the TStE355 carbon steel both in $MgCl_2$-rich brine and NaCl-rich brine. In the case of galvanic corrosion, carbon steel is always the anode with respect to the Cu-base materials being the cathode.This means that the Cu-base materials will be cathodically corrosion protected by the carbon steel. In general, the electrochemical experiments show in agreement with the long-term immersion experiments that the corrosion rate of carbon steel is higher in Q-brine (pH = 4.6) than in NaCl-rich brine (pH = 6.5). But for all conclusions made it always must be kept in mind that electrochemistry describes corrosion only for the starting period of the corrosion process, and determines the initial corrosion rate. For the determination of the long-term corrosion behaviour and the final corrosion rate of the container materials long-term corrosion experiments are necessary, as were performed in this study.The results from the investigation of the element composition and the morphology of corroded Cu, Ni and steel electrode surfaces by means of EPMA / EDX and SEM confirm those obtained from the electrochemical measurements.

8.2 Granitic environment

Among the materials investigated in granitic-bentonite water (Cl^- content up to 50,000 mg/L, temperature up to 90°C) the Ni-base alloy Hastelloy C-22 is the most promising material for the manufacture of corrosion resistance disposal containers to be disposed of in a granitic formation. Under the test conditions applied this material is resistant to pitting corrosion, crevice corrosion and stress corrosion cracking (SCC) in granitic-bentonite water with Cl^- contents up to 50,000 mg/L. Welding procedures such as Electron Beam (EB) and Gas Tungsten Arc (GTA) welding do not influence the corrosion resistance of the material. Furthermore, Hastelloy C-22 does not show any susceptibility to Microbiologically Induced Corrosion (MIC) due to Sulphate Reducing Bacteria (SRB).

The results of electrochemical studies in deaerated granitic-bentonite water (reducing conditions) containing up to 50,000 mg/L Cl^- indicate that Cu and the alloy Cu-Ni 70-30 are resistant to pitting corrosion and that the EBW and GTA welding do not influence the corrosion resistance of these materials. Furthermore, both materials are resistant to crevice corosion in granitic-bentonite water(pH=7.3) containing a very limited amount of oxygen. Cu is resistant to SCC but for Cu-Ni 70-30 a slight sensitivity to SCC was observed under severe test conditions (very slow strain rates of 10^{-6} and $2x10^{-7}$ s^{-1}). Moreover, for Cu and Cu-Ni 70-30 a certain susceptibility to MIC (microbiologically induced corrosion) due to sulphide reducing bacteria (SRB) was determined. Supplementary long-term immersion experiments (T=90°C) under initial oxidizing conditions in granitic water (Cl^- content 98 mg/L, pH=9.1) show that the general corrosion rates of Cu, Cu-Ni 90-10 and Cu-Ni 70-30 are small (1-7 µm/a) and that, as in the experiments under recucing conditions, the Cu-Ni alloys are resistant to pitting corrosion. However, for Cu pitting and intergranular corrosion was observed under the initial oxidizing conditions of the experiments.

Studies at 90°C under initial oxidizing conditions in granitic water (Cl^- content 98 mg/L, pH=9.1) and in granitic-bentonite water (Cl^- content 6258 mg/L, pH=7.3) indicate that the TStE355 carbon steel is resistant to pitting corrosion in the environment having the low Cl^- content and a pH of 9.1. In the granitic-bentonite

environment with the high Cl^- content (6258 mg/L) and a pH of 7.3, the steel suffered from pitting corrosion. In previous investigations of [46] in this granitic-bentonite water no pitting corrosion was observed. A possible explanation for the pitting corrosion of the steel in our experiments is the fact that the total oxygen content in our experimental equiment was higher than in the experiments of [46], which means that the steel was longer exposed to oxidizing conditions.

8.3 Clay environment

The results indicate that the alloy Ti99.8-Pd is the most promising material for the manufacture of containers to be disposed of in clay formations. Among the passively corroded materials (Ti99.8-Pd, nickel-base alloys, stainless steels) only the alloy Ti99.8-Pd is resistant to pitting corrosion under all test conditions applied (T=16°C-140°C, up to 50,000 mg/L Cl^-). The nickel-base alloys Hastelloy C-4 and C-22 are at 16°C and 90°C (anaerobic conditions) also resistant to pitting corrosion. Only under severe test conditions in Synthetic Oxidizing Clay Water (aerobic conditions, T=140°C, Cl^- content higher than 20,000 mg/L) a slight susceptibility to crevice corrosion was observed.

The actively corroded carbon steel suffers from general corrosion (no pitting) and continues to be considered as a candidate material for the realization of the corrosion-allowance container concept. The stainless steels investigated show a lower resistance to pitting corrosion than the nickel-base alloys. The susceptibility of the stainless steels to pitting corrosion increases with increasing temperature and growing Cl^- content. The oxygen level has a significant influence on the pitting resistance of the stainless steels. As oxygen will be consumed in the underground repository, the tested stainless steels will become much more resistant to pitting: $[Cl^-]_{MAX}$ is increased by a factor of about 25, for AISI 316L hMo and UHB 904L, when the conditions change from aerobic to anaerobic.

The presence of the radiolytic product H_2O_2 in the clay solutions does not affect the corrosion behaviour of Ti/0.2Pd, Hastelloy C-4, Hastelloy C-22 and TStE 355 carbon steel. In the case of the stainless steels AISI 316L, AISI 316L hMo, AISI 316Ti, and UHB 904L the addition of H_2O_2 exerts a dual effect on the susceptibility to pitting: a beneficial effect by promoting passivation and inhibiting pitting, and a detrimental effect by increasing the OCP (open circuit potential) significantly and eliminating repassivation completely.

In general it can be stated that pitting corrosion occurs on the stainless steels but at Cl^- concentrations which are significantly higher than those expected in the near field environment of the Belgian disposal concept. Therefore, the stainless steels continue to be considered in the Belgian concept as the first candidate material for containers to be disposed of in clay.

Finally it can be stated that the ‘critical chloride content’ approach used in the clay studies is a useful tool to determine the suitability of stainless steels also in other argillaceous disposal environments containing Cl^- by estimating the maximum chloride level below which pitting is not expected to occur.

9. REFERENCES

[1] G.P.Marsh, G.Pinard-Legry, E.Smailos et al., “HLW Container Corrosion and Design,” Proc. of the Second European Community Conf. and Radioactive Waste Management and Disposal, Luxembourg, April 22-26, 1985, p.314, R.A. Simon (Ed.), Cambridge University Press, EUR 13389 (1986).

[2] E.Smailos, W.Schwarzkopf, R.Köster and K.H.Grünthaler,”Advanced Corrosion Studies on Selected Packaging Materials for Disposal of HLW Canisters in Rock Salt,” Proc. of the Symposium on Waste Management 1998, Tucson, Arizona, USA, February 28-March 3, 1998, Vol.2, pp. 985-994, Arizona Board of Regents (1988).

[3] E.Smailos, I.Azkarate, J.A.Gago, P.Van Iseghem, B.Kursten, T.McMenamin, ”Corrosion Studies on Metallic HLW Container Materials,” Proc. of the 4th European Conf. on Management and Disposal of Radioactive Waste, Luxembourg, 25-29 March 1996, pp. 209-223, T.McMenamin (Ed.), EUR 17543 (1997).

[4] E.Smailos, W.Schwarzkopf and R.Storch,”Corrosion Studies on Packaging Materials for High-Level Waste Disposal in a Rock-Salt Repository,” Proc. of the 12th Scandinavian Corrosion Congress and Eurocorr ’92, Espoo, Finland, June 1992, pp. 327-338 (1992).

[5] E. Smailos, A. Martínez-Esparza, B. Kursten, G. Marx, I. Azkarate,”Corrosion Evaluation of Metallic Materials for Long-Lived HLW/Spent Fuel Disposal Containers,” EUR-Report 19112 (1999).

[6] E. Smailos, J.A. Gago, I. Azkarate, B. Fiehn,”Corrosion Studies on Selected Packaging Materials for Disposal of Heat-Generating Radiactive Wastes in Rock-Salt Formations,” FZKA-Report 5587 (1995).

[7] R.E. Westerman, J.H. Haberman et al.,”Corrosion and Environmental Characterization of Iron-Base Nuclear Waste Package Structural Barrier Materials,” PNL-Report No. 5426 (1986).

[8] E. Smailos, “Corrosion of High-Level Waste Packaging Materials in Disposal Relevant Brines,” Nuclear Technology, Vol. 104, (December 1993) pp. 343-350

[9] E. Smailos, “Influence of Welding and Heat Treatment on Corrosion of the High-Level Waste Container Material Carbon Steel in Disposal Salt Brines,” Corrosion 56, 10 (2000), pp. 1071-1074.

[10] K.-D. Closs, R.Papp, “Fifteen Years of Research and Development on Direct Disposal in Germany: An Overview,“ Nuclear Technology, 121 (1998), pp. 101-113.

[11] K. Janberg, H.Spilker, “Status of the Development of Final Disposal Casks and Prospects in Germany,” Nuclear Technology, 121 (1998), pp. 136-147.

[12] B. Kienzler, A. Loida, W. Maschek, A. Rineiski, “Is Criticality a Matter of Concern for Gorleben?,” 2003 Internat. High-Level Radioactive Waste Management Conf., Las Vegas, Nev., USA, March 30-April 2, 2003, Proc. on CD-ROM.

[13] E. Smailos, „Corrosion Behaviour of Copper-Base Materials in Disposal Relevant Salt Brines,“ Proc. of EUROCORR 2000, Session „Nuclear Corrosion,“ 10-14 September 2000, London, UK.

[14] E. Smailos, D. Schild, G. Gompper, “Corrosion of Ti99.8-Pd under Gamma Irradiation in $MgCl_2$-Rich Brine,“ Material Research Society Symposium Proceedings, Vol. 506 (1998), pp.477-484.

[15] B. Grambow, R. Müller, “Chemistry of Glass Corrosion in High Saline Brines,” Materials Research Society Symposium Proceedings, Vol. 176 (1990), pp. 229-240.

[16] M. Altmaier, V. Metz, V. Neck, R. Müller, Th. Fanghänel, “Solid-Liquid Equilibria of $Mg(OH)_2$(Cr) and $Mg_2(OH)_3Cl^{\bullet}4H_2O$(cr) in the System Mg-Na-H-OH-Cl-H_2O at 25°C,” Geochim. Cosmochim. Acta, 67(2003).

[17] B. Kienzler, B. Luckscheiter, S. Wilhelm, “Waste Form Corrosion Modeling: Comparison with Experimental Results, Waste Management 21(2001), pp.741-752.

[18] M. Kelm, E. Bohnert, “Radiation Chemical Effects in the Near Field of a Final Disposal Site-I: “Radiolytic Products Formed in Concentrated NaCl Solutions,“ Nuclear Technology, 129 (2000), pp.119-122.

[19] H. A. Videla, CORROSION 89, Paper No. 185, NACE Internat., Houston, Texas, 1989.

[20] G. Marx, A. Bestanpouri, W. Schönemann, D. Wegen, Nukleare Entsorgung 4 159 (1989).

[21] G. Marx, C. Nehm, „Radiochemische Korrosionsuntersuchungen an Titan und Titanlegierungen als Containerwerkstoffe in praxisrelevanten Salzlaugen“; BMBF-Bericht (FZK 02E82613), Berlin (1995).

[22] D. Wegen, Dissertation; Freie Universität Berlin (1991).

[23] G. Marx, „Korrosionschemische Untersuchungen an Behältermaterialien unter Plutoniumeinfluß mit Hilfe der Radiotopenmethode“; BMBF-Bericht (FZK 02U58572), Berlin (1990).

[24] C. Nehm, Dissertation; Freie Universität Berlin (1998).

[25] H. Kaesche, Die Korrosion der Metalle; Springer Berlin-Heidelberg-New York (1979) pp. 223-229.

[26] K. Schwabe, Physikalische Chemie, Bd. 2; Akademie-Verlag Berlin (1975).

[27] A. F. Hollemann, E. Wiberg, Lehrbuch der anorganischen Chemie; Walter de Gruyter, Berlin-New York (1985) p. 1001.

[28] C.M. Bethke, „The Geochemist´s Workbench," Release 4.0, University of Illinois, USA, 2002.

[29] „EQ3/6, A Software Package for Geochemical Modeling Version 7.2a," University of California , Lawrence Livermore National Laboratory. Software produced under Designated Unclassified Subject Area (DUSA) "Yucca," 1990-1993.

[30] "Preparation of a synthetic granitic-bentonite water,". Specific Procedure Nº PR-X8-01, CIEMAT, 1996.

[31] ENRESA, Full-scale engineered barriers experiment in crystalline host rock (FEBEX). Bentonita: Origen, propiedades y fabricación de bloques. Publicación Técnica Núm. 04/98, ENRESA, Madrid (1998).

[32] "Corrosion of metals and alloys – Stress corrosion testing. Part 7: Slow strain rate testing". ISO 7539-7, International Standard ISO 1989-12-01.

[33] "Standard practice for slow strain rate testing to evaluate the susceptibility of metallic materials to environmentally assisted cracking", Standard G129, Annual Book of ASTM Standards, Vol.03.01; West Conshohocken, PA, ASTM.

[34] R.N. Parkins, "Slow Strain Rate Testing - 25 Years Experience", Slow strain rate testing for the evaluation of environmentally induced cracking : research and engineering applications, ASTM STP 1210, R. D. Kane, Ed., American Society for testing and materials, Philadelphia, 1993, pp.7-21.

[35] "Standard reference test method for making potentiostatic and potentiodynamic anodic polarization measurements". Standard G5, Annual Book of ASTM Standards, Vol.03.02; West Conshohocken, PA, ASTM.

[36] "Corrosion of metals and alloys – Electrochemical test methods –Guidelines for conducting potentiostatic and potentiodynamic polarization measurements,". COMMITTEE DRAFT, ISO/CD 17475, International Standard ISO 2001.

[37] "Standard practice for calculation of corrosion rates and related information from electrochemical measurements". Standard G102, Annual Book of ASTM Standards, Vol.03.02; West Conshohocken, PA, ASTM.

[38] ASM , "Corrosion", Metals Handbook, Vol.13, p. 118, ASM, International.

[39] "Crevice corrosion testing of iron-base and nickel-base stainless alloys in seawater and other chloride-containing aqueous environments," Standard G78, Annual Book of ASTM Standards, Vol.3.01; West Conshohocken, PA, ASTM.

[40] D.S. Dunn, G.A. Cragnolino and N. Sridhar, “An Electrochemical Approach to Predicting Long-Term Localized Corrosion of Corrosion-Resistant High-Level Waste Container Materials,” Corrosion **56**, 1 (2000) pp. 90-104.

[41] J.-H. Wang, C.C. Su and Z. Szklarska-Smialowska, “Effects of Cl^- Concentration and Temperature on Pitting of AISI 304 Stainless Steel,” Corrosion **44**, 10 (1988), pp. 732-737.

[42] R.S. Glass, G.E. Overturf, R.A. Van Konynenburg and R.D. McCright, “Gamma Radiation Effects on Corrosion – I. Electrochemical Mechanisms for the Aqueous Corrosion Processes of Austenitic Stainless Steels Relevant to Nuclear Waste Disposal in Tuff,” Corrosion Science **26**, 8 (1986) pp. 577-590.

[43] G. Marx, GNF, Berlin, Personal communication (2002).

[44] Z. Szklarska-Smialowska, “Pitting Corrosion of Metals,” NACE International (National Association of Corrosion Engineers, Houston, Texas, USA) (1986).

[45] A.J. Sedriks, “Corrosion of Stainless Steels, 2nd edition,” Wiley-Interscience (New York, USA) (1996).

[46] I. Azkarate, V. Madina, M. Insausti, “Estudios de Corrosion de Materiales para Contenedores de Almacenamiento a Largo Plazo de Residuos de Alta Actividad Situación Alcanzada y Perspectivas,” 5th Workshop of ENRESA Tarragona, Spain (December, 2003).